VNiVERSiDAD D SALAMANCA

CAMPUS OF INTERNATIONAL EXCELLENCE

PhD Dissertation

International Mention

Damage evaluation in constructions based on geomatic and dynamic approaches

Luis Javier Sánchez Aparicio

Ávila, 2016

Department of Cartographic and Land Engineering

Higher Polytechnic School of Avila

University of Salamanca

AUTHOR:

Luis Javier Sánchez Aparicio

SUPERVISORS:

Dr. Diego González Aguilera

Dr. Belén Riveiro Rodríguez

TITLE:

Damage evaluation in constructions based on geomatic and dynamic approaches.

FORMAT:

Doctoral Thesis as a compentidum of publications, with International Doctoral mention.

PHD PROGRAM:

Investigación y desarrollo en geotecnologías (R.D. 1393/2007).

University of Salamanca.

This Doctoral Thesis is composed of a total of four scientific articles that were previously published or accepted for publication in scientific journals of international impact:

- The combination of geomatic approaches and operational modal analysis to improve calibration of finite element models: A case of study in Saint Torcato Church (Guimarães, Portugal).

  Luis Javier Sánchez-Aparicio[a], Belén Riveiro[b], Diego González-Aguilera[a], Luís F. Ramos[c]

  [a]Department of Cartographic and Land Engineering, University of Salamanca, Higher Polytechnic School of Avila, Hornos Caleros 50, 05003, Avila, Spain.

  [b]Department of Material Engineering, Applied Mechanics and Construction, School of Industrial Engineering, University of Vigo, Vigo, Spain.

  [c]ISISE, Department of Civil Engineering, University of Minho, Guimarães, Portugal

  Construction and Building Materials Journal

  DOI: 10.1016/j.conbuildmat.2014.07.106

- Experimental and numerical approaches for structural assessment in new footbridge designs (SFRSCC-GFPR hybrid structure).

  Luis Javier Sánchez-Aparicio[a], Luís F. Ramos[b], José Sena-Cruz[b], Joaquim O. Barros[b], Belén Riveiro[c]

  [a]Department of Cartographic and Land Engineering, University of Salamanca, Higher Polytechnic School of Avila, Hornos Caleros 50, 05003, Avila, Spain.

  [b]ISISE, Department of Civil Engineering, University of Minho, Guimarães, Portugal

  [c]Department of Material Engineering, Applied Mechanics and Construction, School of Industrial Engineering, University of Vigo, Vigo, Spain.

  Composite Structures Journal

  DOI: 10.1016/j.compstruct.2015.07.041

- Photogrammetric, geometrical and numerical strategies to evaluate initial and current conditions in historical constructions: a test case in the church of San Lorenzo (Zamora, Spain).

  Luis Javier Sánchez-Aparicio[a], Alberto Villarino-Otero[a], Jesús García-Gago[a], Diego González-Aguilera[a]

  [a]Department of Cartographic and Land Engineering, University of Salamanca, Higher Polytechnic School of Avila, Hornos Caleros 50, 05003, Avila, Spain.

  Remote Sensing Journal

  DOI: 10.3390/rs801006

- Practical use of multispectral techniques for the detection of pathologies in constructions.

Luis Javier Sánchez-Aparicio[a], Susana Del Pozo-Aguilera[a], Pablo Rodríguez-Gonzálvez[a], Jesús Herrero-Pascual[a], Angél Luis Muñoz-Nieto[a], Diego González-Aguilera[a], David Hernández-López[b]

a Department of Cartographic and Land Engineering, University of Salamanca, Higher Polytechnic School of Avila, Hornos Caleros 50, 05003, Avila, Spain.

b Institute for Regional Development (IDR), University of Castilla La Mancha, 02071, Albacete, Spain

CRC Press - Taylor & Francis Group

ISBN: 978-1-138-02810-4

SUPERVISORS' REPORT

This Doctoral Thesis, titled *Damage evaluation in constructions based on geomatic and dynamic approaches*, and presented by D. Luis Javier Sánchez Aparicio, is fully integrated in the research line: *Modelling and pathological evaluation of historical buildings* of the research unit *TIDOP* (http://tidop.usal.es), member of the University of Salamanca.

As a result of the research activity carried out by the PhD student, during the preparation period of this Doctoral Thesis, several scientific works have been published in prestigious international journals. Complementary to this, the software created must be highlighted, under the title Enhance your Finite Element Models (*EyFEM*), it combines the methodologies developed and used in part of this Doctoral Thesis (see Annex I).

The different publications shown in the present document corroborate and validate the scientific study that has been conducted, and each article that resulted from this study has been published in prestigious international journals indexed in the Journal Citation Report database , within different specialized disciplines: (i) construction (*Construction and Building Materials Journal*); (ii) composite materials (*Composite Structures Journal*)*; and (iii) r*emote sensing (*Remote Sensing Journal*) and engineering & technology (*CRC Press-Taylor & Francis Group*). Following the order of their publication, they are distributed as follows:

- The scientific article: *The combination of geomatic approaches and operational modal analysis to improve calibration of finite element models: A case of study in Saint Torcato Church (Guimarães, Portugal).* Published in the journal *Construction and Building Materials Journal,* indexes from the Journal Citation Report placed it in the Q1 (First Decile) of the *Contruction & Building Technology* field. It ranked the twelfth position, in impact factor out

of the one hundred and twenty four journals indexed on it. DOI: 10.1016/j.conbuildmat.2014.07.106.

- The publication: *Experimental and numerical approaches for structural assessment in new footbridge designs (SFRSCC-GFPR hybrid structure).* Published in the journal *Composite Structure Journal*. This journal, indexed on the first quartile, is the third of twenty four journals. DOI: 10.1016/j.compstruct.2015.07.041.

- The scientific work: *Photogrammetric, geometrical and numerical strategies to evaluate initial and current conditions in historical constructions: a test case in the church of San Lorenzo (Zamora, Spain).* Published in Remote Sensing Journal, indexed and placed in the Q1. It ranked the fifth position out of twenty eight journals, in terms of impact factor. DOI: 10.3390/rs8010060.

- The book chapter: *Practical use of multispectral techniques for the detection of pathologies in constructions (*Accepted for publication*). It reached the sixth place out of seventy five editorials (First Decile) inside the Engineering & Technology discipline. ISBN: 978-1-138-02810-4.*

Based on the requirements imposed by the University of Salamanca for the presentation of Doctoral Thesis based on a compendium of publications, it is considered that the articles, as well as the additional merits, adjust in an optimal way to said necessities. Therefore the methodologies, results and conclusions shown in this document have been validated.

The results thrown during the elaboration of this Doctoral Thesis, have made relevant advances in different engineering fields (strongly associated with the developed topic): (i) the use of geomatic approaches in the evaluation of structural damages present in constructions; (ii) the use of dynamic techniques, based on the Operational Modal Analysis, for the calibration and the damage detection; (iii) the development of procedures for the conversion of point clouds, photogrammetric or laser scanner, able to integrate structural pathologies such as cracks or deformations, into *CAD* models for numerical analysis; and (iv) the use of multispectral classification approaches in the detection and quantification of pathologies in structures.

All of this opens new research lines as well as positioning the procedures shown as solid foundations for their further development.

The Doctoral Thesis concludes with the corresponding conclusion chapter in which, in an accurate and specific way, the main contributions made are shown. In this way, this work can be criticized and projected to further developments integrated in the research line.

Signed, to all extent and consequence, in Ávila, April 5 th 2016.

Dr. Diego González Aguilera.

Dr. Belén Riveiro Rodríguez

RESEARCH STAY REPORT

Luís F. Ramos, Assistant Professor from the Civil Engineering Department at University of Minho, Portugal, certifies that Luis Javier Sánchez Aparicio, PhD Student of the Geotechnologies Research and Development doctorate, has undergone a short stay at University of Minho during his pre-doctoral period, with the duration of 3 months at the University of Minho (Portugal), within the Department of Civil Engineering. During his entire stay he has been followed and tutored by me.

During this period of time, the student has carried out research tasks within the field of pathologic analysis of constructions, summarized as follow:

- Full geometric characterization of Saint Torcato church in Guimarães, Portugal, through laser scanner and photogrammetry. CAD model creation and adjustment for its analysis using the finite element method. Definition of a methodology to fully calibrate and afterwards analyze the model.

- Static and dynamic analysis using finite elements of a hybrid footbridge (*GFRP-SFRSCC*) that suffered from cracking. Ensuring robust calibration of the model, as well as its preparation for a possible damage identification analysis.

- Geometric characterization using laser scanner and dynamic test on the main Tower of Guimarães´ Castle (Guimarães, Portugal).

- Geometric characterization using laser scanner, in order to carry out a Tube Jack test on an irregular masonry Wall. Preparation of the procedure that should be followed to analyze the deformations through the Digital Image Correlation (*DIC*).

In conclusion, I express my high appreciation of Luis Javier Sánchez Aparicio´s professional qualities, his commitment and capacity to carry out high quality and independent research work, besides his ability to fruitfully collaborate with different people and other fields of knowledge, and his high communication skills.

University of Minho, July 30, 2014.

Dr. Luís F. Ramos.

ACKNOWLEDGEMENTS

I may be one of those who think that nothing appears suddenly out of nothing, *Ex nihilo nihil fit*, and that is why the conclusion of the ensuing Doctoral Thesis has been a series of events that were pre-destined to happen. That is why it would be an arduous task to recognize all of those who have influenced on those events at a certain moment. Nevertheless, amidst this vast collective, there are some that stand out for their strong influence and contribution to the Doctoral Thesis, all of whom deserve my deepest gratitude.

Firstly I wish to acknowledge my parents, for their unrelenting determination and sacrifice to provide a thorough academic education for my sister and me, even during hard times, have made it possible. Just as well, I wish to thank Maria, my sister, and Paloma for their constant support during the entire phase. It proved to be very strong during complicated moments, allowing me to continue striving to conclude the Doctoral Thesis.

To Doctors Diego González Aguilera and Belén Riveiro Rodríguez, my tutors, for their adamant and unconditional support, patience and dedication. To Doctor Luís F. Ramos, my tutor during my stay at the University of Minho (Portugal), for his spirit, dedication and concern. Among many other things, I will remember our intense and productive scientific conversations. I would like to thank my *TIDOP* research group colleagues from the University of Salamanca, for the opportunity to exchange experiences, knowledge and the chance to work alongside with them.

Luis Javier Sánchez Aparicio

SUMMARY

It seems inevitable to confirm the steady improvement of materials and construction techniques in the field of civil engineering. The evolution from stones and bricks in masonry walls to self-compacting concretes reinforced with steel fibers or extruded polymers is enormous. However, it is important to remember that, similar to any living being, these construction methods are not impervious to pathological processes. Though their relevance and importance differ greatly depending on the material and the kind of pathological process, they should not be overlooked, since they will influence directly the construction's life span.

Driven by the latter, this Doctoral Thesis focuses on the development of methodologies and solutions that detect, evaluate, materialize and even foresee the pathological conditions which downgrade the bearing capacity of constructions. It endorses as well, global detection and damage assessment methodologies based on geomatics (through the use of laser-scanner and photogrammetric systems) and structure-dynamics (through the Operational Modal Analysis).

In order to corroborate the applicability of the developed procedures, these have been applied in various construction types: ranging from historical buildings, vernacular architecture or buildings in an experimental phase, to "modern" constructions erected with reinforced concrete.

The obtained results lead to the conclusion that the sensors that have been used, as well as the techniques and methodologies that were developed, have earned an essential role in the structural evaluation of constructions. Laser-scanner and photogrammetric systems are capable of providing "plentiful" products in terms of geometric and radiometric qualities. Nevertheless, they require complementary methods in order to mechanically materialize possible building damage (except for the results provided by strategies based on Digital Image Correlation). This need is met using

structure dynamic-based techniques, specifically the Operational Modal Analysis, and the Finite Element Method. Said disciplines offer a wide range of possibilities for quantifying and detecting structural pathologies in constructions.

RESUMEN

Resulta inevitable corroborar el constante avance y perfeccionamiento en el uso de materiales y técnicas constructivas en el campo de la ingeniería civil. Desde el empleo de rocas y ladrillos en mamposterías, hasta hormigones autocompactantes reforzados con fibras de acero o polímetros extruidos. Sin embargo no ha de olvidarse, que al igual que ocurre durante el transcurso vital de cualquier ser vivo, todas estas soluciones constructivas no quedan exentas de procesos patológicos. Que si bien, adquieren importancias diferentes según el tipo de proceso y material afectado, no han de pasarse por alto, condicionando consigo la vida útil de las propias construcciones.

Motivado por ello, la presente Tesis Doctoral centra sus esfuerzos en el desarrollo de metodologías y soluciones, capaces de localizar, evaluar, materializar e incluso predecir aquellas afecciones patológicas que degraden la capacidad portante de las construcciones. Abogando consigo por metodologías globales de detección y cuantificación de daños basadas en las disciplinas de la geomática (a través del empleo de sistemas láser escáner y fotogramétricos) y la dinámica de estructuras (mediante el método de Análisis Modal Operacional).

Con el fin de corroborar la aplicabilidad de los procedimientos desarrollados, estos son empleados en diferentes tipos de construcciones: desde construcciones históricas y vernáculas o en fase experimental hasta construcciones "modernas" erigidas en hormigón armado.

A raíz de los resultados arrojados se concluye que los sensores empleados, así como las técnicas y metodologías desarrolladas, adquieren un protagonismo esencial en el conocimiento estructural de las construcciones. Por un lado, los sistemas láser escáner y fotogramétricos son capaces de suministrar productos "*ricos*" en cualidades geométricas y radiométricas. Sin embargo, requieren de metodologías complementarias para materializar mecánicamente (a excepción de los resultados

provistos por las estrategias basadas en Correlación Digital de Imágenes) posibles afecciones patológicas. La respuesta a dicha necesidad puede ser encontrada en el empleo de las técnicas basadas en la dinámica de estructuras, más concretamente en el Análisis Modal Operacional, y el Método de los Elementos Finitos. El empleo de ambas técnicas ofrece por ende un amplio espectro de posibilidades sobre el cual cuantificar y caracterizar los daños presentes en las construcciones.

Nature, to be commanded, must be obeyed.

Francis Bacon (1605)

TABLE OF CONTENTS

Introduction.....1
Focus of the Thesis.....13
Chapter I: The combination of geomatic approaches and operational modal analysis to improve the calibration of finite element models: a case of study in saint torcato church (guimarães, Portugal). 15
Chapter II: Experimental and numerical approaches for structural assessment in new footbridge designs (SFRSCC-GFPR hybrid structure).....29
Chapter III: Photogrammetric, geometrical and numerical strategies to evaluate initial and current conditions in historical constructions: a test case in the church of San Lorenzo (Zamora, Spain).....42
Chapter IV: Practical use of multispectral techniques for the detection of pathologies in constructions.....65
Chapter V: Conclusions and Future Research Topics.....87
References.....95
Annex I: Enchance your Finite Element Models software.....101
Annex II: Quality Description of the articles published.....107

INTRODUCTION

It is undeniable that a construction's success is greatly based on the constant development in the use of materials and construction techniques, especially in terms of its useful life. They range from solutions that are highly embedded in society, based on the use of walls, arches and lintels that are in turn built in stone masonry, brick or adobe, to innovative structural systems which include the use of polymers or fabrics as resistant materials in self-compacting concrete panels.

However, it is well known that the service loads, environmental actions or accidents may damage those structural systems, therefore decreasing their performance and bearing capacity. Considering the latter, damage can be defined as the undesirable weaknesses of a structural system that risks its safety and performance (Stubbs, 1985). Such weakness, commonly known as the pathological process, can be reflected among other symptoms on cracks, delaminations, bulging or corrosion, depending on the type of the building (Watt, 1999).

In terms of scale, the damage begins at material level, which generally does not imply a total loss of system functionality, but rather that the system is no longer operating in optimal conditions. If this damage is not properly treated, it can grow at different levels (length-scale and time-scale levels) (Farrar & Worden, 2007) and can affect the structural behavior to a point that is not acceptable: the structural failure. For this reason, it is necessary to have systems that are capable of detecting and diagnosing the damages present in structures, with the aim of designing adequate maintenance and renovation

plans that protect the useful life of the constructions.

It is in these systems, where processes focused on the evaluation of the structure's conditions become essential. These processes, commonly known as Structural Health Monitoring (*SHM*) (Worden & Barton, 2004), assume that a current structural damage is closely linked to a temporal factor and affect adversely the useful life of engineering structures (Liang & Yuan, 2015; Lorenzoni et al., 2013; Luís F. Ramos et al., 2010). Therefore, the definition of damage will be limited to variations on the material and/or geometric properties of these structures, including, changes to the boundary conditions and connections, which adversely affect the current or future behavior of the structural system (Farrar & Worden, 2007).

In a first instance, it is possible to classify the *SHM* processes based on their performance capability, as local or global systems (Housner et al., 1997). On one hand, the local methods (such as x-rays, acoustic methods, magnetic or ultrasonic rays) concentrate on a part of the structure and are usually considered to be more sensitive than the global methods. Requiring a prior knowledge of the location of the damaged area. On the other hand, the global strategies (which have less diversity than the local ones) are able to detect those damages that significantly contribute to the global integrity of the structure (Haque et al., 2012).

However, this local/global classification refers solely to purely "*spatial*" criteria which require of complementary levels that evaluate the capacities of damage characterization. On this premise, the classification initially defined by (Rytter, 1993) and later modified by (Worden & Dulieu-Barton, 2004) and by (Yan et al., 2007) provides a valid catalogue on which to analyze the performance of the available methodologies. The classification follows the different levels listed below:

- Level 1 or Detection: includes methods which provide qualitative indicators of the current damage.

- Level 2 or Localization: comprises those strategies which provide information regarding the probable position of the damage.

- Level 3 or Classification: includes procedures that differentiate the type of pathological condition.

- Level 4 or Evaluation: comprehends methodologies through which the area affected by the damage in the construction can be estimated.

- Level 5 or Prediction: composed of the methods which offer information about the safety condition of the structure, and therefore estimate the residual useful life of the construction.

It is noteworthy that there is a hierarchical interconnection between each level. This means that, for example, systems which provide level 3 information intrinsically contain level 1 and level 2 information.

A wide range of nondestructive testing techniques can be used for damage identification purposes. The majority of these procedures can only be applied when the structure is not in operation. Consequently, only a few of these techniques are suitable to be applied in the *SHM* environment. The dynamic-based technique is of greater interest inside this field, in comparison to the quasi-static techniques, which presents a lower sensitivity to damage. This fact positions the dinamic-based tehcnique strategies as the preferred ones. This is due to the fact that they offer a solution capable of evaluating the structural conditions, assess the present damage, and monitor its development (Peeters & De-Roeck, 2001; Ramos, 2007).

In parallel to the classification methods described above, a third classification approach acquires great relevance: model and non-model based strategies. In a non-model based method, the results are compared with the results of a reference state, using as damage detectors the deviances in the certain parameters (wavelet analysis, changes of modal

parameters or changes in derivates of modal parameters) (Ramos, 2007). Furthermore, in a model based technique the response is compared with some form of numerical model, usually a Finite Element Model. This strategy allows a damage assessment up to level 3, according with the Rytter classification, in accordance with another basic pillar in damage detection: damage prognosis. Damage prognosis estimates the remaining useful life of a system (Farrar et al., 2003). This estimation is based on the results provided by predictive models of the current state for which the variables and the damage acting on the structural system need to be correctly defined.

Finite Elements (Zienkiewicz & Taylor, 1994) have been given most of the scientific attention (Saloustros et al., 2015; Adewole & Bull, 2013). These numeric methodologies, unlike the more traditional computation strategies, such as the graphic statics (Huerta, 2008) or the limit analysis (Heyman, 1997), have been positioned as strong solutions to different engineering needs. They allow the evaluation of the structure under study in different situations: dynamic analysis (Ramos et al., 2013), seismic (Milani & Valente, 2015) or static conditions (Gonilha et al., 2014), among others. In contrast to this flexibility, such procedure of numerical evaluation requires extensive knowledge of the intervening variables, in particular, the boundary conditions and mechanical properties of the constituent materials. At this point, the structure dynamics and especially the Operational Modal Analysis (*OMA*) are ranked as one of the preferred complementary techniques (Osmancikli et al. 2015; Türker & Bayraktar, 2014; Ramos et al., 2013). However, this is not the only requirement to obtain adequate numerical simulations in constructions; the calibration of its response (variables, boundary conditions, etc.) and the correct geometrical definition are also critical aspects (Mottershead & Friswell, 1993) for which the disciplines of model updating and geomatics can provide the solution.

On one hand, model updating techniques are focused on the calibration of the system´s different unknown properties which appear as parameters in the numerical model (Simoen et al., 2015), with the aim to minimize the discrepancies between the numerical simulation and the experimental data (observed behavior). A wide number of model updating

techniques have been used in reference text from the approach defined by (Douglas & Reid, 1982) to more complex techniques such as those exposed by (Simoen et al., 2015). They share common aspects in the operational frame: (i) an objective function to be minimized; (ii) the constrain problem; and (iii) the needen of an optimization process.

On the other hand, geomatics are mainly focused on the geometrical definition of the building. This aspect, particularly important in historic constructions, is a relevant topic in the International Scientific Community, positioning these sensors (mainly the laser scanner and the digital cameras) as the most appropriate non-destructive techniques for the geometrical characterization (Conde et al., 2015; Villarino et al., 2014; Riveiro et al., 2011). These sensors are capable of providing a tridimensional, dense and accurate representation of the building, the point cloud. Nevertheless this product, composed by millions of points in a reference space, does not combine directly with the Finite Element Method, since this approach requires a transition between the point cloud to *CAD* models. However, the complexity of this transition is a hot topic in the Scientific Community, limiting the use of this point cloud as a geometric base on which performs simple strategies are performed to construct the *CAD* model manually following two basic approaches (Tognaccini, 2009): (i) orthogonal views; and (ii) sections applied along the main directions and over the mesh. Parallel to these basic approaches, which do not tap the geometrical potentialities offered by these sensors, other types of solutions emerged which exploit the concept of parametric surfaces (planes, cylinders, etc.) (Cabaleiro et al.,2014; Varady, 2008), Non-Rational Uniform B-Splines *(NURBs*) (Piegl & Tiller, 2012) and the voxel approaches (Castellazzi et al., 2015). Beyond the eminently geometrical product provided by the laser scanner or the photogrammetry, the radiometric values of these products, point clouds or images, can provide interesting solutions for the damage detection and quantification.

One of the main applications of the remote sensing field has been the classification of land and terrain from remotely sensed images (Del Pozo et al., 2015; Moody et al., 2014; Pope & Rees, 2014). This approach, commonly known as multispectral classification, assigns

pixels (understanding these as the basic unit of an image) with the same radiometric properties to classes. Said classification capacity allows the use of different bands and sensors (acting on different spectrums) to enhance the extraction of different informational classes. This proves particularly interesting in the detection of pathologies in constructions (Armesto et al., 2010). Besides these properties, the capacity to acquire different images along a period of time and the quantification capacity of this technique can place this solution as a potential global method for damage identification and as a complementary solution for *SHM*.

Nevertheless, the concept of multispectral classification does not acquire a full value in detecting and monitoring pathologies without the presence of the so-called classification algorithms. The two most popular approaches in the classification of multispectral images are divided into (Li et al., 2014): (i) supervised; and (ii) non-supervised classification systems. While the supervised classification systems requires the user´s interaction, assigning training areas of the informational classes to train the system for clustering, the unsupervised classification approach only requires the radiometric information provided by the different image bands without any interaction with the user.

It seems therefore logical, considering the descriptions and classifications mentioned above, that a complete description of damages requires the use of multidisciplinary techniques that are not only able of quantifying and locating the damage, but also have sufficient operating capacity to predict the subsequent behavior (damage prognosis). Consequently, this Doctoral Thesis supports the use of techniques that derive from structure dynamics (through the *OMA*), sensors, and geomatic techniques (laser scanner and photogrammetric systems) as well as tools for image classification (multispectral classifiers), as systems of damage characterization at a global level. All this, without forgetting the support of advanced techniques of numerical Finite Element Analysis and calibration methodologies (model-based methods) that allow to achieve the predictive capacity in the buildings evaluated.

According with these basic operational pillars, the subsequent Chapters (I-IV) presented in this Doctoral Thesis will describe the research activity carried out in the different fields described above: (i) Chapter I geometrical characterization, dynamic identification and model updating; (ii) Chapter II: dynamic identification and model updating; (iii) Chapter III: geometrical characterization and model updating and; (iv) Chapter IV: multispectral analysis.

Once the fields needed for damage identification at global level have been defined, it is necessary to establish a general framework in which the different approaches may be considered. This would enable their integration and futher improvements. To this end, Chapter I (which corresponds to the first publication), develops this integration (except for the multispectral analysis) under a common framework: a historic building with severe damages, considering the numerical simulation of the building as a link.

Without any doubt, the terrestrial laser scanner and photogrammetric (through the Structure from Motion approach or *SfM*) systems have earned great relevance in the geometrical characterization of buildings (Conde et al., 2015, Villarino et al., 2014, Barazzetti et al.,2010). Nevertheless, both terrestrial systems have as main disadvantage the impossibility of acquiring data in areas of difficult access (e.g. roofs, domes or towers) which makes it a requirement to have complementary technologies that solve this problem. It is in this field and due to the flexibility of the photogrammetric sensor itself (in its different versions RGB, multispectral, etc.), where the photogrammetry-*UAV* (Unmanned Aerial Vehicle) has been the ideal solution (Del Pozo et al., 2014; Scaioni et al., 2009).

In other words, the combination of laser scanner and *SfM* (in its terrestrial and aerial versions) seems to be the optimal solution for a complete characterization of complex buildings. However, the need to use several stations, materialized by different point clouds, requires of these entities to be introduced into a common framework. It is in this field where algorithms such as Iterative Closest Points (Besl & McKay, 1992) or Least Square

Surface Matching (Acka & Gruen, 2007) can be used. Nevertheless the registration carried out by these algorithms leads to an error accumulation that needs to be compensated. Algorithms like the Generalized Procrustes Analysis (Toldo et al., 2010) can address this problem and provide the solution.

As mentioned above, the conversion of point clouds into *CAD* models is not a trivial task. Nowadays the common practices are focused on the use of sections, orthogonal views or manual segmentations of the point cloud, not taking the advantages offered by point clouds. Parallel to these strategies, emerge new procedures that can be placed as possible solutions in the conversion to *CAD* models, such as the Functionally Decomposition (Varady, 2008) or NURBs modeling through mesh quadrilaterization (Branch et al., 2008).

Once the geometrical model is generated (and adapted for the subsequent numerical simulation) and its damage is mapped, a correct interpretation of the different variables acting on the numerical model is needed. Here, is where the *OMA* and the calibration of the numerical model become essential.

From the different available possibilities for in-situ testing, one of the most used techniques is the experimental modal identification. More specifically the *OMA*, also known as ambient modal identification, aims to extract the different modal parameters related to the structure (such as frequencies, modal shapes or damping ratios) without an initial excitation or known artificial excitation. This technique includes different methods, focused on the extraction of these variables, (Ramos, 2007): (i) frequency domain such as the Peak Piking or the Enhanced Frequency Domain Decomposition; and (ii) time domain such as the Maximum Likelihood Method or the Stochastic Subspace Identification Method. This method can be amplified with the use of calibration methods, using the modal parameters extracted as ground truth.

The widely used, Douglas-Reid method (Douglas & Reid, 1982) allows the calibration of numerical models (Zordan et al.,2014; Gentile & Saisi,2007). This method minimizes the differences between the numerical model and the experimental variables, requiring only

the resolution of a non-linear equation system and the minimization of an objective function.

It is noteworthy, that the above mentioned chapter addresses the issue of the damage (cracking) from a discrete point of view, considering the damage as a discontinuity in the structure and thus requiring a specific definition of the crack on the numerical model. This results in the need to develop methodologies that are based on the diffuse damage model (De Borst et al., 2004), which are able to detect and quantify the damage without having to materialize the existing pathologies in any specific way (based on a discrete damage model). Moreover, they serve as systems for the precise localization of damage.

Also to note is the applied calibration system. It is based on the "*simplistic*" approach provided by (Douglas & Reid, 1982), whose work structure restricts the calibration to a dynamic scope. It is therefore necessary to move towards robust optimization strategies capable of including on their work structure minimization objective functions (understanding them residual functions which express the discrepancies between the experimental and numerical data) able to work with static components such as deformations.

In response to the aforementioned, the second article presented in this Doctoral Thesis, which is shown as Chapter II, develops a system of robust calibration for numeric models which is able to integrate static and dynamic parameters within a Deterministic structure. This structure considers the model as a conjunct of known or assumed properties which have a relation with the output variables (Simoen et al., 2015). Considering this, the Deterministic model update consists in the determination of the optimal set of variables that act on the system and minimizes the discrepancies between some of the experimental data and the model prediction. This set of variables needs to be constrained, depending on the information that is available from the updating parameters.

Once the general concept of the Deterministic approaches is defined, it seems be logical to assume the possibility to integrate the structure´s present damage as variations of the

mechanical variables that act on it. According with to the previous definition of damage: "*Therefore, the definition of damage will be limited to variations on the material and/or geometric properties of these structures. Including, changes to the boundary conditions and connections, which adversely affect the current or future behavior of the structural system*", adjusting the mechanical values of all elements results in a large number of variables to be optimized, which leads to ill-conditioned problems, on which the Hessian matrix becomes near-singular and difficult to invert accurately. This situation does not guarantee the uniqueness and the stability (concerning to small changes in the variables) of the system, which can be solved through regularization techniques (Titurus & Friswell, 2008) that try to replace the ill-conditioned problem with a well-conditioned one that produces a similar solution. But although this optimization can be solved, two drawbacks need to be considered: (i) the evaluation of a large sensitivity matrix which results in a time consuming problem; and (ii) the non-continuous damage assumption. Taking this into account, Chapter II uses the damage function concept, initially defined by (Teughels& De Roeck, 2003), as a starting point. Taking this approach in consideration, a hybrid system of damage detection and identification has been developed which combines discrete functions and sub-structuring systems under one single operational framework.

As of today, it is inevitable to highlight the importance acquired by the systems of dynamic analysis of structures in the evaluation of their health. The relevance of these systems lies in these techniques' ability to detect and monitor damage (Ramos et al., 2013; Teughels & De Roeck, 2003). They result in a wide variety of methodologies (Rainieri & Fabbrocino, 2014) and indicators (Dong et al., 1994; Stubbs et al., 1992; Pandey et al., 1991) as well, some of which are able of operating jointly with numerical simulations by Finite Elements in order to obtain more robust results (Zordan et al., 2014).

However, and parallel to the mentioned developments in the field of dynamics, emerges the need for indicators that provide equitable values in the field of statics. Although there are several studies that use static data from experimental campaigns (such as the research activity developed in Chapter II), they acquire a purely local character due to the fact that

they derive from punctual data of the structure (Solis et al., 2013).

Inspired by this need, Chapter III introduces two novel parameters of geometric quality. Such indicators, namely the Global Metric Hausdorff (GHm_s) and the Local Metric Hausdorff (GHm_s), which come from the Symmetrical Hausdorff Distance (Hausdorff, 2008), support the large amount of geometric data provided by the geomatic systems, in order to be used in the calibration of numeric models.

Parallel to the above, and considering the importance of the geometry in a correct numerical simulation, Chapter III improves the geometrical strategy developed in the first chapter, based on the Morse theory (Varady, 2008) as a clustering strategy and the parametric fitting of surfaces (based on standard procedures used in reverse engineering), with the inclusion of the non-parametric surfaces called *NURBs* (Piegl & Tiller, 2012). *NURBs* can be considered as high level surface primitives, characterized by their ease of use and their ability to deal with complex surfaces. However these types of surface representations require quadrilateral patches for a correct representation. In this context, the Morse theory and the Spectral analysis of the mesh can provide the solution (Branch et al., 2008): a quadrilaterization of the triangular mesh, on which the *NURBs* approach is applied. According to this, Chapter III considers the work developed by (Branch et al., 2008) and includes algorithms for the generation of manifold meshes (meshes with natural shapes, without degeneration or intersection between elements) (Attene, 2010), strategies developed in Chapter I and the consideration of different pathological processes, such as cracks (as discrete discontinuities in the structural system) and lack of material.

Although at this point it has been possible to address those pathological processes with a stronger relation to the geometric aspects (cracks, distortions or lack of material) we must not forget the existence of certain conditions of great relevance in the behavior of the materials, namely: (i) the existence of biological activity (fungi, algae, etc.); (ii) geological landmarks that determine the mineral composition of stone materials; (iii) the existence of moisture that can cause corrosion processes on reinforced concrete. In order to increase

the value added by the sensors employed on this Doctoral Thesis, multispectral techniques have been proposed in **Chapter IV** as suitable systems for the detection of damage caused by biological activity, humidity, or geological characteristics. However, whilst the concept of the multispectral image implies one image captured through one single sensor (multispectral camera) (Campbell, 2002), this Doctoral Thesis presents the multispectral image as the registration of various geomatic sensors that work in different wavelengths (e.g. RGB camera, infrared or laser scanner). Complementary to this, the use of statistical indicators, such as the confusion matrix, Cohen´s Kappa, or the overall global and user accuracy (Armesto et al., 2010), can show the robustness and quality of the classification made. It is possible to have a system that is suitable for the characterization of the above mentioned pathologies by exploiting, on one hand, the flexibility and the work capacity of large areas of the geomatics sensors and, on the other hand, the other concepts described above. As a result **Chapter IV** shows the practical application of the concepts of multispectral image classification in the evaluation and pathological monitoring of structures. This application is focused on three case studies which include pathological processes with close relation to the building's structure: (i) probable corrosion due to concrete carbonation and efflorescence in concrete bridges; (ii) biological activity (lichen, algae and plants) in historical buildings and; (iii) characterization of the granite of Avila, a special case of altered-facie granite which mechanical properties (frost resistance, bending and compressive strength) are inferior to non-altered granite (García-Talegón et al., 1993).

FOCUS OF THE THESIS

Considering the basic pillars, described in the Introduction, for a successful damage identification at global level, this Doctoral Thesis has been constructed under the following objectives:

I. Evaluation of the applicability of geomatic sensors (Terrestrial Laser Scanner and digital cameras) in buildings with structural damages.

II. Development of modeling strategies and construction of *CAD* models on structures with pathological processes with a clear geometric component (deformations and cracks), suitable for its subsequent numerical analysis.

III. The use of structures' dynamic evaluation strategies based on Operational Modal Analysis (OMA) in the evaluation of damage.

IV. Application and development of methodologies of robust calibration of numeric models, able to locate and interpret the core damage present in buildings, using the above-mentioned techniques.

V. Application of techniques for the analysis of multispectral images in the extraction and quantification of pathologies with an eminently radiometric component (e.g. characterization of materials, humidity in concrete, biological attacks, etc.) that show a close connection with the stability and the useful life of constructions.

In more practical terms and concerning their reach, the sensors used as well as the developed methodologies have been tested in different types of damaged buildings: from historical and vernacular architecture, to reinforced concrete constructions and constructive solutions in an experimental phase.

Chapter I

The combination of geomatic approaches and operational modal analysis to improve the calibration of finite element models: a case of study in saint torcato church (guimarães, Portugal).

Construction and Building Materials 70 (2014) 118–129

Contents lists available at ScienceDirect

Construction and Building Materials

journal homepage: www.elsevier.com/locate/conbuildmat

The combination of geomatic approaches and operational modal analysis to improve calibration of finite element models: A case of study in Saint Torcato Church (Guimarães, Portugal)

Luis Javier Sánchez-Aparicio [a,*], Belén Riveiro [b,2], Diego González-Aguilera [a,1], Luís F. Ramos [c,3]

[a] Department of Land and Cartographic Engineering, University of Salamanca, High Polytechnic School of Avila, Hornos Caleros 50, 05003 Avila, Spain
[b] Department of Material Engineering, Applied Mechanics and Construction, School of Industrial Engineering, University of Vigo, Vigo, Spain
[c] ISISE, Department of Civil Engineering, University of Minho, Guimarães, Portugal

HIGHLIGHTS

- Numerical study applied to historical building with non-intrusive sensors.
- Structure from Motion, allows generating realistic and complete 3D models.
- The methodology presented transforms the data from geotechnologies into CAD models.
- Operational modal analysis for finite element model calibration.
- Modelled features from Structure from Motion can improve the dynamical response.

ARTICLE INFO

Article history:
Received 4 April 2014
Received in revised form 27 June 2014
Accepted 23 July 2014
Available online 20 August 2014

Keywords:
Structure from Motion
Laser scanner surveying
Finite element model
Modal updating
Masonry structures
Orthoimage
Damage survey
CAD modeling

ABSTRACT

This paper present a set of procedures based on laser scanning, photogrammetry (Structure from Motion) and operational modal analysis in order to obtain accurate numeric models which allows identifying architectural complications that arise in historical buildings. In addition, the method includes tools that facilitate building-damage monitoring tasks. All of these aimed to obtain robust basis for numerical analysis of the actual behavior and monitoring task.

This case study seeks to validate said methodologies, using as an example the case of Saint Torcato Church, located in Guimães, Portugal.

1. Introduction

The conservation of historic buildings requires understanding their structural behavior, and consequently: (i) their boundary conditions, (ii) the characteristics of the constitutive materials (iii) the origin of the damage that the building suffers and (iv) their vulnerability [1]. Therefore the creation of accurate numerical models is imperative in order to obtain adequate restoration systems.

Masonry walls are very common in the vast majority of existing monuments. Cracked elements, associated with different events (settlements and/or excessive displacement loadings) are a common problem that reduces the service life of these structures [2]. The fracture phenomena (cracks) are caused by the masonry's high brittleness to tensile stresses. Furthermore, the structural behavior is highly dependent of the structural geometry. This is why four conditions are required to carried out proper analysis: (i) having a complete and accurate geometric characterization of the structure; (ii) knowing the material's mechanical properties (iii) characterizing all the loads acting in the structure; and (iv) providing

Abbreviations: UAV, Unmanned Aerial Vehicle; SfM, Structure from Motion; PW, Photogrammetry Workbench; MAC, Modal Assurance Criterion; DR, Douglas–Reid Method; ICP, Iterative Closest Point; NURBS, Non-Uniform Rational B-Splines.

* Corresponding author. Tel.: +34 920353500; fax: +34 920353501.
E-mail addresses: luisj@usal.es (L.J. Sánchez-Aparicio), lramos@civil.uminho.pt (L.F. Ramos).
[1] Tel.: +34 920353500; fax: +34 920353501.
[2] Tel.: +34 986 813 661; fax: +34 986 811 924.
[3] Tel.: +351 253510200; fax: +351 253510217.

http://dx.doi.org/10.1016/j.conbuildmat.2014.07.106
0950-0618/

numerical models that correctly simulate the characteristic behavior of the structure (non-linear material behavior, ground settlement, contact between bricks, etc.).

Modern restoration techniques for built heritage are characterized by minimal intervention, compatibility, durability and reversibility [3]. Identifying and to monitoring the pathological condition of the building plays a key role in understanding the current behavior of the structure and the choice of restoration methods to be accomplished [4].

Traditional measuring methods often had a significant dependence of the worker's skills and they normally have associated high time cost. These methods were replaced by direct interpretations done over the building plans (design models) [5–7]. The constant progress of the numeric method of finite elements and computer processing allows the generation of increasingly complex geometric models; that is why it is more and more imperative the necessity of relying on sensors capable to provide massive detailed data and features for the model. Is in this field where geomatic sensors like terrestrial laser scanner [8,9] or digital camera [10] have acquired important roles, due to the capacity of acquire accurate geometrical information needed by the numerical models.

In the present paper, the proposed methodology for data acquisition combines and enhances the laser scanning and digital camera system providing, beside the characteristics defined above, the versatility of adaptation to different infrastructures. All of this within a single application, a hybrid point-cloud, which greatly eases the preparation of geometrically precise numerical models that also serve as a basis for the monitoring of the structure through the analysis of, either the point-cloud or by the analysis of the obtained orthoimages.

The paper relies on the application of the proposed methodology on a case study, St. Torcato Church, close to the city of Guimarães, Portugal [1]. This historical construction has moderate to severe damage and needs to be strengthened. The methodology has been carried out to upgrade and calibrate the finite element model using a global dynamic identification, including crack and geometric improvement, in order to complement with the static and dynamic monitoring system and a future numerical analysis. All this will be made in order to obtain the current stress state of the building and asses the effectiveness of subsequent restoration mechanism that aims at stabilizing the damage.

Within this context, this article attempts to demonstrate a methodology for data acquisition and processing and it is organized in the following way: Section 1 is the introduction; Section 2 presents the instruments for data acquisition which are the laser scanner and the set formed by the UAV and digital camera; Section 3 wherein the methodology for obtaining the hybrid point-cloud and the calibration of the model is shown; Section 4 the data obtained by the laser scanner and the digital camera sensors is analyzed separately, for the presented case study and for the potential of the hybrid point-cloud (this applies not only to the numerical finite-element analysis but also to damage analysis monitoring); and finally in Section 5, the conclusions are drawn.

2. Materials and methods

As described in Section 1, the aim of this methodology is to generate precise finite-element numerical models for subsequent structural analysis. These must be precise, in terms of geometry accuracy and they must contain the necessary data to monitor and track the evolution of damages in the structure. All this within an accurate georeferenced framework and with non-intrusive sensors as the main source.

2.1. Laser scanner system: the terrestrial laser scanner

Currently the terrestrial laser scanning system has acquired great relevance by offering a wide range of advantages; one of the greatest one is the acquisition of non-contact three-dimensional geometry of the analyzed surface, preventing any disruption and allows to accurately capture geometry, providing a high density of data (millions of points) [11]. This feature includes that it does no dependency on specific lighting conditions [12]. It is therefore the combination of accuracy, speed and range of measures that has placed the system as the most powerful tool for three-dimensional modeling and reconstruction of monuments [13,14].

In order to establish a valid methodology to make more accurate finite element models, two different laser scanning systems have been analyzed based on different measurement principles (Table 1): (i) Riegl LMS-Z390i based on time of flight principle (ii) Faro Focus 3D based on the phase shift principle. For details on these measurement principles, refer to [15].

2.2. Imaging system: UAV and "Structure from Motion"

While the laser scanning system allows fast capture and processing of data, it has some drawbacks such as the difficulty for transport and the restriction of stationing in certain elevated places inside historic buildings, these places often are critical. Therefore, it is necessary to use additional platforms and sensors capable of providing accurate data from any position; for this the onboard digital camera on an Unmanned Aerial Vehicle (UAV) platform is used (Fig. 1).

The chosen photogrammetric platform was designed by Roca et al. [16]. It is made of aluminum and carbon fiber, and comprises a total of eight MK-3638 SLOW-FLY APC propeller motors controlled by a central 12 × 3.8 Brushless Control V2.0 that can manage separately the rotational speed of each of the motors. All of this provides the system with great stability and robustness against failure in flight.

In addition to this platform, a low-cost sensor, a Canon EOS 450D digital camera that had been previously geometrically calibrated (Table 2), and a Canon EF 20 mm wide-angle lens were assembled. The wide-angle lens is meant to minimize the amount of images taken.

In recent years photogrammetric data processing systems (SfM) have taken a great relevance; they are able to include into their structure the advantages of computer vision (automation and flexibility) and those of photogrammetry (accuracy and reliability) [17] in order to obtain dense three-dimensional models (point clouds) that can compete in accuracy with the laser scanner system [18]. Within this field highlights the Photogrammetry Workbench (PW) software, which implements the "Structure from Motion" system, ensuring automation (in the transformation of 2-D images to 3-D point clouds), flexibility (by allowing work with any type of camera, calibrated and non-calibrated) and quality (to ensure precision and quite acceptable resolutions).

3. Methodology

3.1. Generating the CAD model and its integration with finite elements

The early stage in the laser scanning and the Structure from Motion (SfM) data processing, have been omitted in this article, since our main interest is focused on establishing a robust methodology that serves as a template for subsequent restoration actions. This template will be based on the hybrid point cloud, which comes from the combination of data obtained from laser scanning, the SfM and the analysis of the products that are obtained from them. For more details about SfM flow see either [19].

Also is imperative to building an accurate CAD model which allows us to evaluate the actual behavior of the construction as a basis for the numerical analysis. However, at an early stage, the point cloud provided by the laser scanning and the SfM present superabundant information in different coordinate systems. As a result, this data is not suitable for CAD model building. Following a semi-automatic method that allows adapting the point cloud to an accurate and suitable CAD model for numerical analysis is presented (Fig. 2).

This methodology requires a multi-phase post-processing that involves three main steps: (i) data fusion at the same coordinate system through registration algorithms; (ii) point cloud resampling and (iii) point cloud simplification (removing certain architectural details without relevance) and parameterization for CAD model conversion.

3.1.1. Hybrid point cloud registration

A complete documentation of historical buildings requires the use of multiple point cloud data set. Is a requirement therefore to place all of these point clouds in the same coordinate system in order to be processed together.

Table 1
Comparison of technical specifications between laser scanner system Riegl LMS Z-390i and Faro Focus 3D.

	Riegl LMS Z-390i	Faro Focus 3D
Measurement principle	Time of flight	Phase shift
Wavelength	1550 nm	905 nm
Measurement range	1–400 m	0.6–120 m
Accuracy nominal value	6 mm a 50 m in specific lighting and reflectance conditions	2 mm a 25 m in specific lighting and reflectance conditions
Field of view	360° Horizontal 80° Vertical	360° Horizontal 305° Vertical
Capture rate	11,000 points/s	122,000/976,000 points/s
Beam divergence	0.3 m rad	0.19 m rad

Fig. 1. Image of the UAV platform and the digital camera (left). Image taken during the data collection of the point cloud SfM (right).

Table 2
Canon EOS 450D digital camera geometric calibration settings.

Parameter	Value
Sensor size	$W = 22.2425$ mm $H = 14.8336$ mm
Principal point	$X_p = 10.8716$ mm $Y_p = 7.4449$ mm
Focal length	$f = 20.4222$ mm
Radial distortion	$K_1 = 2.157e{-}004$ mm $K_2 = -4.189e{-}007$ mm $K_3 = 0$ mm
Tangential distortion	$P_1 = 4.321e{-}005$ mm $P_2 = -1.003e{-}005$ mm

The proposed methodology is based on a registration system coarse to fine. In an initial stage a point cloud pair-wise registration is carried out. This step takes as a base the ICP (Iterative Closest Point) algorithm [20], that minimize the difference between two points clouds, requiring a total of $n - 1$ alignments, where n is the number of point clouds.

Using pair-wise registration causes an error propagation along the registration of all the point cloud scans. In order to minimize this error accumulation a global registration, based on Generalized Procrustes Analysis [21], was used considering the pair-wise registration, previously made, as the rough registration needed.

3.1.2. Hybrid point cloud resampling and CAD conversion

Traditionally the step procedure from the raw point cloud to the CAD model could be made through three different approaches [22]: (i) orthogonal views; (ii) sections applied along directions and over the mesh and (iii) Non-Uniform Rational B-Splines (NURBS) generated from the mesh. The two first approaches require a high manual work made by the user, whereas the NURBS approach demands high computational cost.

In this article an alternative and semi-automatic approach is presented, which combines NURBS and parametric shapes approximations with the addition of a segmentation process described below, in order to build a suitable CAD model for structural applications. While NURBS-based method was used for complex shapes like (vault or domes), the parametric-based method was used for the rest of the structure.

Once the registration procedure has been completed, the resulting point cloud needs to be resampled (due to the high amount of data) in order to generate a suitable CAD model for the numerical analysis. In this case several methodologies could be applied based on [23]: (i) Principal Component Analysis; (ii) Quadric-Based Polygonal Surface Simplification; (iii) Clustering methodologies and (iv) Radial Based Function. For the proposed methodology a resampling based on curvature has been applied, in order to decimate flat surfaces without losing detail in features areas. This curvature based resampling follows the next steps: (i) creating a local neighborhood of the analysis point; (ii) local surface based on quadratic approximation and (iii) extraction of the normal and principal curvatures.

After that, the resulting point cloud is meshed, since the majority of segmentation procedures are also performed over meshes. The segmentation process is performed by Functionally Decomposed Surface Models [24]. Once the segmentation is done, the different surfaces created are approximate to NURBS and parametric shapes. As a result a manageable CAD model is generated and could be imported and used for a FEM package.

Additionally to the mentioned above, some relevant features like cracks, can be included into the CAD model that defines more realistically the building's behavior. It is sufficient to extract the area of interest from the point cloud, either SfM or laser, to mesh that area and to incorporate it into the CAD model (Fig. 3).

3.2. Crack recognition and characterization

Digital image analysis is a tool of great potential in the field of pathological characterization of buildings. Several authors demonstrate the feasibility of this analysis to characterize either from the terrestrial laser scanner [25,26] or from the image captured by a digital camera [27,28].

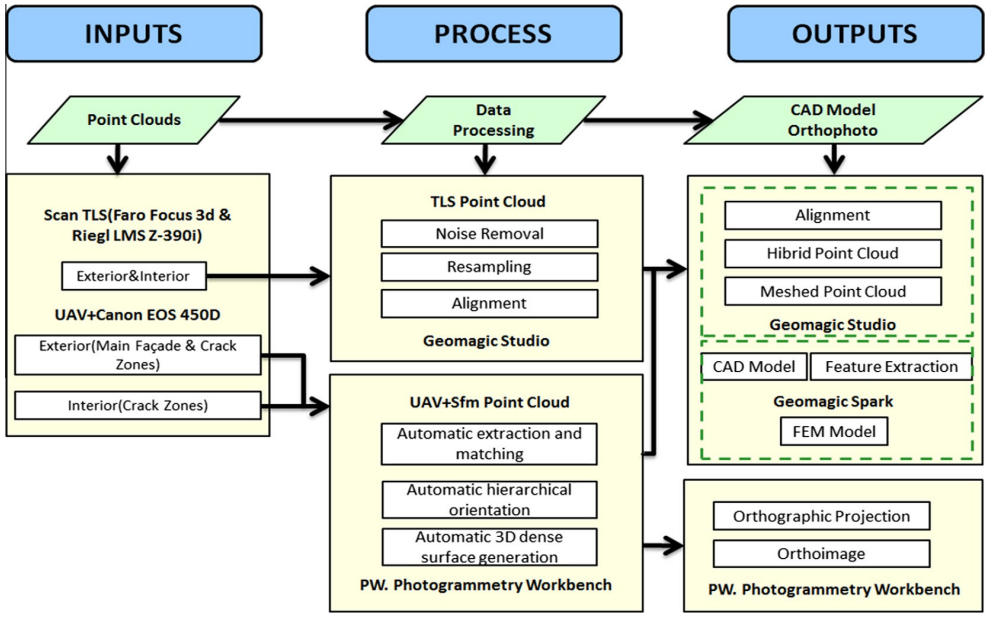

Fig. 2. Workflow for the proposed methodology.

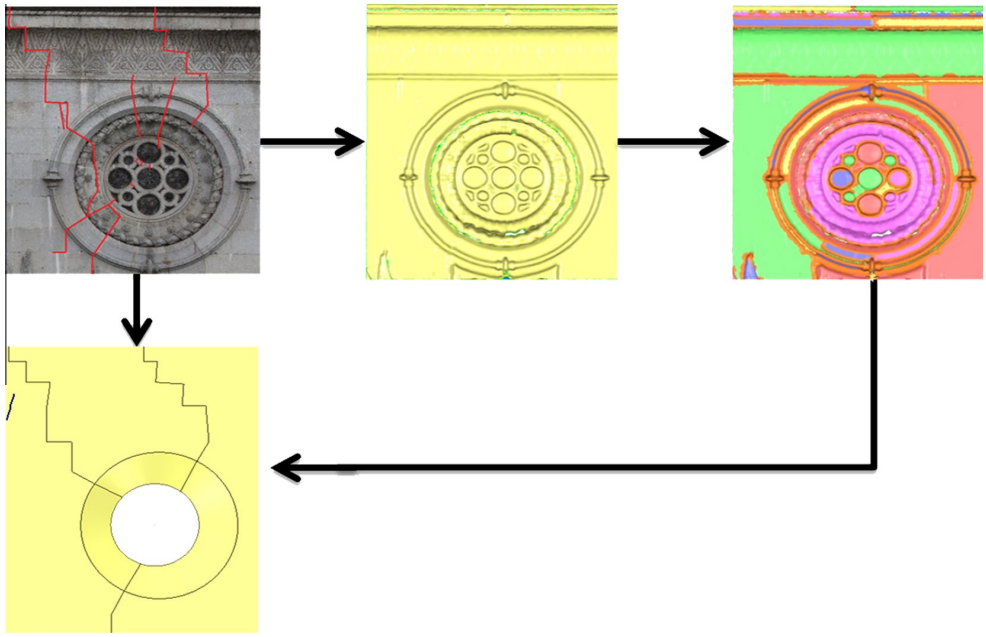

Fig. 3. Graphical description of the proposed methodology. From left to right: point cloud, mesh model, segmentation model, CAD model with major cracks.

Besides offering robust tools for generating three-dimensional models from two-dimensional data (digital image), PW can also obtain orthoimages on specific areas and specific levels, providing the user with precise documentation from anywhere in the building.

Given the high density of points gathered during the three-dimensional reconstruction, the production of orthoimages will require only two points to provide adequate scale, taken from the laser point cloud and a reference plane, in order to run an orthographic projection. The pixel size of this projection is calculated according to the density of the cloud of points, close to the resolution of the initial images [29].

Given the fact that the obtained orthoimage stands as a product without geometric distortions and in real scale, it is sufficient to

directly measure on it and so obtaining crack characterization (length and opening).

3.3. Finite element numerical model

The geometric accuracy and high level of detail provided by the laser scanning systems and Structure from Motion, provide complex CAD models. In order to solve this geometric complexity, for the discretization elements it is required: (i) high flexibility to adapt themselves to the geometry and (ii) great compatibility with automatic meshing algorithms [7]. All this makes the tetrahedral discretization elements with an isoparametric formulation the most suitable for the meshing of complex CAD models.

3.4. Calibration of the finite element numerical model

The analytical results obtained from the calculation model are sensitive to material properties and boundary conditions [30] thus making necessary to gather experimental data to optimize the numerical model.

Among the different possibilities availables today for the implementation of in-situ tests on historic buildings, experimental modal identification is the most popular method [1]. This technique is a non-intrusive system with the capability to identify the global properties of the structure. It allows to obtain vibration frequencies, damping coefficients and mode shape of historic buildings, which may be related to various physical properties (Young modulus, density, stiffness of connections between parts, etc.) which makes possible to validate the analytical models [31].

This publication builds on the data obtained from the accelerometers configuration adopted in 2009. The campaign counted a total of 35 measuring points with 9 sets spread throughout the Church, for more details see [1] (Fig. 4).

The basic objective of these methods is to improve the correlation between the experimental data and those obtained from finite element model, through small changes in a group of model parameters [32]. The criterion often used to assess the correlation is the MAC (Modal Assurance Criterion), this being defined from the following formula (1) [33]:

$$\mathrm{MAC}_{u,d} = \frac{[(\varphi_i^u)^T(\varphi_i^d)]^2}{(\varphi_i^u)^T(\varphi_i^u)(\varphi_i^d)^T(\varphi_i^d)} \tag{1}$$

where φ_i^u y φ_i^d correspond to the mode shape vector on experimental and numerical model respectively for a vibration mode *i*.

As noted above, the goal is to minimize the existing differencies between the experimental behavior and numerical model, considering the experimental values as references. Used in 2007 for the calibration of the numerical model for the Monza Cathedral bell tower [34], the methodology proposed by Douglas–Reid [35] (DR) can be used for calibration of finite element numerical models. This method tries to minimize the difference between theoretical and experimental parameters through the natural frequencies, or another modal parameter, using the following approach:

$$R_i^{\mathrm{FE}}(X_1, X_2, \ldots, X_n) = \sum_{k=1}^{N}[A_{ik}X_k + B_{ik}X_k^2] + C_i \tag{2}$$

To solve these equations, a total of $2n + 1$ values are required to be calculated, taking into account initial values, as well as lower and upper bounds for all updating parameters.

Using the methodology followed by [34], the next step consists of determing the modal frequencies and minimize their difference according to the following objective functions (3) and (4):

$$J = \sum_{i=1}^{m} w\varepsilon \tag{3}$$

$$\varepsilon = f_i^{\mathrm{EXP}} - f_i^{\mathrm{FE}}(X_1, X_2, \ldots, X_n) \tag{4}$$

where *J* is the objective function to be minimized, *w* are the weights considered through engineering criterion and *e* represents the error function (difference between the frequency obtained by operational modal analysis f_i^{OMA} and numerical analysis f_i^{FE}).

The main drawback of this methodology lies in the consideration of a unique modal parameter; frequency. To obtain more

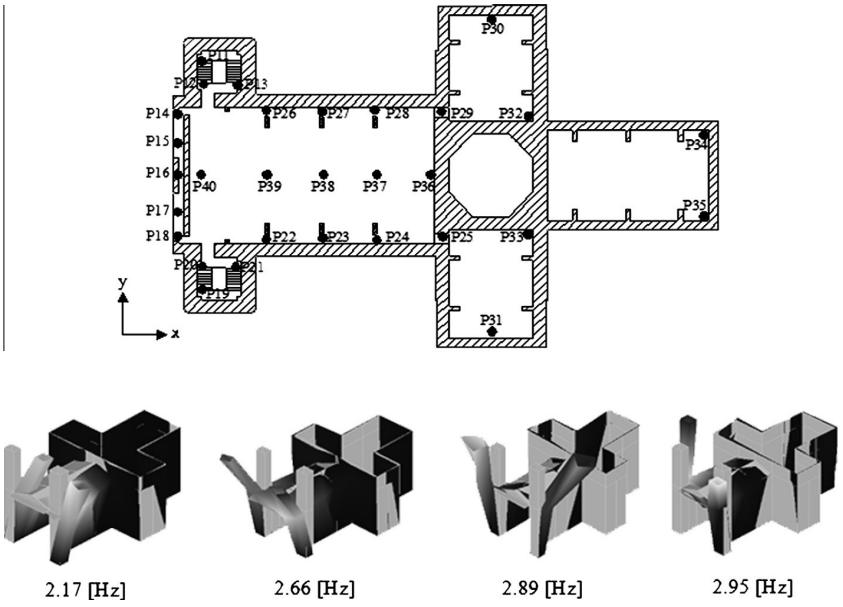

Fig. 4. Scheme of the arrangement of the 35 accelerometers on the Church (above). Mode shape obtained from operational modal analysis (bellow).

accurate results the objective function must be modified, including the MAC values (5):

$$J = 1/2\left[W_f \sum_{i=1}^{m}\left(\frac{f^2_{i,\mathrm{FEM}} - f^2_{i,\mathrm{EXP}}}{f^2_{i,\mathrm{EXP}}}\right)^2 + W_m \sum_{i=1}^{m}(1 - \mathrm{MAC}_{i,\mathrm{FEM}})^2\right] \quad (5)$$

where J is the objective function to be minimized, W_f and W_m are the weights considered for the frequency and vibration modes, f is the frequency and MAC the Modal Assurance Criterion values, both values corresponding to the vibration mode i.

4. Experimental result and discussion

Located in the village of St. Torcato, within the municipality of Guimarães (northern Portugal), the Church of St. Torcato is a clear example of historic building built in stone material, showing moderate-severe structural damage made evident mostly by cracks in its main façade. Starting at the entrance arch keystone, it extends through the rosette to the coronation, splitting this element in two macroblocks [1] (Fig. 5).

Such crack increases the width along its development up to the roof. The movement in opposite directions of the main façade towers due to the settlement suffered by the building is remarkable, as well as some "chrusing" type cracks caused by the compressive stress concentration resulting from eccentric loads originating in the towers.

Built in style "Neo-Manuelinio" the Church of Saint Torcato mix Classics, Gothic, Renaissance and Romanesque elements in its extension [6]. This gives it a special and complex aesthetic that along its length, with a height of about 50 m in the towers, prevents effective tridimensional data capture with laser scanner, topographic techniques or manual measurements [36]. The binomial Structure from Motion and laser scanning is the ideal solution allowing abundant and accurate three-dimensional data capture anywhere in the building.

The results obtained are hereby analyzed independently, according to the source sensor (laser scanner or digital camera) and the resulting numerical model of the combination of these and the calibration using operational modal analysis.

4.1. Terrestrial laser scanner

For the study we have considered the two most popular measuring systems for survey of buildings and civil infrastructures: the laser time of flight and phase difference [25].

Multiple tests have been carried out in the exterior as well as in the interior of the Church. Since the point-cloud is defined by density of points, the acquisition rate and range, the laser scanner LMS Z-390i Riegl (based on time of flight) is considered to be the most suitable for data capture in the exterior. Besides, it has a larger range compared to the Faro Focus 3D laser. Indoors, the data acquisition speed of the Faro Focus 3D scanner (122,000 points/s) compared to the speed of the Riegl LMS laser Z-390i (11,000 points/s), together with its portability proved to be the most important advantages for gathering the data in the interior of the Church.

While in both cases the laser system provides a sufficient and suitable density of points to accurately monitor deformations [37], the amount of data and distinctive features provided might be insufficient of the extraction and monitoring of cracks (for example, it does not record texture) (Fig. 6).

The final model had a total of 29 scans and 267,601,626 points: (i) 14 scans were done of the outside with the Riegl LMS laser Z-390i, (ii) 3 interior shots were taken with the Riegl LMS laser Z-390i and (iii) 12 interior scans were made with the Faro Focus 3D laser. However, the top of the towers and the rooftop of the Church could not be modelled because no suitable location was found for the laser to reach those areas. In addition, the data collection was hampered by additional conditions: the excessive laser beam skew angle on the ledge, top of the towers and the openings between the chapels preventing a complete and accurate characterization of the building and of the critical areas. Thus requiring a complementary technique capable of solving such weaknesses, UAV and SfM.

4.2. UAV and Structure from Motion

The point-clouds collected by laser scanning do not provide a sufficient amount of data for a full geometric characterization of the outer shell: either the distance from scanner to object the range is too large, the point of view is insufficient or the laser system cannot be placed in a certain location, such as in the upper region of the façade beyond the central cornice.

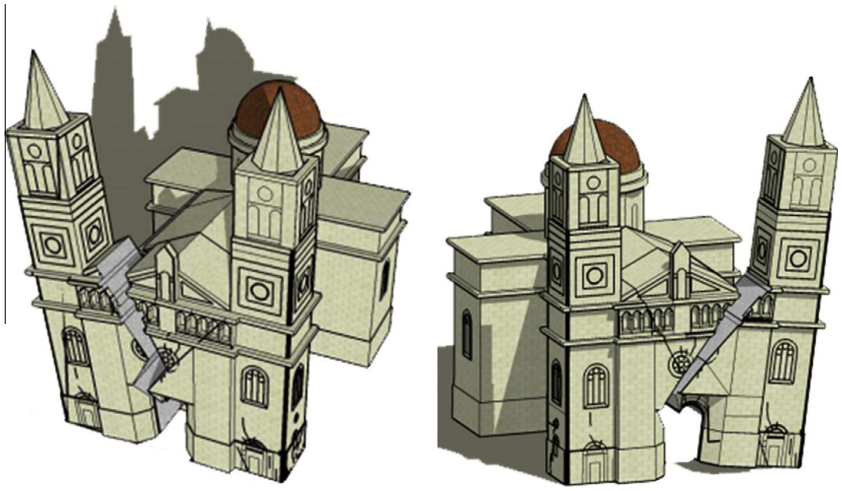

Fig. 5. Representation of the possible structural failure collapse mechanisms of the Church of Saint Torcato. It is possible to observe the formation of two macro-blocks.

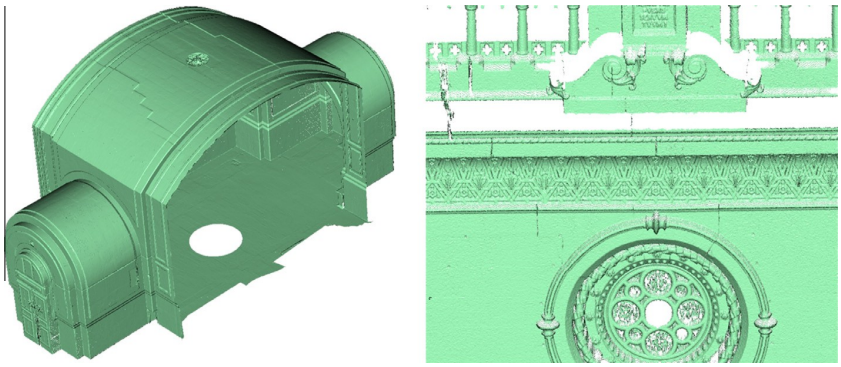

Fig. 6. Settlement of the entrance vault detail (left). Settlement of the entrance vault detail (right).

In addition to the aforementioned, the obliqueness phenomenon must be considered. As shown by authors such as [38,39], this phenomenon is highly correlated with the value of uncertainty in obtaining a point's spatial coordinates. This phenomenon is of great importance in obtaining accurate products and it is highlighted by this case study, where it is critical in certain areas, such as in the inclination of the towers or in the cracking of the central façade.

All this requires a supplementary technology to the laser scanning, this is UAV + SfM; a non-intrusive way of solving the problems described above through its great portability and ability to collect data. Besides, it gathers an extra supply of analyzable features, which makes it possible to get complete point-cloud models, which form the foundation for accurate and thorough CAD models. These models profit from the features obtained from the hybrid point-cloud, such as cracks (Fig. 7).

This model, generated through the described technique, is comprised of a total of 398 photographs taken by UAV platform: (i) 273 photos of the main façade dividen in 3 vertical strips (1 for each tower and one for the main façade) and (ii) 125 photos of the cracks on chapels, also divided in 3 vertical strips. Alongside these photographs, 117 additional shots were taken without UAV platform (terrestrial photogrammetry): (i) 85 photos of the arches of the chapels of the main nave and (ii) 32 photos at the level of the Church choir.

Both techniques, terrestrial laser scanner and SfM, complement to each other, and their combination is the ideal solution for restoring built heritage. While the laser scanner provides the system a set of precise, dense and fast capture data with which it is possible to monitor structural movement and generate a CAD model suitable for numerical analysis, the UAV + SfM system combines with it perfectly supplying the geometric data of the areas that were unreachable through the previous system. In addition, it characterizes completely the structure's pathological conditions by obtaining direct and georeferenced data.

Fig. 7. Front elevation of the point cloud obtained through SfM technique and PW software (left). Detailed comparison between the laser scanner point cloud and the one obtained in PW software (right).

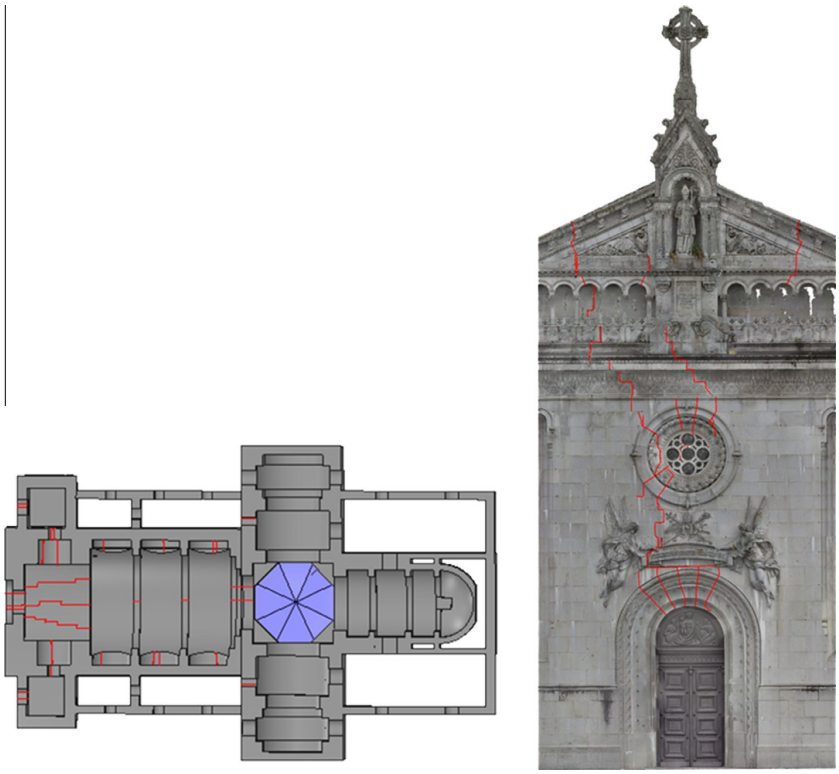

Fig. 8. Results of the inspection for damages: plan view at ground level (left). Main façade orthoimage inspection for damages (central part) (right).

However, the resulting data of both sensor show different coordinate system but the high redundancy allows the creation of a single model applying the methodology explained in Section 3, that finally is converted into a valid CAD model of the building for the subsequent analysis. An average value of 0.0125 with a standard deviation of 0.0065 was found in the coarse registration process. Later, in the fine registration process this values down to 0.0035 with a standard deviation of 0.0011. The final hybrid point cloud had a total of 40,359,060 points (that represents a 10% of the original set).

4.3. Characterization of structural pathologies

The characterization of cracks plays a fundamental role in structure monitoring in terms of stability and safety. Traditionally such monitoring was conducted with graduated cards, mechanical or electronic gauges, or LVDT (linear variable differential transformer). However, this equipment has significant drawbacks [27]: (i) firstly, there is a need for permanent plates, that may become damaged or can be lost, (ii) they provide data only from certain points and certain directions, (iii) the cracking is not directly measured; it is assumed that its activity is correctly defined by the variation of the reference points. In addition to this, some of these methods strongly rely on temperature (this is the case of electronic gauges).

Thanks to the combined use of the shown spatial-data capture techniques, it is possible not only to obtain high density point-clouds and photorealistic textures (this is the case of UAV + SfM system) but also high quality orthoimages in any position and on determined surfaces, thus solving the problems described above. All supplemented with direct product georeferencing, which makes perfectly viable to monitor the movement of the structure and the evolution of damage that may arise.

The aforementioned methods combined with an accurate numerical model will comprise all the necessary tools for sizing and evaluating the restoration system of the building.

The first damage inspection of the monument [6] was carried out in 1998. The inspection indicated that the façade suffered structural damages, made evident by cracks running from its bottom, in the keystone to the coronation. In addition, patologies are observed in the entrance dome keystone under the choir, in the arcs are that make up different bays of the main nave and in cracks on the side of the building.

It is on the main facade where the building shows a greater amount of these pathological conditions, spread along as cracking and displacement on elements of arches and vaults (Fig. 8). Fig. 8 results of the inspection for damages: plan view at ground level (left). Main façade orthoimage inspection for damages (right).

4.4. Geometrical CAD model

Made by the proposed methodology, the Saint Torcato CAD model has greater geometric complexity than the one exposed by Lourenço and Ramos [6]. Within this geometric improvement is remarkable a better characterization of the main façade and towers, including architectural details over the balcony and along the towers.

Since most of the façade shows structural pathological conditions, it is therefore expected that the dynamic response of the structure will be influenced in part by such cracking. The high correlation between the CAD model and the actual photogrammetric point cloud allows to incorporate these characteristics into the

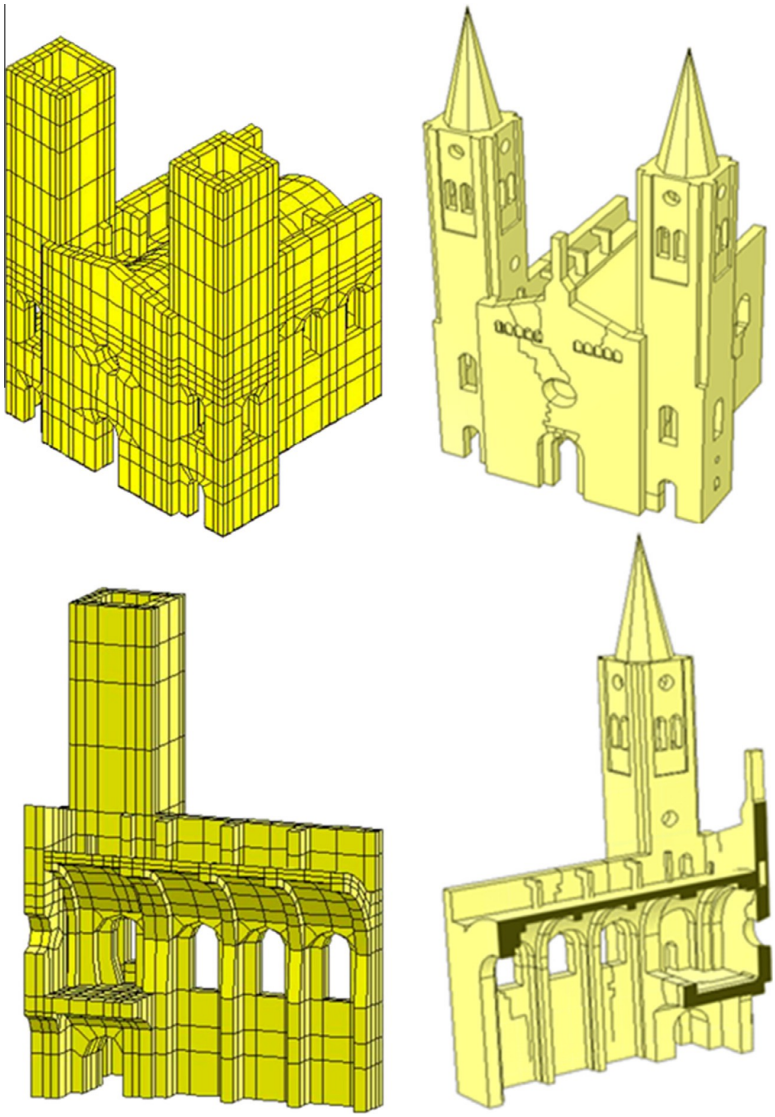

Fig. 9. Isometrics views of the initial geometric model (left) and the one generated by the proposed methodology (right).

CAD model directly, only requiring the meshing of the area under study. Also this model, presents different wall thickness, increasing the model realism (Fig. 9).

4.5. Definition of the numerical calculation model

While the geometric aspect has been completely improved by the methodology presented, the material characterization (homogeneous and isotropic), since at the time no experimental test were carried out, the input loads and boundary conditions remain the same than the initial one. For the loads have been consider: (i) gravitational loads; (ii) truss self-weight and (iii) roof self-weight.

Complementary to this loads conditions, it is necessary to correctly simulate the elastic behavior (Winkler model) of the ground in which the structure stands and also a proper simulation of the behavior of the transcept. Such behavior has been emulated through CONTACT173/TARGET170 elements [40].

The discretization of the model has been carried out considering a 4-node isoparametric tetrahedral element (SOLID65) with a maximum size of 0.60 m. In order to increase the robustness of the tetrahedral mesh, element softening has been carried out using Laplace algorithm [40].

All this results in a total of 218,244 discrete elements into the numerical model (212537 SOLID65, 5707 CONTACT173/TARGET170) (Fig. 10).

4.6. Modal analysis, calibration of the numerical model

The next step required to obtain an accurate finite element model is to calibrate their elastic parameters and thus adapt the dynamic behavior of the numerical model to the real one. In order to accurately calibrate the numerical model it is necessary to follow a three-step procedure: (i) initial hypothesis, (ii) manual calibration and (iii) robust calibration. The initial hypothesis considered were: the elastic properties of masonry, the major

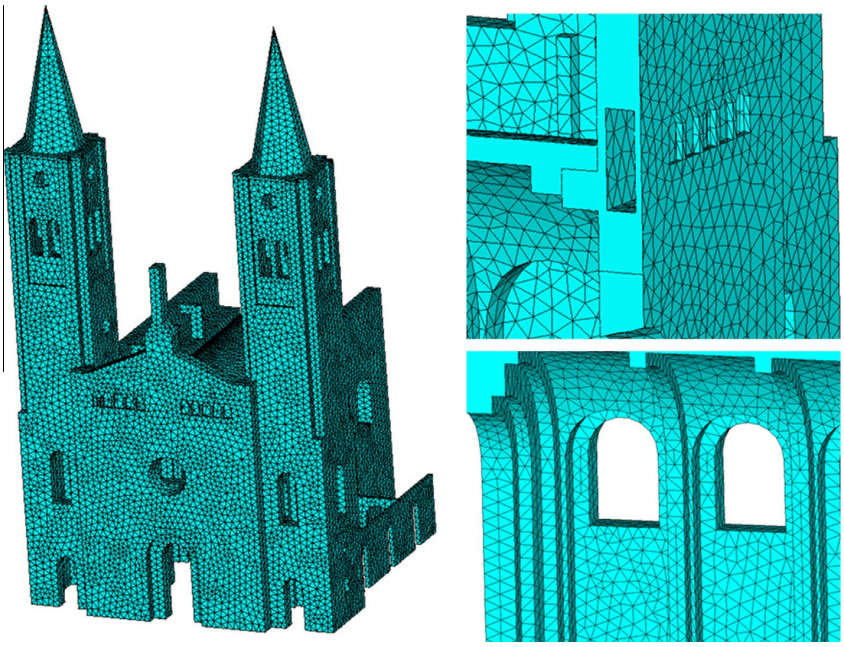

Fig. 10. Isometric view of the mesh model (left). Mesh detail of the balcony and chapels (right).

Table 3
Summary of the adopted values for the calibration of the numerical model.

	Initial values	Lower bound	Upper bound	Updated value
$E_{MASONRY}$ (GPa)	10	5	15	9.19
$\delta_{MASONRY}$ (kg/m^3)	2500	2400	2700	2600
$K_{NFAÇADE}$ (GPa/m)	0.0001	0.00005	0.01	0.0004
$K_{TFAÇADE}$ (GPa/m)	0.1	0.05	1	0.53
$K_{NFIRSTCAP}$ (GPa/m)	1	0.05	5	0.40
K_{NSOIL} (GPa/m)	0.585	0.0585	5.85	0.627
$K_{NTRANSCEPT}$ (GPa/m)	0.1	0.005	1	0.29
$K_{TRANSCEPT}$ (GPa/m)	0.0001	0.00001	0.01	0.00002

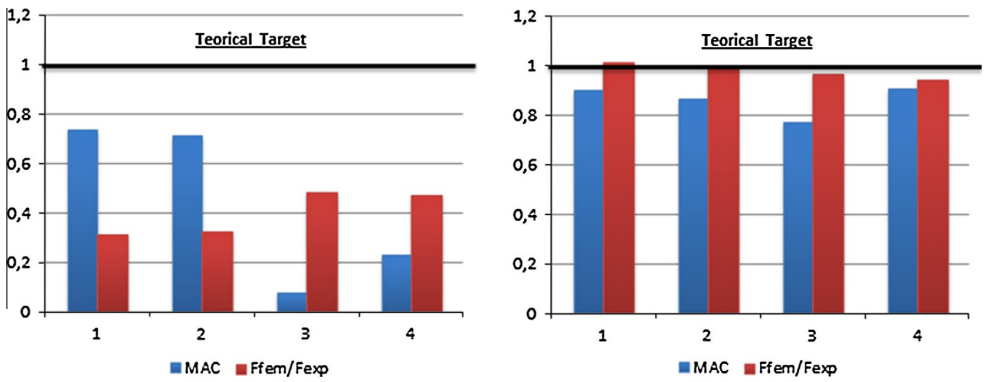

Fig. 11. Comparison between representative values of dynamic response (frequencies and MAC): value ratio of the initial model proposed by Lourenço (left). Ratios obtained with the hereby proposed methodology (right).

cracks on the main façade and the main nave, the elastic behavior of the soil, and the simulation of the connection between the nave and the transcept.

Within the manual calibration stage, numerous tests have been required, evaluating separately each of the considered elastic variables and rejecting those that did not bring improvements to the numerical model. Finally, have been chosen a total of eight parameters, namely: Young modulu's of the masonry ($E_{MASONRY}$) and its density ($\delta_{MASONRY}$), the normal ($K_{NFAÇADE}$) and shear ($K_{TFAÇADE}$) stiffness of the major cracks on the main façade, the normal ($K_{NFIRSTCAP}$)

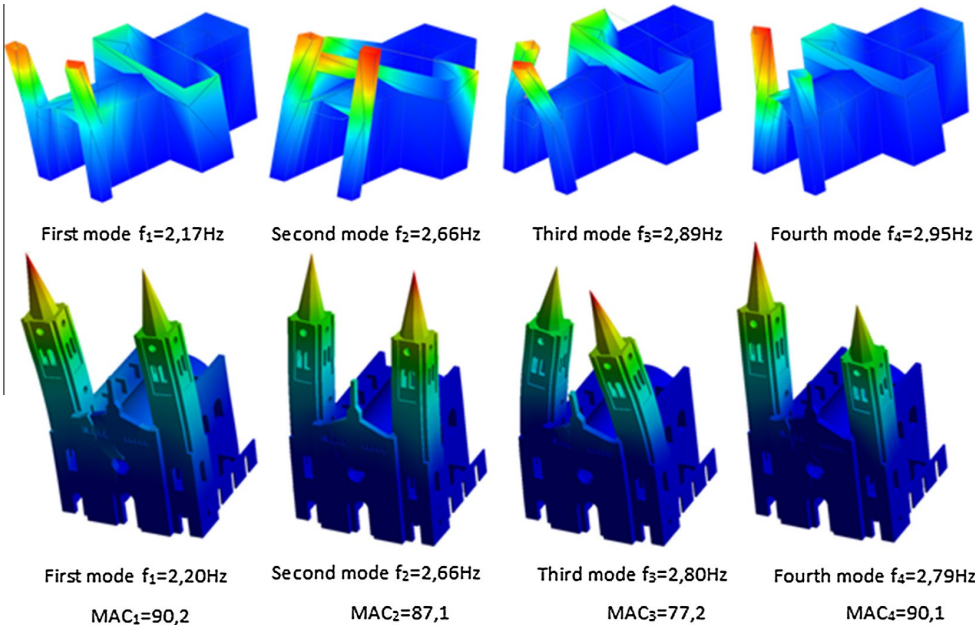

Fig. 12. Comparison between the vibrational model form the OMA and those from the hereby presented finite element numerical model.

stiffness of the major cracks on the main nave, the soil's normal stiffness (K_{NSOIL}), as well as the simulation of the connection between the main nave and the transcept through a normal stiffness ($K_{NTRANSCEPT}$) and a shear one ($K_{TTRANSCEPT}$). During the last step, the accurate calibration of the previously discretized parameters through DR methodology (described above) was required, providing the results presented below (Table 3).

The now calibrated elastic properties of the masonry show a globally damaged material. The high elasticity obtained in the simulation of the transept confirmed that the building, as it progressed, suffered settlements and cracking. However, the rise in rigidity of the elastic properties in comparison to the initially calculated in [6], denote soil compaction. As shown in (Fig. 11) (Fig. 12), the relative ratios between the experimental and numerical frequencies, with a value close to one for the standard MAC indexes denote a high correlation between the experimental dynamic behavior of the building and the numerical one. Through the simulation of the cracks, it was possible to correctly simulate the dynamic behavior and the high existing elasticity in the central area of the building.

5. Conclusions

The methodology presented aims to compile the information from different sensors in order to establish a complete geometric characterization of historic buildings. The combined method for data acquisition solves most common problems encountered today like the preparation of accurate CAD models and the analysis of structure characteristics (displacements and cracking).

Using the laser scanner alone would not solve some of the problems that arise today, i.e. the lack of data in areas that are not accessible to the system or the difficulty of cracking identification. That is why it is essential to incorporate a complementary data capture system able to meet solving problems. The perfect complement for an accurate, quick and complete data capture is the Image Structure from Motion System on UAV platform. Other advantages provided by this second capture system, lies in the potential that digital image analysis gives to the graphical product. This digital image analysis makes possible to completely characterize cracking (length and opening).

The binomial SfM-laser scanner is a reliable foundation from which to analyze appropriate restoration actions, following the procedure: (i) analysis of the causes through the numerical model (ii) displacement and stress state along the structure (iii) analysis of the effectiveness of the system (analysis of the numerical model including restoration activities, analysis of cracks and collapses systems).

The methodology presented can be applied to other infrastructures, such as tunnels or bridges, given the high versatility of the sensors described and the wide range of possibilities that they offer. All this is complemented by a global dynamic analysis of the structure that allows a reliable calibration of the numerical model through the elastic system variables.

The Saint Torcato Church (Guimarães, Portugal) represents an ideal case study for evaluating the potential of the method developed. Based on the geometric characterization performed through the presented methodology, several research works are taking place, in order to improve the characterization of the different materials by Ground Penetration Radar and Boroscopic Camera, for further FEM analysis.

References

[1] Ramos LF, Aguilar R, Lourenço PB, Moreira S. Dynamic structural health monitoring of Saint Torcato church. Mech Syst Signal Process 2013;35(1–2):1–15.
[2] Grimm CT. Masonry cracks: a review of the literature 1988:257–80.
[3] ICOMOS. Recommendations for the analysis, conservation and structural restoration of architectural heritage. In: International scientific committee for analysis and restoration of structures of architectural heritage; 2003.
[4] Vercher J, Gil E, Mas A, Lerma C. Diagnosis/intervention creteria in damaged slabs by severe corrosion of prestressed joists. J Perform Constr Facil 2013;45:45.
[5] Betti M, Vignoli A. Assessment of seismic resistance of a basilica-type church under earthquake loading: modelling and analysis. Adv Eng Softw 2008;39(4):258–83.
[6] Lourenço PB, Ramos LF. Investiçasão sobre as Patologias do Santuário de São Torcato. Final Report. University of Minho 1999;99-DEC/E-5.

[7] Taliercio A, Binda L. The Basilica of San Vitale in Ravenna: investigation on the current structural faults and their mid-term evolution. J Cult Heritage 2007;8(2):99–118.
[8] Armesto J, Roca-Pardiñas J, Lorenzo H, Arias P. Modelling masonry arches shape using terrestrial laser scanning data and nonparametric methods. Eng Struct 2010;32(2):607–15.
[9] Pieraccini M, Dei D, Betti M, Bartoli G, Tucci G, Guardini N. Dynamic identification of historic masonry towers through an expeditious and no-contact approach: application to the "Torre del Mangia" in Siena [Italy]. J Cult Heritage 2014;15(3):275–82.
[10] Riveiro B, Solla M, de Arteaga I, Arias P, Morer P. A novel approach to evaluate masonry arch stability on the basis of limit analysis theory and non-destructive geometric characterization. Automat Constr 2013;31:140–8.
[11] Lubowiecka I, Armesto J, Arias P, Lorenzo H. Historic bridge modelling using laser scanning, ground penetrating radar and finite element methods in the context of structural dynamics. Eng Struct 2009;31(11):2667–76.
[12] Park HS, Lee HM, Adeli H, Lee I. A new approach for health monitoring of structures: terrestrial laser scanning. Comput-Aided Civ Infrastruct Eng 2007;22(1):19–30.
[13] Guidi G, Frischer B, Russo M, Spinetti A, Carosso L, Micoli LL. Three-dimensional acquisition of large and detailed cultural heritage objects. Mach Vision Appl 2006;17(6):349–60.
[14] Yastikli N. Documentation of cultural heritage using digital photogrammetry and laser scanning. J Cult Heritage 2007;8(4):423–7.
[15] Pfeifer N, Briese C. Laser scanning: principles and applications summary. In: Third international exhibition and scientific congress on geodesy, mapping, geology, geophysics, Novosibrisk, Russia; 2007.
[16] Roca D, Lagüela S, Díaz-Vilariño L, Armesto J, Arias P. Low-cost aerial unit for outdoor inspection of building façades. Automat Constr 2013;36:128–35.
[17] Barazzetti L, Binda L, Scaioni M, Taranto P. Photogrammetric survey of complex geometries with low-cost software: application to the 'G1' temple in Myson, Vietnam. J Cult Heritage 2011;12(3):253–62.
[18] TAPEnADe. Case study: Maya bass-relief. Copan (Honduras); 2012.
[19] Westoby MJ, Brasington J, Glasser NF, Hambrey MJ, Reynolds JM. 'Structure-from-Motion' photogrammetry: a low-cost, effective tool for geoscience applications. Geomorphology 2012;179:300–14.
[20] Besl PJ, McKay ND. A method for registration of 3-D shapes. IEEE Trans Pattern Anal Mach Intell 1992;14(2):239–56.
[21] Toldo R, Beinat A, Crosilla F. Global registration of multiple point clouds embedding the generalized procrustes analysis into an ICP framework. 3DPVT 2010 Conference; 2010.
[22] Tognaccini R. La Chiesa di Santa Maria del Mar a Barcelona-Dal Rilievo Tridimensionale all'Analisi Strutturale. Pisa, Italy: University of Pisa; 2009.
[23] Nguyen V-S, Bac A, Daniel M. Simplification of 3D point clouds sampled from elevation surfaces; 2013.
[24] Varady T. Automatic procedures to create CAD models from measured data. Comput-Aided Des Appl 2008;5(5):577–88.
[25] González-Jorge H, Gonzalez-Aguilera D, Rodriguez-Gonzalvez P, Arias P. Monitoring biological crusts in civil engineering structures using intensity data from terrestrial laser scanners. Constr Build Mater 2012;31:119–28.
[26] Armesto-González J, Riveiro-Rodríguez B, González-Aguilera D, Rivas-Brea MT. Terrestrial laser scanning intensity data applied to damage detection for historical buildings. J Archaeol Sci 2010;37(12):3037–47.
[27] Barazzetti L, Scaioni M. Crack measurement: development, testing and applications of an automatic image-based algorithm. ISPRS J Photogramm Remote Sens 2009;64(3):285–96.
[28] Lubowiecka I, Arias P, Riveiro B, Solla M. Multidisciplinary approach to the assessment of historic structures based on the case of a masonry bridge in Galicia [Spain]. Comput Struct 2011;89(17–18):1615–27.
[29] Deseilligny MP, DeLuca L, Remondino F. Automated image-based procedures for accurate artifacts 3D modeling and orthoimage generation. Icomos 2012;113.
[30] Friswell MI, Mottershead JE, Ahmadian H. Finite-element model updating using experimental test data: parametrization and regularization. Philos Trans R Soc Lond Ser A: Math, Phys Eng Sci 2009;359(1778):169–86.
[31] Ramos LF, De Roeck G, Lourenço PB, Campos-Costa A. Damage identification on arched masonry structures using ambient and random impact vibrations. Eng Struct 2010;32(1):146–62.
[32] Mottershead JE, Friswell MI. Model updating in structural dynamics: a survey. J Sound Vib 1993;167(2):347–75.
[33] Allemang RJ, Brown DL. A correlation coefficient for modal vector analysis; 1982.
[34] Gentile C, Saisi A. Ambient vibration testing of historic masonry towers for structural identification and damage assessment. Constr Build Mater 2007;21(6):1311–21.
[35] Douglas BM, Reid WH. Dynamic test and system identification of bridges. J Struct Div 1982;108(10):2295–312.
[36] Scaioni M, Barrazzetti L, Brumana R, Cuca B, Fassi F, Prandi F. Rc-Heli and Structure from Motion techniques for the 3-D reconstruction of a Milan dome spire. ISPRS 2009. XXXVIII-5/W1.
[37] Gordon S, Lichti D, Stewart M, Franke J. Structural deformation measurement using terrestrial laser scanners. In: 11th FIG symposium on deformation measurements. Santorini, Greece; 2003.
[38] Lichti D, Gordon S. Error propagation in directly georeferenced terrestrial laser scanner points clouds for cultural heritage recording. Athens (Greece): FIG Working Week; 2004.
[39] Schaer P, Skaloud J, Landtwing S, Legat K. Accuracy estimation for laser point cloud including scanning geometry. In: 5th International symposium on mobile mapping technology. Padova (Italy); 2007.
[40] ANSYS. ANSYS manual sets. USA; 2012.

Chapter II

Experimental and numerical approaches for structural assessment in new footbridge designs (SFRSCC-GFPR hybrid structure).

Composite Structures 134 (2015) 95–105

Contents lists available at ScienceDirect

Composite Structures

journal homepage: www.elsevier.com/locate/compstruct

Experimental and numerical approaches for structural assessment in new footbridge designs (SFRSCC–GFPR hybrid structure)

Luis Javier Sánchez-Aparicio [a,*], Luís F. Ramos [b,1], José Sena-Cruz [b,1], Joaquim O. Barros [b,1], Belén Riveiro [c,2]

[a] Department of Land and Cartographic Engineering, University of Salamanca, High Polytechnic School of Avila, Hornos Caleros, 50, 05003 Avila, Spain
[b] ISISE, Department of Civil Engineering, University of Minho, Guimarães, Portugal
[c] Department of Material Engineering, Applied Mechanics and Construction, School of Industrial Engineering, University of Vigo, Vigo, Spain

ARTICLE INFO

Article history:
Available online 20 July 2015

Keywords:
GFRP pultruded profiles
Experimental tests
Operational Modal Analysis
Finite Element Model Updating
Damage identification
Civil structures

ABSTRACT

Within the civil engineering field, the use of the Finite Element Method has acquired a significant importance, since numerical simulations have been employed in a broad field, which encloses the design, analysis and prediction of the structural behaviour of constructions and infrastructures. Nevertheless, these mathematical simulations can only be useful if all the mechanical properties of the materials, boundary conditions and damages are properly modelled. Therefore, it is required not only experimental data (static and/or dynamic tests) to provide references parameters, but also robust calibration methods able to model damage or other special structural conditions. The present paper addresses the model calibration of a footbridge bridge tested with static loads and ambient vibrations. Damage assessment was also carried out based on a hybrid numerical procedure, which combines discrete damage functions with sets of piecewise linear damage functions. Results from the model calibration shows that the model reproduces with good accuracy the experimental behaviour of the bridge.

1. Introduction

In the last few years, new civil engineering designs have emerged in the field of the construction of footbridges, considering new materials [1,2] and constructive [3–5] solutions. Within these new materials, have received special attention the use of fiber reinforced polymer (FRP) and glass fiber reinforced polymer (GFRP), offering better resistance to environmental agents and the advantages of high stiffness-to-weight and strength-to-weight ratios when compared to conventional construction materials [6,7]. They also can be combined with traditional materials, like concrete or steel, offering particularly effective flexural properties [8–10]. These hybrid structures are particularly suitable for footbridge structures thanks to the possibility of an easy and quick erection.

However, several characteristics restrict the use of this type of materials: (i) high deformability (low elastic and shear modulus); (ii) brittle failure; (iii) behaviour at elevated temperatures; and (iv) lack of specific design codes [11]. Due to the small service loads, these structures usually are light and slender. For these reason the interaction with pedestrians or wind can arise some structural problems [12,13]. Considering the mentioned above, several tests are needed in order to assess the structural behaviour of these structures in different scenarios. The diversity of materials and the interaction between them makes the Finite Element Methods (FEM) as the most feasible solution to evaluate and simulate these structures.

In contrast with the potentialities that the FEM can offer, some choices (mechanical properties of the materials or structural conditions) may give erroneous numerical results. Within this context, this paper attempts to demonstrate a methodology to evaluate, through experimental tests and robust numerical calibration strategies, the structural behaviour of a pedestrian bridge prototype. The bridge was experimentally tested with several static and dynamic tests and with the main results, a model calibration was performed to tune the mechanical parameters.

In order to obtain a robust finite element model, which represent accurately the structural behaviour of the footbridge a

Abbreviations: GFRP, Glass Fibre Reinforced Polymer; SFRSCC, Steel Fibre Reinforced Self-Compacting Concrete; FEM, Finite Element Method; FEMU, Finite Element Model Updating; MAC, Modal Assurance Criterion.

* Corresponding author. Tel.: +34 920353500; fax: +34 920353501.
E-mail addresses: luisj@usal.es (L.J. Sánchez-Aparicio), lramos@civil.uminho.pt (L.F. Ramos), jsena@civil.uminho.pt (J. Sena-Cruz), barros@civil.uminho.pt (J.O. Barros), belenriveiro@uvigo.es (B. Riveiro).
[1] Tel.: +351 253510200; fax: +351 253510217.
[2] Tel.: +34 1 986814052; fax: +34 986811924.

http://dx.doi.org/10.1016/j.compstruct.2015.07.041
0263-8223/

damage assessment was carried out, based on an hybrid numerical procedure, which combines discrete damage functions with sets of piecewise linear functions to evaluate the damage present at the structure. Special attention was paid to the influence of the supports, the interaction between structural components and the damage response of the SFRSCC deck.

This paper is organized as follows: Section 1 is the introduction; Section 2 a general structural description of the hybrid footbridge is presented; Section 3 presents the static and dynamic tests performed on the footbridge; Section 4 a robust dynamical-static calibration process is carried out; and finally in the Section 5 the conclusion are drawn.

2. GFRP–SFRSCC hybrid footbridge

2.1. Description of the structure

The studied prototype at full scale was developed in the framework of research project PONTALUMIS – Development of a prototype of a pedestrian bridge in GFRP-ECC, involving ICIST/Instituto Superior Técnico, ISISE/University of Minho and company ALTO – Perfis Pultrudidos, Lda. The footbridge design was carried out considering the main potentialities of the used materials. Therefore, the composite Steel Fiber Reinforced Self-Compacting Concrete (SFRSCC) material was placed in zones where compressive stresses exist, whereas GFRP girders were used to carry the tensile stresses. The cross section of the bridge is characterized by the following: (i) a SFRSCC deck; (ii) SFRSCC jackets placed in the vicinity of the supports; and (iii) GFRP girders (Fig. 1).

The connection between the structural components (SFRSCC deck and GFRP pultruded girders) was made through two different solutions: (i) for the contact areas located above the jackets an epoxy resin layer with 2 mm of thickness was used; and (ii) for the remaining contact zones the same adhesive solution was used in combination with a redundant mechanical connection based on M10 stainless steel bolts, with 300 mm of spacing (two per main girder's flange), in order to extend the bridge life time due to rheological effects, vandalism and accidental loads.

Complementary to the previous structure, a group of secondary girders were placed between the main ones. This solution prevents any distortion caused by eccentric loads. Positioned at the support, quarterspan and midspan sections, this profiles were constituted by I-shaped ($200 \times 100\ mm^2$) GFRP pultruded profiles and connected to the main girders by means of equal length angle GFRP ($60 \times 8\ mm^2$) profiles and stainless steel bolts (M10) threaded rods and nuts.

The footbridge structure presents a total length of 11.00 m on two pairs of supports (two pinned and two sliding), as show (Fig. 2). More details can be found elsewhere [11].

2.2. Mechanical properties of the footbridge components

Made by E-glass fiber rovings and mats embedded in a isophthalic polyester, the main and secondary pultruded profiles have been characterized by the following tests [11]: (i) tension (EN ISO 527) [14]; (ii) compression (ASTM D 695) [15]; and (iii) shear test (10° off-axis tension test), according to the recommendations of Hodgkinson [16]. Allowing the evaluation of several material mechanical properties, namely: (i) longitudinal elasticity modulus in tension ($E_{L,t}$); (ii) transverse elasticity modulus in compression ($E_{T,c}$); (iii) in-plane shear modulus (G_{LT}); (iv) longitudinal tensile strength ($f_{tu,L}$); and (v) in-plane shear strength ($T_{u,LT}$). These properties are summarizes in Table 1.

For the SFRSCC material, a specific mixture composition was used (details about the mix design are available in [17]: (i) cement; (ii) limestone filler; (iii) water; (iv) superplasticizer; (v) fine sand; (vi) river sand; (vii) crushed stone; and (viii) fibers. The compressive strength and flexural properties of the SFRSCC were assessed according to standards NP EN 12390-3 [18] and RILEM TC 162-TDF, respectively [19], providing the following mechanical information: (i) Young's modulus; (ii) compressive strength (f_{cm}); (iii) cracking strength in flexure ($f_{ct,L}$); (iv) equivalent flexural tensile strengths ($f_{eq,2}$ and $f_{eq,3}$); and (v) residual flexural tensile strengths ($f_{R,1}$ to $f_{R,4}$) (see Table 2).

The epoxy adhesive used to bond the main girders to the SFRSCC deck has an elasticity modulus in tension of $E_a = 8.8$ GPa and a tensile strength of $f_{au} = 17.3$ MPa [20]. The redundant mechanical connection into the span between jackets was materialized by stainless steel anchors (M10 × 55). This solution present a bearing capacity of $f_{bk} = 700$ MPa (according to the manufacturer). For the present study case, three different types of connections had been considered: (i) epoxy layer; (ii) epoxy layer and bolt; and (iii) bolt L-union between secondary and main girders. This connection were materialized through interface elements, considering the mechanical properties obtained in the different experimental program carried out (Table 3).

3. Experimental programs

3.1. Static test

In order to ensure the correct erection, disposition and performance of the different structural elements in the footbridge several static tests were performed [11]. These experimental tests were mainly focused on the characterization of the bending response of the footbridge, as well as the deformation recovery after unloading. For this purpose, the footbridge was loaded with multiple close-spaced water reservoirs, with a total weight of 8.8 kN/m^2. These reservoirs were placed in different uniformly and distributed configurations (load case A–C, see Table 4). All the loading and unloading operations were performed as fast as possible in order to minimize creep effects on the concrete. As a result, three load configuration (A–C) were evaluated: (i) load distributed on the entire span with a width of 1.20 m; (ii) load in the central part of the span with a length of about 2.70 m and a small gap of 0.30 m in the vicinity of midspan; and (iii) load in the central part of the span with a length of 5.10 m and a small gap of 0.30 m in the vicinity. In order to evaluate the different load setups, different sensors were placed along the footbridge: (i) electrical transducers (with a precision of 0.01 mm); and (ii) axial strains electric strain gauges (Fig. 3).

As results of the static tests (see Table 4 and Fig. 3), the acquired data was distributed into five groups, namely: (i) midspan deflection ($\delta_{ms,Avg}$); (ii) axial strains on the SFRSCC deck ($\varepsilon_{c,Avg}$); (iii) axial strains on the web of the main girders ($\varepsilon_{w,Avg}$); (iv) axial strains on the bottom flanges of the main girders ($\varepsilon_{c,Avg}$); and (v) curvature at midspan (ζ).

3.2. Dynamical identification test

A dynamical identification campaign, based on the Operational Modal Analysis (OMA) approach, was performed with the aim of identifying the modal properties of the structure. With a sensitivity of 10 V/g, range of ±0.5 g, and 8 μg rms broadband resolution, a total of eighteen uniaxial piezoelectric accelerometers were place on different locations on the vertical direction (Fig. 4).

By using Enhanced Frequency Domain Decomposition (EFDD) technique [22] each mode is estimated as a decomposition of the system's response spectral densities into several single degree of freedom systems.

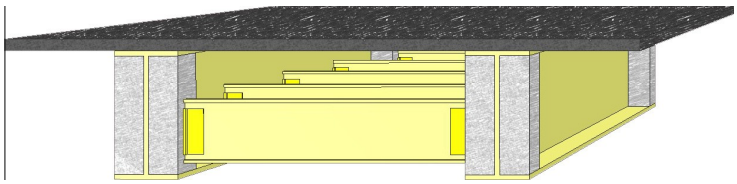

Fig. 1. Isometric view of the footbridge (in dark-grey the SFRSCC concrete, in light-grey the SFRSCC jackets and in yellow the GFRP profiles). (For interpretation of the references to colour in this figure legend, the reader is referred to the web version of this article.)

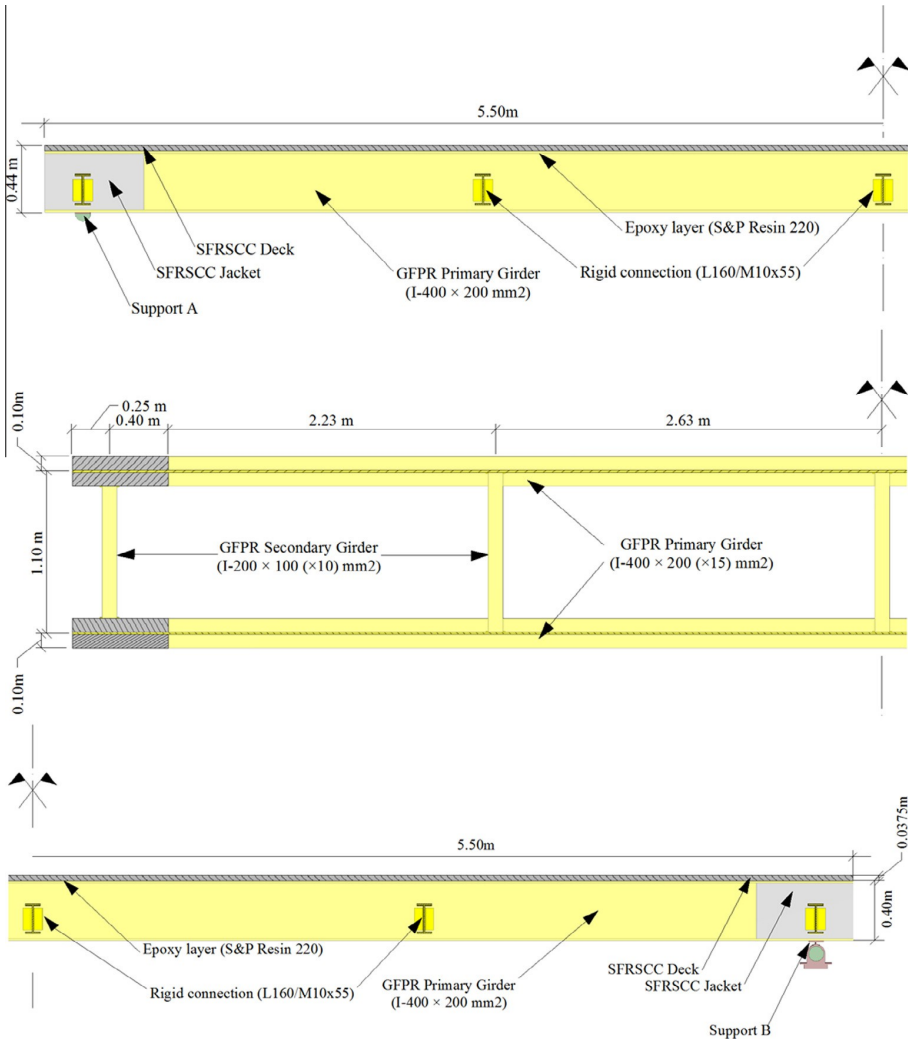

Fig. 2. Section views of the SFRSCC–GFPR footbridge (units in meters). Longitudinal sections (above and middle). Transversal view (below).

Table 1
Mechanical properties of the GFRP pultruded profiles [11].

Part	$E_{L,t}$ (GPa)	$E_{T,c}$ (GPa)	G_{LT} (GPa)	$f_{tu,L}$ (MPa)	$T_{u,LT}$ (MPa)	p (kN/m^3)
GFRP web	23.98 ± 1.61	4.55 ± 0.52	3.49 ± 0.43	278.90 ± 23.78	20.42 ± 1.15	18.00
GFRP flange	35.71 ± 1.83	3.57 ± 0.36	–	336.94 ± 37.51	–	18.00

Table 2
Mechanical properties of the SFRSCC material used [11].

$E_{c,28}$ (GPa)	f_{cm} (MPa)	$f_{ct,L}$ (MPa)	$f_{eq,2}$ (MPa)	$f_{eq,3}$ (MPa)	$f_{R,1}$ (MPa)	$f_{R,2}$ (MPa)	$f_{R,3}$ (MPa)	p (kg/m^3)
37.75 ± 1.3	75.95 ± 10.0	6.21 ± 1.2	10.42 ± 2.4	10.56 ± 2.4	10.17 ± 2.1	10.27 ± 2.34	9.71 ± 2.34	2325.78

Table 3
Mechanical properties obtained in the experimental program [21].

Variable	Epoxy layer	Epoxy layer and bolts	Bolt union
K (N/m^3) × 10^6	288.55 ± 59.75	300.57 ± 71.79	140.02 ± 9.63

A total of 16 vibration modes were identified. It is noted that, in this modal identification, several modal shapes present an asymmetric behaviour. This phenomenon can be attributed to the presence of damage in the structure especially in the first and fourth quarterspan (Fig. 5).

Following this antisymmetric behaviour in the different vibration modes, a visual inspection was carried out. Some micro-cracks on the SFRSCC deck were detected, the average value of the crack width being about 0.06 mm, in the vicinity of the quarterspans and an isolate crack in the midspan, with an average value of 1.5 mm (Fig. 6).

4. Finite element updating strategy

4.1. Numerical model of the footbridge

In order to simulate the structural (static and dynamic) behaviour of the footbridge a tridimensional FE model was built using the commercial software TNO Diana [23]. With a total of 24,334 elements high-order elements (CHX60) [23], with 10 cm as the maximum dimension (Fig. 7). For the epoxy connections (main girder-deck and secondary girder-primary girder) interfaces elements were chosen, avoiding the use of highly distorted solid elements, since the width of these connections are about 2 mm. As a result, 3,240 interface elements (Q24IF) were used.

The numerical model includes the following structural components: (i) GFRP main girders; (ii) GFRP secondary girders; (iii) bolted connections with a GFRP L union; (iv) SFRSCC deck; (v) SFRSCC jackets; (vi) epoxy-bolt layer; and (vii) epoxy layer. All the structure is supported by two groups of pinned supports (in the left side) and other two groups of sliding supports (right side). Both supports are modelled by 88 spring elements in the main directions (SP2TR).

Finally, the material properties (mean and deviation values) obtained by the different tests carried out (see Tables 1–3), were consider for the FE model. Also a perfect normal bond was assumed at the GFRP-epoxy and SFRSCC-epoxy interfaces, consider only the interface stiffness [1].

4.2. Cost function and optimization algorithm

Finite Element Model Updating (FEMU) strategy can be employed in a wide range of applications [24–26]: (i) design; (ii) simulation; (iii) prediction; and (iv) damage identification. In this context, several approaches can be carried out [27]: (i) Deterministic approaches; (ii) Bayesian finite element strategies; and (iii) Fuzzy approaches.

For the present study case, a deterministic strategy was followed. The success of this approach is based on minimizing the residual vector (r) of the objective function (J), considering the data derived from the experimental campaigns, defined by the Eq. (1).

$$r = \frac{1}{2}\left\| \begin{matrix} J^{sta} \\ J^{din} \end{matrix} \right\|^2 \tag{1}$$

where ||•|| denotes the Euclidean norm, r is the residual vector of J^{sta} and J^{din} (static and dynamic residuals, respectively). The objective function terms ($J = J^{sta} + J^{din}$) are given by:

$$J^{sta} = \frac{1}{2} W_\delta \sum_{j=1}^{m} \left(\frac{\delta_j^{num} - \delta_j^{exp}}{\delta_j^{exp}} \right)^2 \tag{2}$$

$$J^{din} = \frac{1}{2}\left[W_f \sum_{i=1}^{m} \left(\frac{f_i^{num} - f_i^{exp}}{f_i^{exp}} \right)^2 + W_\phi \sum_{i=1}^{m} \left(\phi_i^{num} - \frac{\phi_i^{exp}}{|\phi_{ref}^{exp}|} \right)^2 \right] \tag{3}$$

where W_f, W_φ, and W_δ are the weights considered for the frequency, vibration modes and static displacements, respectively, f is the frequency, ϕ the modal displacements, δ the static displacements, and ϕ_{ref} is a scaling factor (normalization) that enable a comparison between the experimental and numerical modes displacements. For the dynamic functions (J^{din}) the i index indicates the mode shape and for the static one (J^{sta}) the j index indicates the load case.

Generally, the residuals values (r) of the objective function (J) to be minimized shows a non-linear relation with the unknowns. For these purpose a non-linear least squares function was used to solve the problem. Inside this non-linear least squares framework the Trust Region Reflective iterative algorithm was employed. In each iteration, the search area is reduced to a zone known as "*trust region*" [28]. Finally, the objective function (J) was approximated to a quadratic minimizer by the truncated Taylor series.

As exposed in [27], the gradient-based optimizations method, in our case the Gauss–Newton approach with the Trust Region Reflective algorithm, requires the computation of the Jacobian (or sensitivity matrix) and Hessian matrix. Both matrix can be solved following a special structure integrated into the least squares problem Eqs. (4) and (5).

$$\nabla J(\theta) = \sum_{i=1}^{m} r_i(\theta) \nabla r_i(\theta) = Jacob(\theta)^T r(\theta) \tag{4}$$

$$\begin{aligned} \nabla^2 J(\theta) &= Jacob(\theta)^T Jacob(\theta) + \sum_{i=1}^{n} r_i(\theta) \nabla^2 r_i(\theta) \\ &\cong Jacob(\theta)^T Jacob(\theta) \end{aligned} \tag{5}$$

Table 4
Static test results for the three different load configurations [11].

Setup	$\delta_{ms,Avg}$ (mm)	$\varepsilon_{c,Avg}$ (μm/m)	$\varepsilon_{w,Avg}$ (μm/m)	$\varepsilon_{f,Avg}$ (μm/m)	ζ (10^{4}m^{-1})
A (along the entire span)	38.07	−190	320	1102	30.6
B (central part of the span)	23.27	−145	220	712	20.3
C (central part of the span)	43.28	−252	392	1208	34.6

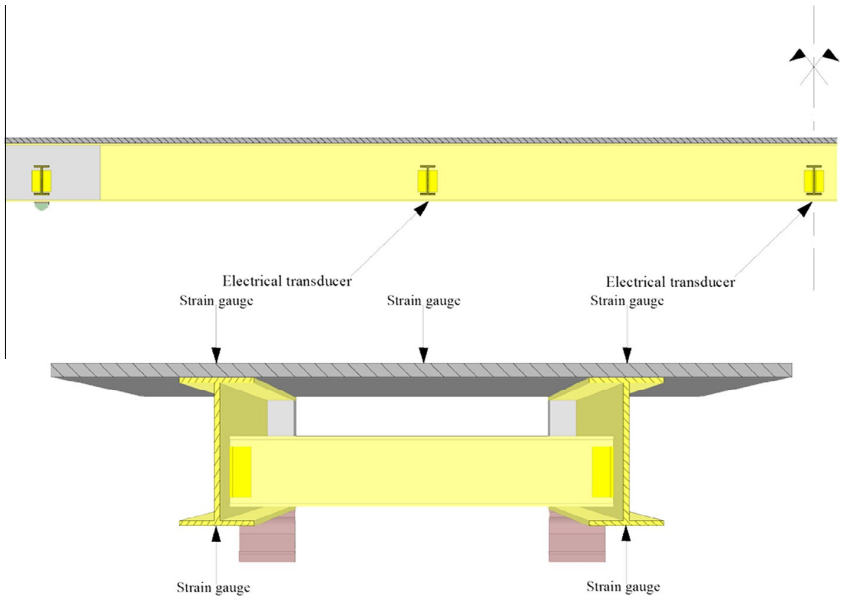

Fig. 3. Cross-section of the footbridge: Longitudinal cross-section, with the electrical transducers (above). Transversal cross-section, at mid-span, with the strain gauges sensors (below).

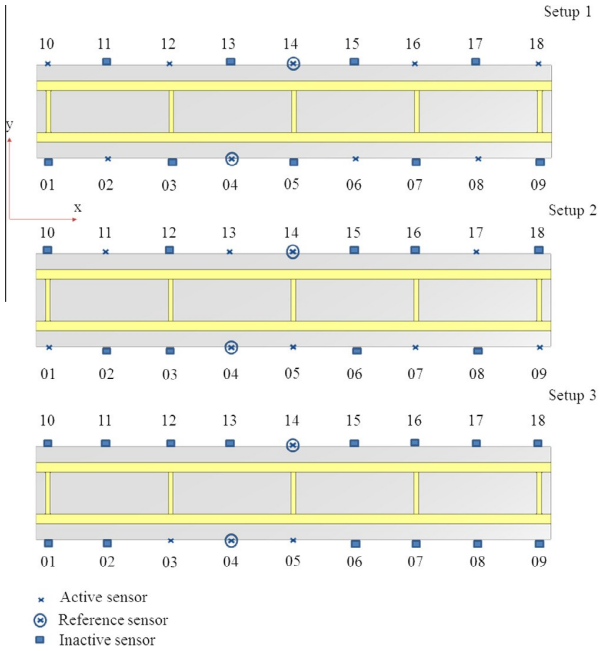

Fig. 4. Modal identification test: accelerometers positions and test setups.

where *Jacob* is the Jacobian matrix, r the vector which contains the residuals, θ the different variables that will be optimized, ∇J is the first derivate of the objective function and $\nabla^2 J$ the second one. The index n indicates the number of unknowns consider during the optimization.

Aiming at avoiding unrealistic results, boundary constraints were applied to the updating parameters, based on the deviation values obtained in the different mechanical test (see Tables 1–3) and other values provided in literature [13,20,21]. With respect to the model updating, only the first six vibration modes were considered (see Table 5).

4.3. Robust model updating

Given the complexity of the structure, several calibration stages were considered, namely: (i) initial model updating; (ii) support stiffness model updating; and (iii) damaged model updating. As model robustness indicators for results quality check, the following quantities were used: (i) relative error between frequencies; (ii) modal assurance criterion [29]; and (iii) relative error between displacements for the different load cases.

In the first stage, on the initial model updating only the Young's modulus of the main materials (SFRSCC deck, pultruded profiles flanges and webs) and the stiffness of the different epoxy solutions (with and without bolt redundancies, see Section 2.2) were calibrated (see Table 6). It should be stressed that, for the pultruded profile material and given its orthotropic behaviour, in order to reduce the number of updating variables a constant relation between longitudinal and transversal Young's modulus was

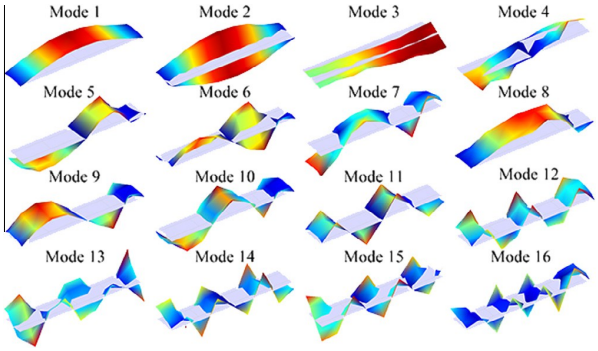

Fig. 5. Results of the 16 modes obtained from the Operational Modal Analysis campaign (the x axis was consider along the longitudinal direction, the y along the transversal and z along the orthogonal direction) [11].

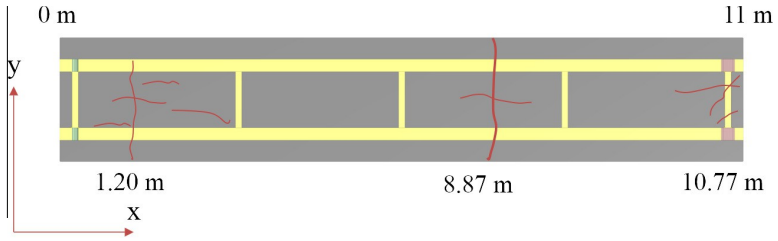

Fig. 6. Damage inspection on the footbridge (cracks are in red color). (For interpretation of the references to colour in this figure legend, the reader is referred to the web version of this article.)

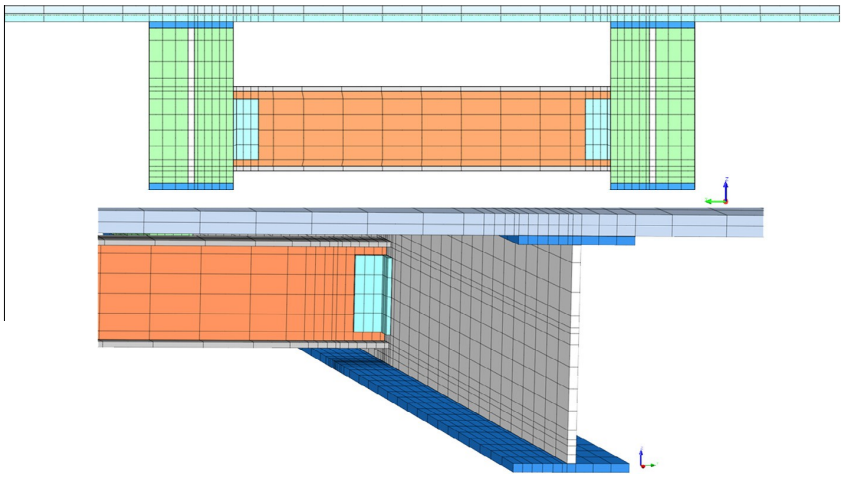

Fig. 7. Front view of the mesh model (above). Mesh detail of the inner part (below).

Table 5
Results values from the Enhanced Frequency Domain Decomposition.

Mode shape	Frequency		Damping ratio		Description
	Mean value (Hz)	CoV (%)	Mean value (Hz)	CoV (%)	
1	6.40	0.28	1.89	18.69	1st Vertical bending mode
2	8.16	0.01	1.26	11.77	1st Lateral Torsional mode
3	12.13	0.63	1.96	16.28	1st Lateral bending mode
4	20.78	12.28	1.57	62.08	2nd Torsional mode
5	22.16	6.14	0.92	20.59	2nd Vertical bending mode
6	23.74	0.09	0.76	11.65	3rd Torsional mode

Table 6
Results of the initial model robust calibration.

	Initial values	Lower bound	Upper bound	Updated values
E_{SFRSCC} (GPa)	37.75	33.82	41.68	39.90
$E_{GFRP\text{-}FLAN}$ (GPa)	35.71	30.22	41.20	41.12
$E_{GFRP\text{-}WEB}$ (GPa)	23.98	19.15	28.81	28.80
K_{EPOXY} (N/m^3)	14.43×10^{10}	5.53×10^{10}	23.33×10^{10}	17.3×10^{10}
$K_{EPOXY\text{-}BOLT}$ (N/m^3)	15.03×10^{10}	4.27×10^{10}	25.79×10^{10}	25.2×10^{10}

established ($E_{L,t}/E_{t,c}$): (i) 5.27 for the GFPR webs; and (ii) 10.00 for the GFPR flanges. This relation was considered in the different calibration procedures.

Following the results obtained in Table 4 with above considerations, the model has high static and dynamic deviations with an average error in frequencies and displacement of 33.06% and 55.04%, respectively (see Tables 7 and 8). Also, the third mode shape was not identified numerically.

Taking into account the previously results, it follows that the structural consideration of the initial model do not fit with the real behaviour of the footbridge (high structural stiffness). As a subsequent calibration, the footbridge supports were modelled with a different approach. Elastic springs in the main directions of both supports were considered, and subsequently a sensitivity analysis was performed, taking into account the initial values proposed by [13]. The results obtained in this analysis shows that the elastic springs are extremely sensitive, especially in the x and y direction. The same initial values and bounds have been considered for the elastic modulus, obtaining the presented in Table 9.

Analyzing the results obtained in terms of quality index (Figs. 8 and 9), an average relative error of 3.5% (relative error between frequencies) was obtained. Additionally, an average MAC value of

Table 7
Summary of the dynamical results obtained with the initial considerations, in terms of relative error in frequencies and MAC values.

Vibration mode	f_{exp} (Hz)	f_{num} (Hz)	Error (%)	MAC (%)
1	6.40	10.69	67.05	98
2	8.16	10.80	32.39	99
3	12.13	–	–	–
4	20.79	20.04	-3.59	82
5	22.16	25.86	16.70	89
6	23.74	27.09	14.10	88

Table 8
Summary of the results obtained in the initial model, through the static correlation values considered (relative error in displacement).

Load case	$disp_{exp}$ (mm)	$disp_{num}$ (mm)	Error (%)
A	−38.07	−16.08	−57.77
B	−23.27	−11.29	−51.50
C	−43.28	−19.10	−55.86

Table 9
Results obtained in the robust calibration of the spring model.

	Initial values	Lower bound	Upper bound	Update values
E_{SFRSCC} (GPa)	37.75	33.82	41.68	34.10
$E_{GFRP\text{-}FLAN}$ (GPa)	35.71	30.22	41.20	38.94
$E_{GFRP\text{-}WEB}$ (GPa)	23.98	19.15	28.81	28.81
E_{EPOXY} (N/mm^3)	14.43×10^{10}	5.53×10^{10}	23.33×10^{10}	9.72×10^{10}
$E_{EPOXY\text{-}BOLT}$ (N/m^3)	15.03×10^{10}	4.27×10^{10}	25.79×10^{10}	21.52×10^{10}
K_{Ax} (N/m)	10.00×10^{6}	10.00×10^{5}	10.00×10^{7}	4.37×10^{6}
K_{Ay} (N/m)	10.00×10^{5}	10.00×10^{4}	10.00×10^{6}	8.78×10^{5}
K_{Bx} (N/m)	10.00×10^{3}	10.00×10^{2}	10.00×10^{5}	1.69×10^{4}
K_{Bx} (N/m)	10.00×10^{5}	10.00×10^{4}	10.00×10^{6}	4.24×10^{5}

92.0% (with a minimum value of 86% in the sixth mode) was obtained and an average displacement relative error of 5.0%. Therefore, it can be stressed that the results obtained by the second model are more accurate compared with the previous one. But - from the obtained results (the different modal shapes and error in frequencies) it is observable that the different modes considered have negative and positive frequencies errors. Said phenomena indicates a wrong relation between stiffness of the different structural parts, and also burden the model calibration (Fig. 8).

Evaluating more in deep the different measurement points through the COMAC index (Co-ordinate Modal Assurance Criterion) [30] as a damage indicator (see Fig. 9), large discrepancies can be observed at different points (2, 9, 11 and 18), whose origin can be attributed to the structural damage (Fig. 6).

Considering the exposed above, it is expected that trough appropriate damage identification and quantification the results will improve. From the damage inspection previously showed (Fig. 6), it is possible to conclude that mainly three areas can be improved with the damage calibration (the vicinity of first and fourth quarter-spans with a generalize damage) and the third quarter-span (due to the presence of an isolate crack).

4.4. Damage function

Based on the classification defined by [31], four levels of damage assessment can be established: (i) level 1 or Detection; (ii) level 2 or Localization; (iii) level 3 or Assessment; and (iv) level 4 or Prediction of the remaining service life. The FEMU strategy allows a damage assessment up to level 3. This implies that this model-based approach is able of detecting, locating and quantifying the damage acting on the structure. Such potential is related to the understanding of damage in the structure. When the structure suffers damage it implies a degradation of the mechanical properties which can be simulated by the decrease of stiffness of the surrounding elements in the said area. The calibration of this structure, as well as the damage identification and extension, can

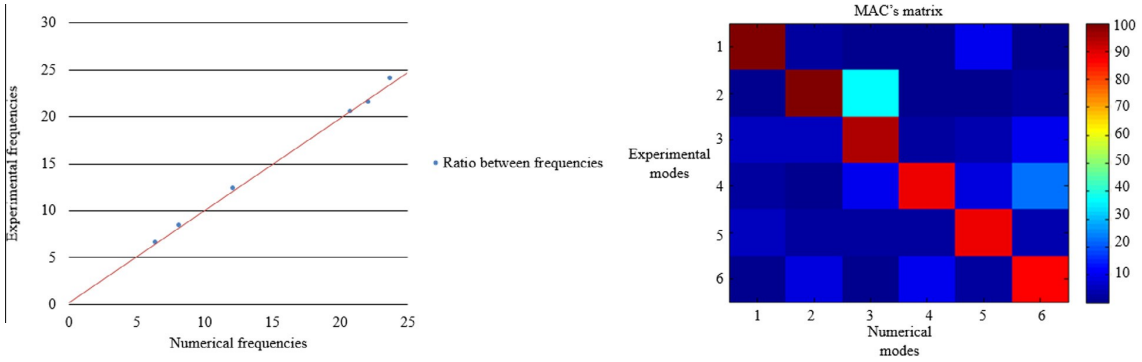

Fig. 8. Frequency pair between spring model updated and OMA (left). MAC matrix with the first six modes (right).

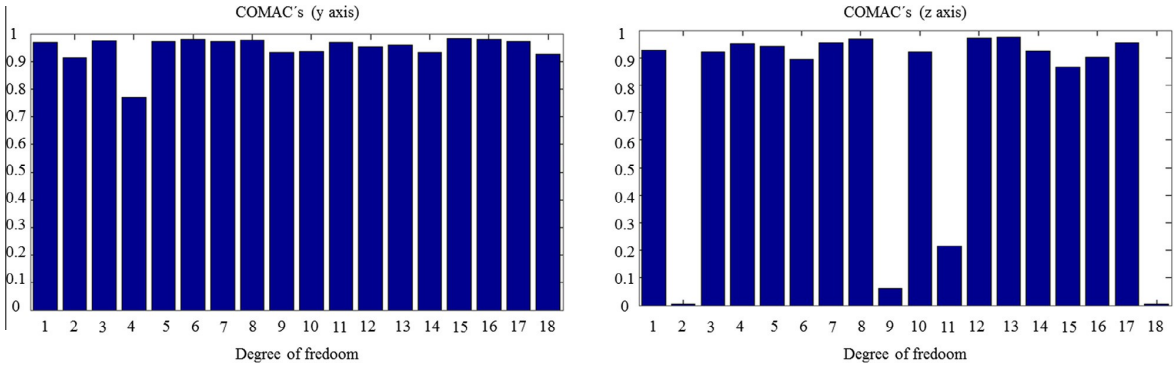

Fig. 9. COMAC values obtained in the spring model updating: COMAC values in *y* direction (left) and COMAC values in *z* direction (right).

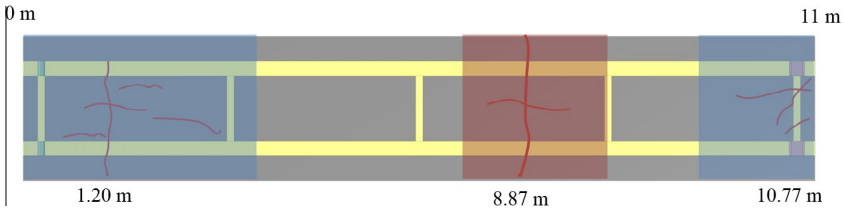

Fig. 10. Schematic representation of the damage identification strategies employed during the robust model updating. In blue the areas with substructure damage functions and in red the area with a discrete damage function. (For interpretation of the references to colour in this figure legend, the reader is referred to the web version of this article.)

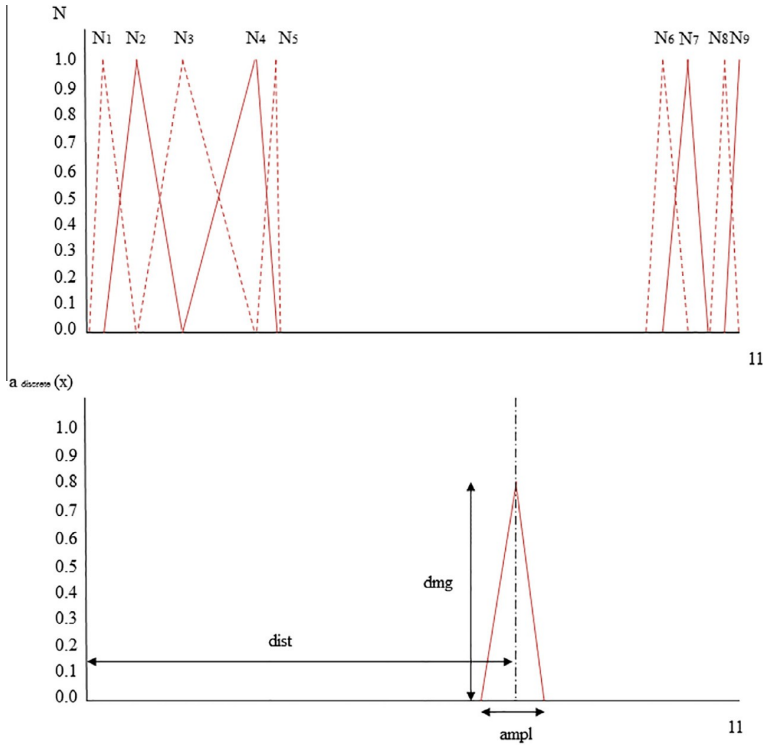

Fig. 11. Different shape functions used during the robust model updating. Substructure damage functions (above). Discrete damage function (below).

be made through the adjustment of the mechanical properties of the different elements affected by this damage.

However, adjusting the stiffness of all elements results in a large number of variables to be tuned, leading to an ill-conditioned problem that can be minimized through different approaches. One approach is the regularization technique [32]. Nevertheless, two drawbacks must be considered. On the one hand, as exposed above, evaluate the function sensitivity implies assessing the sensitivity of each variable, which results in a time consuming solution. On the other hand, less "real" results obtained by the updating of each element (non-continuous damage assumption) are obtained.

In order to solve these drawbacks, the damage quantification can be made through three different approaches: (i) discrete approach that considers the crack as a macroblock splitter through interface elements [33]; (ii) diffused approach that considers a degradation zone [25] on the surroundings of the damage area; and (iii) sub-structuring the model and applying damage functions [24,27].

Generally, the third approach could be applied successfully in different structures [32], but in contrast with the procedure showed in this updating analysis, a reference undamaged model is not available.

For these purpose, a twofold methodology was applied: (i) sensitivity analysis, maintaining the variables previously obtained, of the different damage areas through different FE bands along the damage quarter-spams; and (ii) applying a damage strategy, with different damage functions assumptions, to materialize the damage present in the structure (Fig. 10).

For the present case of study and considering the damage inspection (see Fig. 6), and the COMAC's values (see Fig. 9), an adaptation of the second and third approach was used (Fig. 10): sub-structuring technique with piecewise linear functions show in Eq. (6) for the first and fourth quarter spams (with a general damage), and a discrete damage shape function for the isolate crack shown in Eq. (7) (see Fig. 11).

Table 10
Summary of the updated variables (without consider the damage variables) obtained in the damage model calibration.

	Initial values	Lower bound	Upper bound	Update values
E_{SFRSCC} (GPa)	37.75	33.82	41.68	39.66
$E_{GFRP\text{-}FLAN}$ (GPa)	35.71	30.22	41.20	39.29
$E_{GFRP\text{-}WEB}$ (GPa)	23.98	19.15	28.81	28.81
E_{EPOXY} (N/m^2)	14.43×10^{10}	5.53×10^{10}	23.33×10^{10}	9.49×10^{10}
$E_{EPOXY\text{-}BOLT}$ (N/m^2)	15.03×10^{10}	4.27×10^{10}	25.79×10^{10}	13.13×10^{10}
K_{Ax} (N/m)	10×10^6	10×10^5	10×10^7	4.77×10^6
K_{Ay} (N/m)	10×10^5	10×10^4	10×10^6	8.98×10^5
K_{Bx} (N/m)	10×10^3	10×10^2	10×10^5	1.44×10^4
K_{Bx} (N/m)	10×10^5	10×10^4	10×10^6	4.77×10^5

$$N_{substructure,i}\begin{cases}\frac{x-x_{i-1}}{x_i-x_{i-1}} & x \in [x_{i-1}, x_i] \\ \frac{x_{i+1}-x}{x_{i+1}-x_i} & x \in [x_i, x_{i+1}] \\ 0 & otherwise\end{cases} \tag{6}$$

$$a_{discrete}(dmg, dist, ampl)\begin{cases} dmg\left(\frac{x_i - x_{dist-ampl}}{x_{dist} - x_{dist-ampl}}\right) & x \in [x_{dist-ampl}, x_{dist}] \\ dmg\left(\frac{x_{dist+ampl} - x}{x_{dist+ampl} - x_{dist}}\right) & x \in [x_{dist}, x_{dist+ampl}] \\ 0 & otherwise\end{cases} \tag{7}$$

where $N_{substructure}$ indicates the shape function for the substructure approach, x the centroid of the damage elements, x_i the border centroid between substructures, $a_{discrete}$ the damage function for the discrete approach, dmg the damage value of the function (between 0 and 1), $dist$ the distance from the origin to the point (into the discrete damage function), and $ampl$ the discrete damage aperture.

After defining the different shape functions, the damage can be applied following Eqs. (8) and (9),

$$K_{damage,i} = N_i(1 - a_i) \tag{8}$$

$$a_i = p * N_i \tag{9}$$

where $K_{damage,i}$ is the stiffness matrix which contains the damage values of the different elements affected by the damage for the shape function N_i, a_i is the damage coefficient and p is the design variables to be minimized. As a result the different values of the affected elements can ben obtained. Finally, once the different damage strategies were correctly defined, the Jacobian matrix *Jacob* needs to be re-formulated with the following considerations, Eq. (10):

$$\text{Jacob}_\theta = \begin{cases} \frac{\partial J}{\partial \theta} \rightarrow \text{if } \theta \text{ is an undamage variable} \\ \frac{\partial J}{\partial \theta} = \frac{\delta J}{\delta a_{sub}} N_{sub}(\theta) \rightarrow \text{if } \theta \text{ is an substructure variable} \\ \frac{\partial J}{\partial \theta} = \frac{\delta J}{\delta a_{dis}} \left[\frac{\delta N_{dis}(\theta)}{\delta \text{dmg}} \quad \frac{\delta N_{dis}(\theta)}{\delta x_{dist}} \quad \frac{\delta N_{dis}(\theta)}{\delta ampl}\right] \\ \rightarrow \text{if } \theta \text{ is an discrete variable} \end{cases} \tag{10}$$

where J is the objective function, θ variable to be updated, a and N (with the index *sub* for substructure and *dis* for discrete) the damage and shape functions and dmg, x_{dist}, $ampl$ the different variables of the discrete damage function. For the resolution of the derivatives, a finite difference approach was consider.

Table 11
Summary of the results, for the damage model, through the dynamical correlation values considered (relative error in frequencies, MAC values).

Vibration mode	f_{exp} (Hz)	f_{num} (Hz)	Error (%)	*MAC* (%)
1	6.40	6.61	3.28	100
2	8.16	8.33	2.08	100
3	12.13	12.33	1.65	96
4	20.79	20.51	−1.35	90
5	22.16	21.52	−2.89	89
6	23.74	24.09	1.47	86

Table 12
Summary of the results obtained in the damage model, through the static correlation values considered (relative error in displacement).

Load case	$disp_{exp}$ (mm)	$disp_{num}$ (mm)	Error (%)
A	−38.07	−39.15	2.82
B	−23.27	−23.80	2.27
C	−43.28	−43.71	0.98

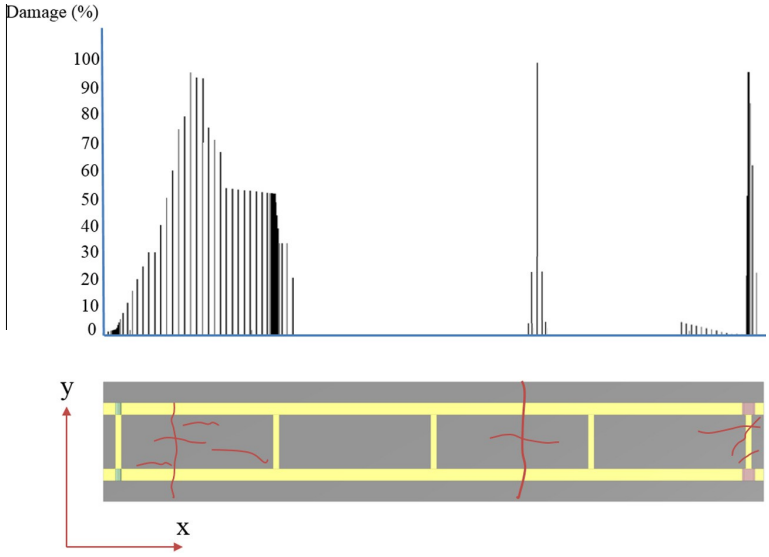

Fig. 12. Graphical comparison between the numerical and experimental damage obtained by the proposed methodology.

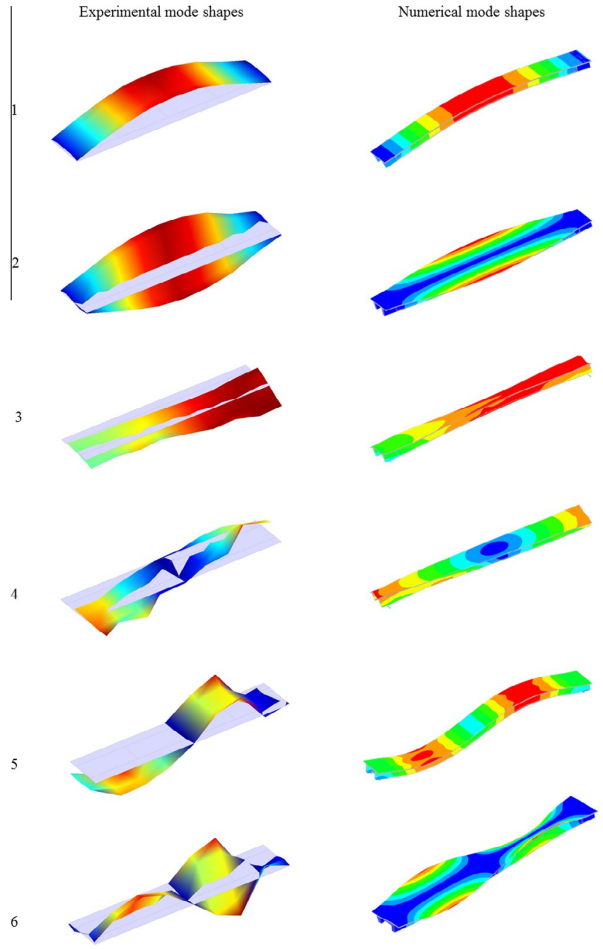

Fig. 13. Experimental and numerical mode shapes of the first six modes.

4.5. Robust calibration with damages functions

The damage presented by the footbridge can only be observed only in the intrados of the footbridge's deck. Considering this, only the lower elements of the footbridge's deck has been updated (by the proposed damage identification). As a result of the robust calibration a new model of the footbridge has been obtained (Table 10). This model presents a damage along its deck as show (Fig. 12).

Regarding the damages of the first and fourth quarterspans, as it was expected, a general damage was obtained with higher values next to the more damage areas, according with the visual inspection (Fig. 6). Also, through the discrete function, it was possible to identify the isolate crack, which is in the third quarterspan, at a distance of the deck origin equal to 7.60 m (in contrast to 7.37 m obtained in the visual inspection), originate by the presence of a transversal crack.

As a result, the final model shows a better similarity with the experimental results (see Tables 11 and 12). In terms of updating results, an average error in frequencies of 2.12% and an average MAC value of 93.50%. Considering the static behaviour, it was also observed an improvement in the results with an average error equal to 2.02%.

Finally (Fig. 13) presents a comparison between the different mode shapes identified experimentally and tuned numerically.

5. Conclusions

Nowadays, the evaluation of new constructive solutions and therefore the evaluation of new infrastructures implies a multidisciplinary task. Such analysis must involve: (i) mechanical tests of the different components; (ii) experimental programs to understand the global behaviour of the structure; and (iii) accurate numerical simulations to design, evaluate and predict its structural behaviour. Nevertheless, the interaction between different components (joints), boundary conditions and damage, are unavoidable considerations within a numerical simulation. In order to solve this, in the present paper it was shown a robust calibration method based on a non-linear least-squares method complemented by a hybrid strategy to detect and quantify the damage. The proposed methodology was validated with a high innovative structure: a hybrid footbridge based on a SFRSCC deck and GFPR pultruded profiles. The model updating analysis was carried out with results from experimental data (static and dynamic tests). It considers the stiffness of the different joints (L-union and GFPR main girders-deck union), non-perfect supports and damage as a set of linear damage functions.

Finally, an accurate damage identification analysis was performed, arising in an accurate model. However, there are always further needs of investigations in order to improve results, mainly the MAC's values for the fifth mode shape and to consider the cracks direction in the damage functions as a design variable to better improve their effects.

References

[1] Mendes P, Barros J, Sena-Cruz J, Teheri M. Influence of fatigue and aggressive exposure on GFRP girder to SFRSCC deck all-adhesive connection. Compos Struct 2014;110:152–62.
[2] Nguyen H, Mutsuyoshi H, Zatar W. Hybrid FRP-UHPFRC composite girders: part 1 – experimental and numerical approach. Compos Struct 2015;125:631–52.
[3] Bel Hadj Ali N, Rhode-Barbarigos L, Pascual Albi AA, Smith IFC. Design optimization and dynamic analysis of a tensegrity-based footbridge. Eng Struct 2010;32:3650–9.
[4] Yeh F-Y, Chang K-C, Sung Y-C, Hung H-H, Chou C-C. A novel composite bridge for emergency disaster relief: concept and verification. Compos Struct 2015;127:199–210.
[5] Chen Z, Cao H, Zhu H, Hu J, Li S. A simplified structural mechanics model for cable-truss footbridges and its implications for preliminary design. Eng Struct 2014;68:121–33.
[6] Cabral-Fonseca S, Correia JR, Rodrigues MP, Branco FA. Artificial accelerated ageing of GFRP pultruded profiles made of polyester and vinylester resins: characterisation of physical–chemical and mechanical damage. Strain 2012;48:162–73.
[7] Liao K, Schultheisz CR, Hunston DL. Effects of environmental aging on the properties of pultruded GFRP. Compos Part B Eng 1999;30:485–93.
[8] Gonilha JA, Correia JR, Branco FA. Creep response of GFRP–concrete hybrid structures: application to a footbridge prototype. Compos Part B Eng 2013;53:193–206.
[9] Keller T, Schaumann E, Vallée T. Flexural behavior of a hybrid FRP and lightweight concrete sandwich bridge deck. Compos Part A Appl Sci Manuf 2007;38:879–89.
[10] Deskovic N, Triantafillou TC, Meier U. Innovative design of FRP combined with concrete: short-term behavior. J Struct Eng 1995;121:1069–78.
[11] Gonilha J, Barros J, Correia J, Sena-Cruz J, Branco F, Ramos L, et al. Static, dynamic and creep behaviour of a full-scale GFRP-SFRSCC hybrid footbridge. Compos Struct 2014;118:496–509.
[12] Thambiratnam DP, Perera NJ, Abeysinghe CM, Huang M-H, De Silva SS. Human activity-induced vibration in slender structural systems. Struct Eng Int 2012;22:238–45.
[13] Gonilha JA, Correia JR, Branco FA. Dynamic response under pedestrian load of a GFRP–SFRSCC hybrid footbridge prototype: experimental tests and numerical simulation. Compos Struct 2013;95:453–63.
[14] ISO. ISO 527-1:2012. Plastics-determination of tensile properties. Genève. 2012.
[15] ASTM. ASTM D 695. Standard test method for compressive properties of rigid plastics. West Conshohocken, Pennsylvania. 2002.
[16] Hodgkinson JM. Mechanical testing of advanced fibre composites. Elsevier; 2000.
[17] Barros J, Pereira E, Santos S. Lightweight panels of steel fiber-reinforced self-compacting concrete. J Mater Civil Eng 2007;19:295–304.

[18] IPQ IpIQ. NP EN 12390-3:2011. Testing hardened concrete part 3: compressive strength of test specimens, Caparica; 2011.
[19] RILEM. International RILEM workshop on test and design methods for steel fibre reinforced concrete-background and experiences; 2003.
[20] Firmo JP, Correia JR, França P. Fire behaviour of reinforced concrete beams strengthened with CFRP laminates: protection systems with insulation of the anchorage zones. Compos Part B Eng 2012;43:1545–56.
[21] Gonilha J, Aquino A, Correia J, Branco F. Experimental evaluation of the GFRP/ECC connection–shear connection tests: phase 1. ICIST internal project report A. 5; 2010.
[22] Gade S, Møller N, Herlufsen H, Konstatin-Hansesn H. Frequency domain techniques for operational modal analysis. 1st IOMAC Conference; 2005.
[23] Diana T. Finite element analysis user's manual-release 9.4. 4. TNO DIANA; 2011.
[24] Teughels A, De Roeck G. Damage assessment of the Z24 bridge by FE model updating. Key engineering materials. Trans Tech Publ; 2003 [p. 19–26].
[25] Ramos LF, Marques L, Lourenço PB, De Roeck G, Campos-Costa A, Roque J. Monitoring historical masonry structures with operational modal analysis: two case studies. Mech Syst Signal Processing 2010;24:1291–305.
[26] Mishra AK, Chakraborty S. Development of a finite element model updating technique for estimation of constituent level elastic parameters of FRP plates. Appl Math Comput 2015;258:84–94.
[27] Simoen E, De Roeck G, Lombaert G. Dealing with uncertainty in model updating for damage assessment: a review. Mech Syst Signal Processing 2015;56–57:123–49.
[28] Coleman TF, Li Y. An interior trust region approach for nonlinear minimization subject to bounds. SIAM J Optim 1996;6:418–45.
[29] Allemang RJ, Brown DL. A correlation coefficient for modal vector analysis. Proceedings of the 1st international modal analysis conference. SEM, Orlando; 1982. p. 110–6.
[30] Foti D. Dynamic identification techniques to numerically detect the structural damage. Open Constr Build Tech J 2013;7:43–50.
[31] Rytter A. Vibrational based inspection of civil engineering structures: unknown; 1993.
[32] Titurus B, Friswell M. Regularization in model updating. Int J Numer Meth Eng 2008;75:440–78.
[33] Sánchez-Aparicio LJ, Riveiro B, González-Aguilera D, Ramos LF. The combination of geomatic approaches and operational modal analysis to improve calibration of finite element models: a case of study in Saint Torcato Church (Guimarães, Portugal). Constr Build Mater 2014;70:118–29.

Chapter III

Photogrammetric, geometrical and numerical strategies to evaluate initial and current conditions in historical constructions: a test case in the church of San Lorenzo (Zamora, Spain).

remote sensing

MDPI

Article

Photogrammetric, Geometrical, and Numerical Strategies to Evaluate Initial and Current Conditions in Historical Constructions: A Test Case in the Church of San Lorenzo (Zamora, Spain)

Luis Javier Sánchez-Aparicio *, Alberto Villarino, Jesús García-Gago and Diego González-Aguilera

Received: 16 September 2015; Accepted: 8 January 2016; Published: 13 January 2016
Academic Editors: Fabio Remondino, Parth Sarathi Roy, Randolph H. Wynne and Prasad Thenkabail

Department of Land and Cartographic Engineering, University of Salamanca, High Polytechnic School of Avila, Hornos Caleros, 50, 05003 Avila, Spain; avillarino@usal.es (A.V.); jesusmgg@usal.es (J.G.-G.); daguilera@usal.es (D.G.-A.)
* Correspondence: luisj@usal.es; Tel.: +34-920-353-500; Fax: +34-920-353-501

Abstract: Identifying and quantifying the potential causes of damages to a construction and evaluating its current stability have become an imperative task in today's world. However, the existence of variables, unknown conditions and a complex geometry hinder such work, by hampering the numerical results that simulate its behavior. Of the mentioned variables, the following can be highlighted: (i) the lack of historical information; (ii) the mechanical properties of the material; (iii) the initial geometry and (iv) the interaction with other structures. Within the field of remote sensors, the laser scanner and photogrammetric systems have become especially valuable for construction analysis. Such sensors are capable of providing highly accurate and dense geometrical data with which to assess a building's condition. It is also remarkable, that the latter provide valuable radiometric data with which to identify the properties of the materials, and also evaluate and monitor crack patterns. Motivated by this, the present article investigates the potential offered by the combined use of photogrammetric techniques (DIC and SfM), as well as geometrical (NURBs and Hausdorff distance) and numerical strategies (FEM) to assess the origin of the damage (through an estimation of the initial conditions) and give an evaluation of the current stability (considering the deformation and the damage).

Keywords: digital image correlation; structure from motion; global metric Hausdorff; local metric Hausdorff; non-uniform rational B-Splines; finite element modelling; vernacular architecture; historical construction

1. Introduction

The conservation of built heritage is today considered a fundamental aspect of modern society. Their artistic, cultural, and intrinsic value make these constructions extremely important. Complementary to this, the lack of the building's own mechanical values and the characteristic behavior of its masonry, the complex interaction between components, and the lack of documentation, make the analysis of such constructions remarkably difficult. Currently, and derived from these considerations, numerous regulations propose the integration of different approaches among which are [1]: (i) the study of the construction's history; (ii) inspection; (iii) monitoring; and (iv) structural analysis.

Regarding the numerical calculations, the static graphic [2] and limit analyses [3] traditionally provided the necessary tools to study the stability and bearing capacity of historical structures [4]. However, such numerical strategies have among their drawbacks the difficulty to evaluate damages [1].

In contrast with these models, the Finite Element Method (FEM) has been widely used for the evaluation of historical buildings at different levels; from complex and large constructions through macromodelling techniques [5], to the use of micromodelling strategies [6], where the units are independently discretized, or homogenized [7]. However, the large number of involved variables, as well as interaction with other structures, conditions the results.

It is in the field of built constructions where remote sensors and especially photogrammetric and laser scanner systems have proven great worth for their analysis [3,8–10]. These sensors are able to provide accurate and dense geometric and radiometric values with which to assess these buildings, as well as obtaining the data through non-intrusive means. Despite this, the data they provide (in form of dense and accurate point clouds) is largely untapped, since it is only used for the construction of simplified CAD models [10].

On one hand, the present article introduces two novel robustness parameters (based on geometrical components) in order to increase their applicability, obtained from the symmetrical Hausdorff distance [11]. These parameters, called Global Hausdorff metric (GHm_s) and Local Hausdorff metric (LHm_s), help ascertain whether the variables or simulated conditions improve or worsen the numerical results, in comparison with the real deformation provided by the photogrammetric and laser scanner systems.

On the other hand, the article introduces a methodology based on a Non-Uniform Rational B-Splines (NURBs) modelling strategy, with the purpose of providing an accurate geometrical model (with the current deformation and damage) for the evaluation of the current stability of the construction. This strategy is able to take advantage of the properties provided by the Structure from Motion products: (i) density; (ii) accuracy; and (iii) photorealistic texture, within a numerical environment.

In order to confirm the feasibility of the proposed geometrical strategies (GHm_s, LHm_s and NURBs modelling), they are applied to a case study: the dome of the church of San Lorenzo in Sejas de Aliste (Zamora, Spain). This construction, built in brick masonry, has suffered severe structural damages, shown through significant deformation, cracking and plastic hinges that reduce its bearing capacity. It seems necessary to perform a structural evaluation in order to design efficient restoration actions.

The article is organized as follows: Section 1 consists of an introduction and brief state of the art, Section 2 describes the different image-based techniques that were employed; Section 3 is made up of the description of the construction, the current deformation, damage, and the numerical aspect through the FEM; Section 4 describes two robustness indices based on geometrical discrepancies, a manual calibration of the model and a complementary strategy to evaluate the current stability of the construction (considering the complex geometry and the presented cracking); and finally, Section 5 shows the conclusions.

2. Image Based Approaches: Digital Image Correlation and Structure from Motion

The great diversity of approaches today, along with their flexibility, place image-based procedures as a suitable solution for the analysis of constructions [3,9,12], materials [13,14], and pathologies [8].

The different methodologies that comprise this approach, particularly in the field of numerical evaluation of constructions, highlight: (i) Digital Image Correlation (DIC); and (ii) image-based modelling procedures. While the former provides mechanical data of materials and constructive solutions (in the form of displacement and strains), the latter allows the definition of a dense, accurate, and photorealistic geometrical model of the construction. Their combination provides relevant information for the numerical analysis of the structure.

2.1. 2D Digital Image Correlation

A wide variety of methodologies has been developed and used to study material and union behavior. Some of these are [14,15]: (i) Moiré interferometry; (ii) Holography interferometry; (iii) Shearography; and (iv) Digital Image Correlation.

Remote Sens. **2016**, *8*, 60

These methodologies prove to have important advantages, compared to traditional methods based on strain gauges or LVDT's (Linear Variable Differential Transformer) such as their non-invasiveness and their full-field data information. In comparison, traditional methods provide only local information and require direct contact with the tested material. Within this wide range of techniques, the use of Digital Image Correlation (DIC) stands out.

To characterize the materials used in the dome, various compression tests were performed separately on each material (three in each material) during the experimental campaign that was carried out. Considering the procedure defined by [16], an extra specification, such as the mortar joint material (made by gympsum mortar), was considered.

In order to verify the flexibility and accuracy of the shown method, one standard sensor was used for both the DIC and the SfM: a digital reflex camera Canon 500D. However, in contrast to the image-based modelling strategy, DIC requires the preparation of the analyzed specimen, following the approach defined by [16]: (i) MIG (Mean Intensity Gradient) evaluation [17] of the speckle pattern; (ii) camera pose estimation [18]; and (iv) camera calibration [19].

Once the specimen has been correctly pre-processed, different images were captured during the test (Figure 1). Also, concerning the test setup, a large focal distance and working distance were used in order to minimize the geometrical distortion, out of plane displacements (approximation to a telecentric lens system) [20], depth of field, and light conditions.

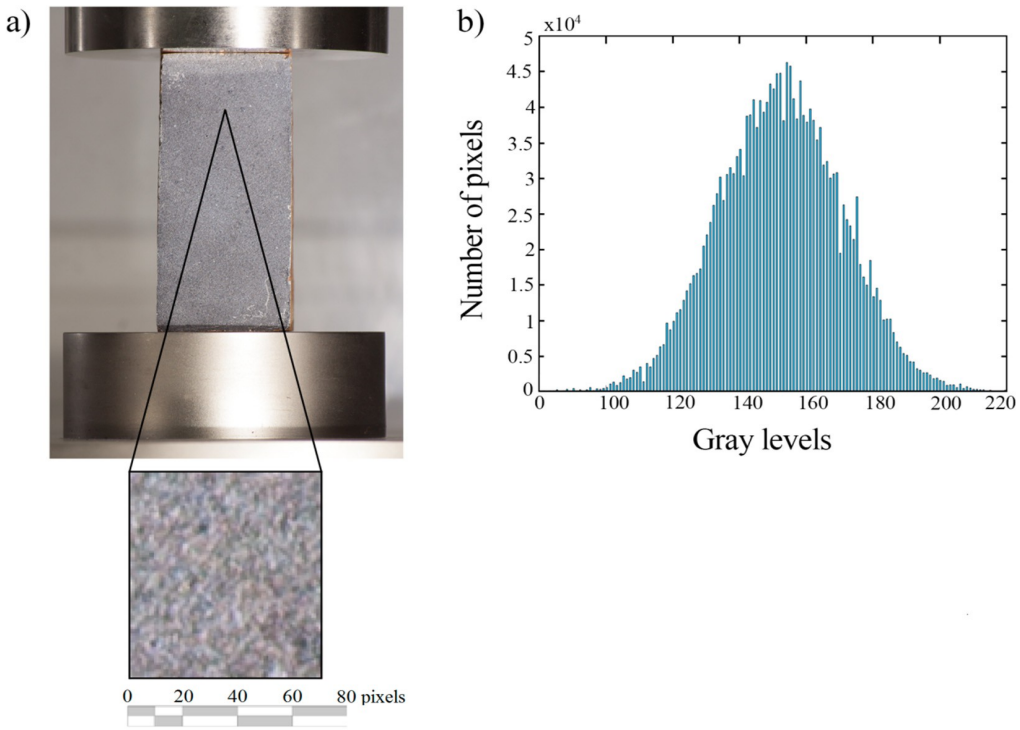

Figure 1. (**a**) Detail view of the brick and speckle pattern applied during the Digital Image Correlation (DIC) test; (**b**) Histogram of the speckle pattern.

The basic principle of DIC is the tracking (or matching) of the different areas of the images which were captured during the test (before and after deformation occurs), called subsets. As an initial approximation of this tracking, a correlation coefficient (generally the Zero Normalized Cross Correlation) [20] is used. Later, this initial approximation is optimized by the use of a non-linear

strategy (such as the Inverse Compositional Gauss Newton method) [20] which allows the evaluation of the displacement suffered by the subset along the different captured images (Figure 2) [16].

Complemented to this optimization process an interpolation process (based on splines) is used with the aim of obtain sub-pixel accuracy [20]. Considering multiple subsets in the image, their analysis can provide a full-field displacement. Later, the strains suffered by the specimen during the test, which allow the evaluation of its mechanical properties, can be obtained by a direct relationship between the obtained displacement on the measurement point and the initial length of the virtual extensometers [16]. A total of three virtual extensometers were placed on the ROI: (i) A-A′ and B-B′ in the longitudinal direction; and (ii) C-C′ in the transversal direction.

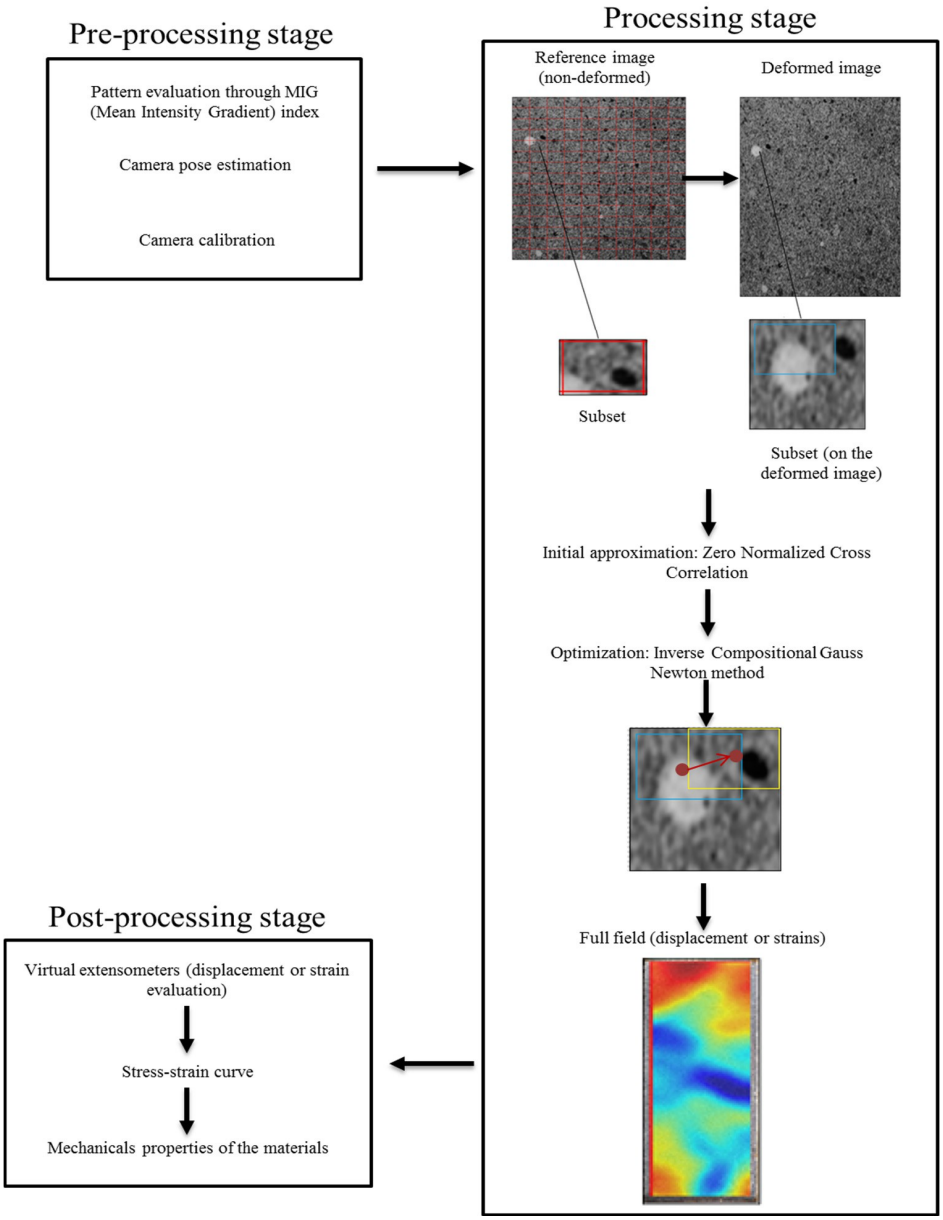

Figure 2. Digital Image Correlation general outline. In red the reference subset, in blue the initial seed, and in yellow, the final location of the subset.

Remote Sens. **2016**, *8*, 60

Concerning accuracy, there are different studies [15,21,22] that endorse the DIC's precision for the assessment of the material's mechanical properties. For a standard test configuration, the accuracy may range from values of 0.01–0.04 pixels. Considering a conservative threshold at 0.1 pixels, and an acceptable accuracy for the test of 0.01 mm (from which the critical pixel size is set at 0.1 mm), the test's configuration is shown in (Table 1).

Table 1. Summary of the different properties set during the Digital Image Correlation (DIC) test carried out with a Canon EOS 500D and a macrolens system 70–300 mm.

Values Adopted during the Digital Image Correlation (DIC) Test	
Aperture	7.1
Focal length (mm)	200
Working distance (mm)	2700
Pixel size (mm)	0.063
Acquisition frequency (Hz)	0.33

Once the stress-strain curve has been obtained (by a relationship between the stress applied by the compression press and the strains obtained by DIC) (Figure 3b), it is possible to extract the mechanical properties of the materials as follows (Table 2): (i) the Young Modulus was considered as the ratio between one third of the maximum force achieved and the mean strain provided by the longitudinal extensometers (A-A′ and B-B′); (ii) for the Poisson ratio, the relationship between the strains provided by the longitudinal extensometers and those obtained by the transversal extensometer (C-C′) was taken into account; and (iii) the compression strength was considered as the maximum pressure supported by the specimen.

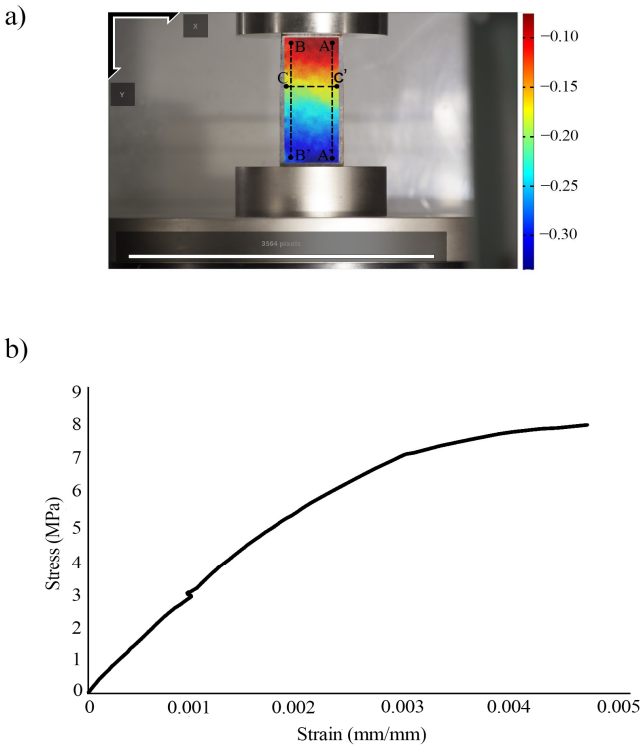

Figure 3. Results after the experimental campaign (2D DIC). (**a**) Deformation measurement, expressed in pixels, between two captures and positioning of the virtual extensometers; (**b**) Stress-strain curve obtained with the virtual extensometer A-A′.

Table 2. Mechanical properties obtained by the performed DIC test.

Mechanical Properties Obtained by the DIC Test		
	Clay brick	Gypsum mortar
E (GPa)	3.10 ± 0.30	1.15 ± 0.06
ν (-)	0.22 ± 0.05	0.23 ± 0.02
fc (MPa)	7.80 ± 0.90	2.12 ± 0.10

To assess the accuracy of the previously mentioned procedure, a comparative study was carried out, between the strain rate applied by the compression press (with an average value of -1.77×10^{-6} s^{-1}), and the one obtained by the different performed DIC tests and the different virtual extensometers used (with an average value of -1.93×10^{-6} s^{-1}). The results obtained demonstrate the accuracy and suitability of the applied configuration and algorithms, with an estimated precision of 0.056 pixels (which correspond to an approximate value of 3.53 μm). This value proves to be lower than the previously shown critical value.

2.2. Image-Based Modelling: Structure from Motion

In recent years the image-based modelling strategy, called Structure from Motion (SfM), has positioned itself as an attractive alternative to laser scanning systems. Its flexibility—as it can be integrated into different types of platforms (e.g., UAV [9])—low-cost, and qualities of the point cloud (high density, photorealistic texture, and accuracy) place the solution at a vantage position in the evaluation of historical buildings [23].

This technique integrates within its operating structure the advantages of computer vision (automation and flexibility) and photogrammetry (accuracy and reliability) [23] to obtain high density three dimensional models whose accuracy can compete with those of the laser scanner system [24,25].

For this case study, a standard SfM strategy is applied, comprising the following stages: (i) automatic extraction and keypoint matching by applying the Affine-Scale Invariant Feature Transform (ASIFT) algorithm [26]; (ii) automatic hierarchical orientation of images; and (iii) dense model generation through the MicMac algorithm. For further details on this methodology see [12]. Concerning the photogrammetric network a convergent protocol was used, combining a total of 32 cameras with high overlap (around 90%) and throwing a mean GSD (Ground Sample Distance) of 1.61 mm. Complementary to these, different circular targets (along the lower part of the pendentive) were used to scale the model (this measurement were taken by a total station using a radiation approach).

As a result of the implementation of the above-mentioned methodology it is possible to obtain a dense and photorealistic texture point cloud (Figure 4a). Afterwards, applying CAD conversion techniques (meshing, surface parameterization, extrusions, revolutions, *etc.*), or even generating true-ortho-images, increase further the applicability of the obtained product. More precisely, they help to accurately build CAD models suitable for subsequent numerical simulations, as well as complementary products, which analyze patterns of deformation and cracking for the pathological characterization of the structure [9] (Figure 4b).

Concerning the total error, associated with this point cloud, a quadratic error propagation was used Equation (1). Into this approach, two sources were considered: (i) the error coming from the bundle adjustment of the photogrammetric network; and (ii) the error corresponding to the scaling process Equation (2).

$$\varepsilon_t = \sqrt{{\varepsilon_p}^2 + {\varepsilon_s}^2} \quad (1)$$

$$\varepsilon_s = \sqrt{2{\varepsilon_i}^2 + {\varepsilon_m}^2} \quad (2)$$

where ε_t represents the total error; ε_s the scale error; ε_p the error associated with the photogrammetric network; ε_i the origin error stablished as $\sqrt{2} * (\frac{pixelsize}{\gamma})$, where γ is the subpixel accuracy of the target detection algorithm (estimated in 0.5); and ε_m the error associated with the total station.

As a result a budget error of ε_t = 4.38 mm was obtained (with values of ε_P = 3.22 mm, ε_i = 1.14 mm, ε_m = 2.50 mm, and ε_s = 2.97 mm).

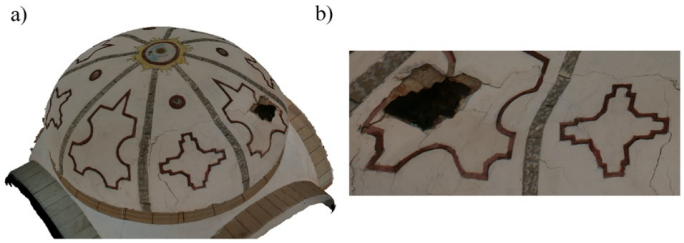

Figure 4. (**a**) 3D model obtained by the proposed methodology; (**b**) Detail view of the most damaged section through the texture model.

3. Structural Evaluation of San Lorenzo's Dome

3.1. San Lorenzo Church

The church is built with irregular masonry walls (slabs of slate) fixed with lime mortar and at the corners finished with granite masonry. The parish church of San Lorenzo in Sejas de Aliste is located in the region of Aliste, Zamora province (Spain), 32 m long and 17 m wide, it belongs to the family of temples with transept crossing, Latin cross-shaped floor plan, and transept and nave at different heights (Figure 5).

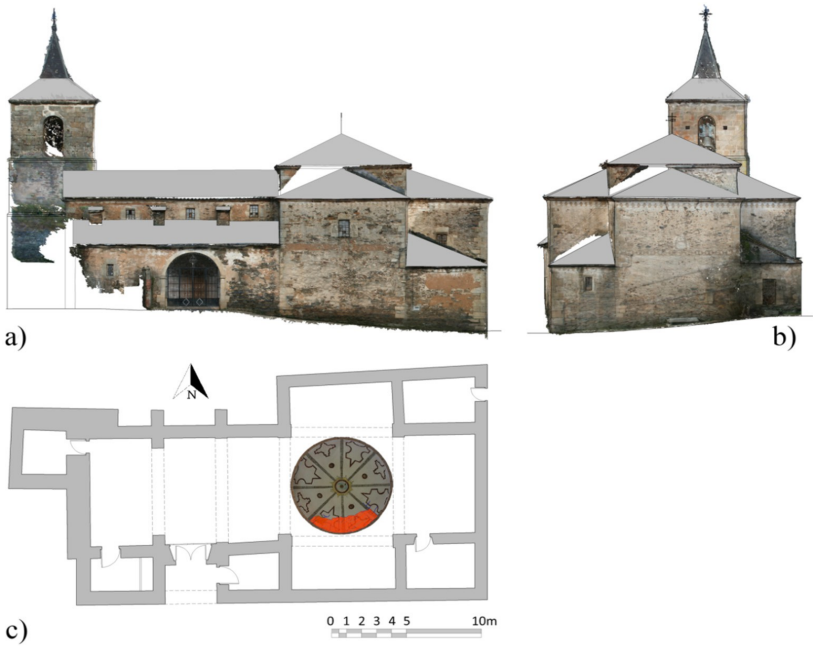

Figure 5. San Lorenzo church: (**a**) Orthophoto of the main façade through the methodology proposed; (**b**) Orthophoto of the west façade (chancel) of the construction; (**c**) Floor plan-view of the church, red color indicates the damaged area of the dome.

Remote Sens. **2016**, *8*, 60

The transept crossing is the most representative element of this temple. Its importance in the building is highlighted in the interior through the semi-elliptical dome that shelters the whole crossing. Its eight ribs marked with bands stand out. The transept is highlighted in the outside as well, covering the dome with a hipped roof that rises above the nave and transept height. This roof is built with a pavilion-shaped chestnut-timber framing, with regularly placed rafters that lean on the main beams and bear the load of the roof, made up of curved tiles and wooden roof boards (Figure 6a). Overall stability is obtained by use of tie beams at the top of the bearing walls, which collect the loads of the rafters and the hip rafters or main beams. Angle-ties, placed at 45° in each corner under the hip rafters prevent the transversal deformation of the tie beams (Figure 6a).

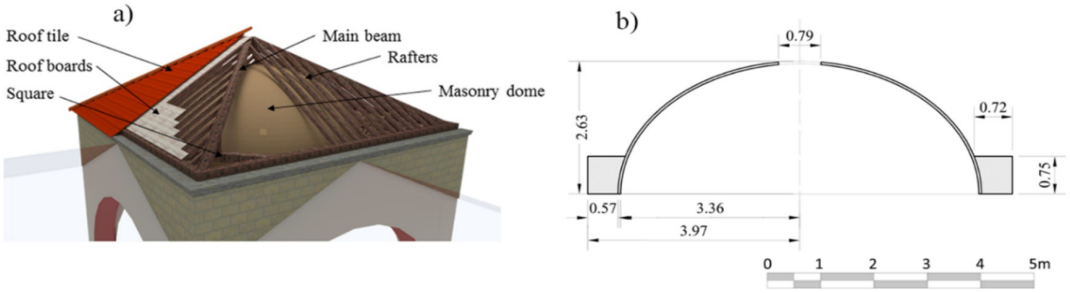

Figure 6. (**a**) Constructive section of the church's transept; (**b**) Transversal section of the dome geometry (initial state estimated by the Structure from Motion (SfM) point cloud) with dimensions in meters.

Concerning the dome, the construction has an estimated diameter of 6.72 m and a total height (measured from the pendentive) of 2.63 m. This structure was built with traditional tile brick and gypsum mortar, reaching a total thickness of 5.00 cm. It resembles, from a construction point of view, a Catalan vault (Figure 6b). It is also worth mentioning the presence of an infill (basically composed of a mixture of sand, clay and fragments of bricks with a medium compaction) at the support of the dome. This infill reaches a total height of 0.75 m and an average thickness of 0.65 m, and its presence contributes to the stability of the construction.

3.2. Present Damage and Deformation

The characterization of both, deformations and cracking patterns, is key to understanding the structure in terms of stability and safety. The high density, accuracy, and photorealistic texture of the point cloud obtained by the proposed methodology (Section 2.2) can address this task foregoing any need of physical contact with the structure. Through evaluation of the obtained product, it is possible to obtain a hypothesis for the origin of the damage.

It is worth noting that there is widespread damage in the area enclosed by three ribs (corresponding to the southern part of the dome). This area has two main cracks, in the parallel direction, which are interconnected through the presence of two plastic hinges. At its maximum, there is a deflection of 19.70 cm (compared to the initial estimated model) (Figure 7).

These structural pathologies seem to be related to the presence of assymetric loads acting on part of the dome's shell (Figure 7a). More specifically the current damages, which are located under the south wing, can be attributed to a failure of the timber structure.

On one hand, the evaluation of photogrammetric products (which are the result of the previously defined SfM strategy) allows an estimation of the possible causes of the dome's damage. However, it is required to have numerical strategies to verify these assumptions and assess the current state of the construction. For the present case study, and considering the hypothesis of failure of the timber structure several numerical analyses were performed: (i) numerical evaluation of the timber structure for the worst load case: snow; (ii) evaluation of the dome's stability under self-weight; and (iii) numerical evaluation of the interaction timber-dome as a result of a timber failure.

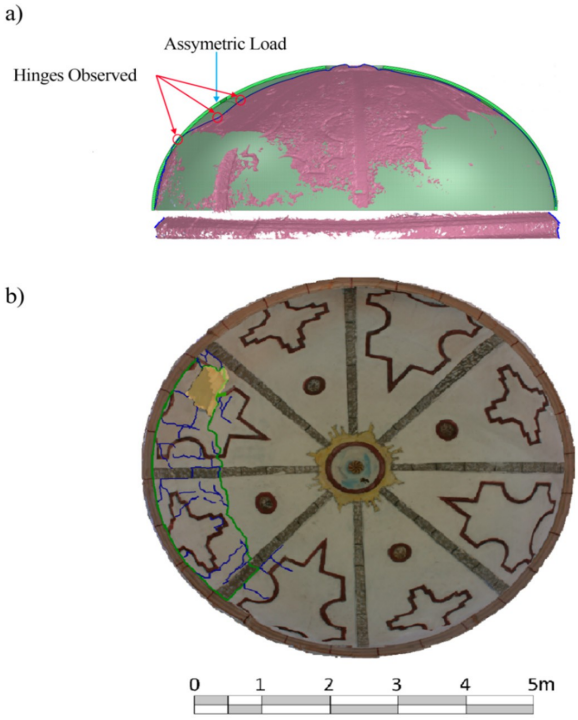

Figure 7. Results of the visual inspection over the different photogrammetric products: (**a**) Surface comparison between the initial proposed model and the most deformed one estimated by the SfM point cloud; (**b**) Damage inspection in the orthophoto, in green the main observed cracks, in blue the secondary cracks, in yellow the material removal.

Previous investigations carried out by [16], verified the stability of the timber structure for the most adverse load case: the presence of snow. Yielding a maximum deflection of 2.35 cm, it proves to be insufficient in order to interact with the dome. Considering these results, it is possible to conclude that the interaction between the cover and the dome seems to be linked with the presence of pathological agents (mainly moisture and biological organisms) which reduce the bearing capacity of the timber structure until it fails and rests on the dome.

3.3. Numerical Simulation of the Initial State of the Dome: Self-Weight and South Wing Support

Understanding the degradation mechanisms present in the construction requires a geometrical model of its initial state, a material characterization, as well as its boundary conditions, and load assessment. According to these, several numerical simulations (through non-linear static analysis) were performed in order to understand the causes and the construction's initial conditions. Several improvements, regarding the geometric and mechanical aspects, are introduced in comparison to the previous investigations performed by [16]: (i) consideration and modelization of the infill-dome interaction; and (ii) account of gypsum as union material.

Regarding the mechanical aspect, a macromodelling strategy of the masonry was followed. This technique blends the bricks, mortar joints as well as the brick-mortar interface into one continuum assuming homogeneous material properties (Table 3). Also, the recommendations exposed by reference [6,27] were considered. An initial estimation of the masonry's Young modulus was estimated using the formulas displayed in [28], setting the initial Young modulus at 2.54 GPa. However, further visual inspections showed the presence of an erratic masonry with low overlap between units. In accordance with this, a reduction of the initial Young modulus was considered for subsequent

simulations (half of the initial estimated), yielding a final value of 1.22 GPa, analogous to those used in similar studies [7,29].

Table 3. Mechanical properties adopted for the macromodelling of the masonry.

Mechanical Properties for the Masonry Structure		
E_m (GPa)	Young Modulus	1.22
δ_m (kg/m^3)	Density	1800.00
ν_m (-)	Poisson coefficient	0.25
$f_{t,m}$ (MPa)	Tensile strength	0.16
$f_{c,m}$ (MPa)	Compressive strength	1.60
$d_{t,m}$ (mm)	Ductility index in tensile	0.093
$d_{c,m}$ (mm)	Ductility index in compression	1.6
$\beta_{c,m}$ (-)	Shear retention	0.2

For the numerical simulation of the infill, a Morh-Coulomb failure criterion was considered, with its mechanical properties set according to the visual inspection (medium compaction) and the recommendations shown by [7,29,30] (Table 4).

Table 4. Mechanical properties adopted for the infill simulation.

Infill Mechanical Properties		
E_i (GPa)	Infill Young Modulus	0.80
δ_i (kg/m^3)	Infill density	1800.00
G (GPa)	Infill shear modulus	$E_i/2$
f_i (MPa)	Cut-off tension	0.02
Φ_i (deg)	Infill friction angle	39
c_i (MPa)	Infill cohesion	$1 \times f_i$

Concerning the load (for the numerical evaluation of the interaction between timber structure and the dome), a value of 8000 N was considered, resulting from the combination of different loads: (i) 650 N/m^2 for the arabic tiles and wooden board; and (ii) 400 N/m^2 for the snow load. Finally, the numerical model (for both simulations), had a total of 46,181 high order solid elements (CTE30) [31] (Figure 8a).

It is possible to observe that in the absence of external loads acting on the dome, the structure seems to be stable under its own weight (Figure 8b). In spite of this, considering the support of the south wing (roof tile, boards, and rafters), the dome begins to present damage (cracking) and its deformation tendency (Figure 8c) seems to be similar to the one shown in the photogrammetric model (Figure 7a).

However, in terms of deformation, considering for this purpose six control nodes along the damage area (Figure 8a), the model exhibits high rigidity. This suggests that the initial mechanical conditions are inadequate to reproduce the damage and deformation presented in the dome (Table 5).

Table 5. Comparison between the obtained and expected displacement of the control nodes in the numerical model (initial considerations).

Control Node	Displacement Obtained (mm)	Displacement Expected (mm)
54	1.95	148.00
20256	0.48	46.00
56	1.57	198.00
21125	0.54	52.00
443	2.12	196.00
64123	0.57	25.00

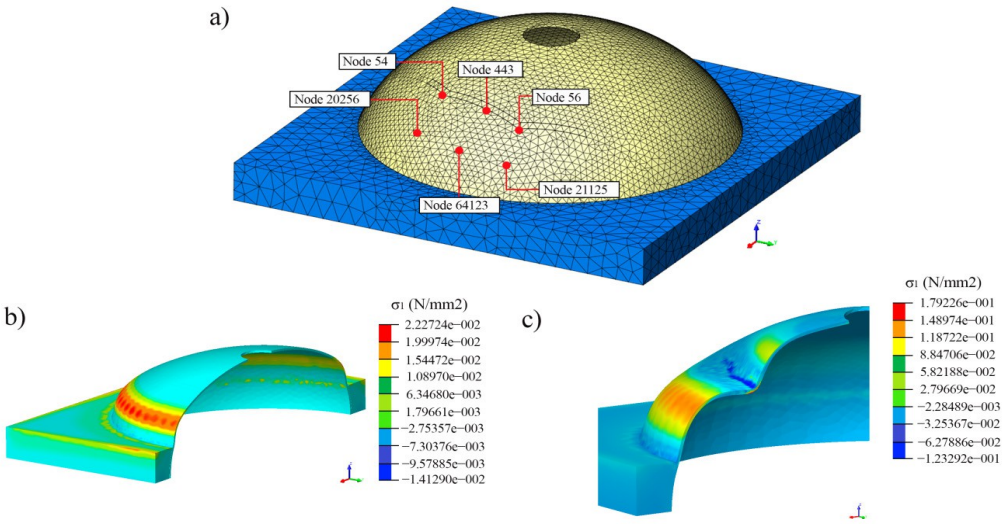

Figure 8. (**a**) Isometric view of the mesh and the control points (nodes) used for the numerical simulations; (**b**) First principal stress distribution, expressed in N/mm^2 for the self-weight case; (**c**) First principal stress distribution, expressed in N/mm^2, for the numerical model which considers the asymmetric load.

The high discrepancies shown in the previous numerical simulation suggest the need for an optimization of the mechanical properties. However, performing such an optimization requires inevitably having robustness indices to quantify the level of improvement/worsening introduced by the different variable's variations.

Exploiting the advantages offered by the SfM or laser scanner systems, two novel robustness parameters (based on geometric discrepancies) are proposed: (i) a global parameter, based on the similarity between the numerical and real model; and (ii) a local index which provides data about the geometrical variations introduced by the new variables considered in different areas of the construction.

4. SfM, NURBS Modelling, Global and Local Hausdorff Metrics: Geometrical Strategies to Improve the Knowledge about the Initial and Current State of the Constructions

4.1. Global and Local Hausdorff Metrics as Geometric Accuracy Indices

The Hausdorff distance or Hausdorff metric is used in a wide range of fields, such as point cloud [32] and meshes [33] comparison, object recognition [34], and image comparison and matching [35]. This metric proves to be a robust strategy for the similarity evaluation of two compact and non-empty sub-sets within a metric space. It is formulated as follows Equations (3) and (4):

$$d(y, X) = \min_{x \in X} ||y - x||_2 \quad (3)$$

$$d_H(Y, X) = \max_{y \in Y} d(y, X) \quad (4)$$

where $||.||_2$ stands for the Euclidean norm; *min* the minimum value (distance); *max* the maximum distance; X and Y are the two compact sub-sets defined by the numerical and photogrammetric nodes; and x and y the considered points inside these sub-sets.

It is worth mentioning that, considering the previously defined concept of Hausdorff distance, the value of the norm does not have a symmetrical nature; it is therefore different in each direction ($d_H(X,Y) \neq d_H(Y,X)$). For that reason, the symmetrical Hausdorff distance d_{SH} Equation (5) is used as metric comparison to avoid potential errors of geometrical similarity. This way a more robust solution is provided for geometry comparison.

$$d_{SHi} = \max\{d_H(y, X), d_H(x, Y)\} \quad (5)$$

where d_{SHi} is the symmetrical Hausdorff distance; of sub-set i, between models (numerical and photogrammetric); and x and y are two points that respectively belong to sub-sets X and Y.

On the other hand, understanding the global structural behavior of the analyzed construction inevitably requires several numerical analyses in order to adapt the simulated behavior to the real one. It is necessary to take into account the consideration that new conditions or new values of variables may worsen or improve the global and/or local result of the structure. It is therefore possible to define, out of the previously shown comparison metric Equation (3), two novel geometrical indices of robustness that represent improvements or worsening in the new numerical simulations in comparison to a reference model, considering the different variations of the variables or conditions: Global Hausdorff metric Equation (6); and Local Hausdorff metric Equation (7).

$$GHm_s = \left(\frac{\sum_{i=1}^{n} d_{SH}(\mathrm{i}) - \sum_{i=1}^{n} d_{SH_b}(\mathrm{i})}{\sum_{i=1}^{n} d_{SH_b}(\mathrm{i})} \right) \times 100 \quad (6)$$

$$LHm_s(\mathrm{i}) = \frac{d_{SH}(\mathrm{i})}{d_{SH_{ref}}(\mathrm{i})} \quad (7)$$

where GHm_s represent the Global Hausdorff metric index and LHm_s the Local Hausdorff metric index, $d_{SH(i)}$ the symmetrical Hausdorff distance to cluster i considered for the model; $d_{SHb}(i)$ the symmetrical Hausdorff distance for cluster i of the base model (the model that results from the geometrical discrepancies between the initial model and the photogrammetric one); and $d_{SHref}(i)$ the symmetrical Hausdorff distance from cluster i to the reference one (which may be the base model).

On one hand, GHm_s is able to provide a global value, expressed in percentage, for the improvement/worsening of the numerical simulation model in comparison to the model that was considered as base model. On the other hand, LHm_s provides a comparison of the variations between the numerical model and the reference model at a local level (values lower than one indicates a local improvement and values higher than one, a worsening).

For this case study, the reference model was considered to be the base model, obtained by the application of Equation (3) between the photogrammetric model and the non-deformed numerical model (Figure 9).

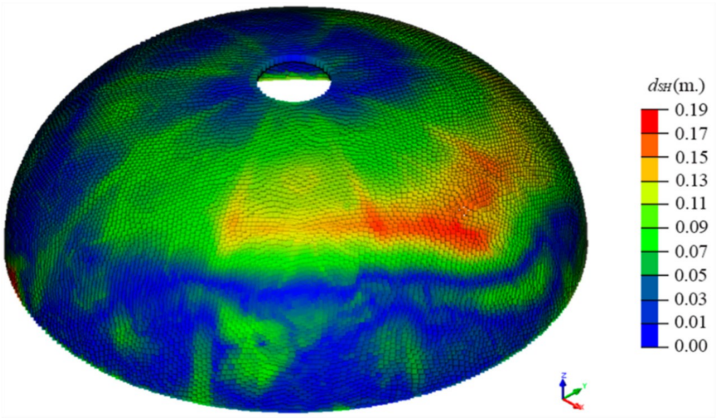

Figure 9. Graphical distribution of the different considered symmetrical Hausdorff distance (d_{SH}) (expressed in m) for the base model.

Finally, and considering GHm_s and LHm_s as the robustness indexes, a manual calibration was carried out, according to the established lower and upper bounds (Table 6) (Figure 10). According to [36], which provides a range of mechanical properties for historical masonry constructions, the upper and lower bounds were established with a safety factor of 1.35, since nowadays only visual inspection and geometrical survey are available (without an extensive experimental campaign).

Table 6. Parameters and variables considered during the manual calibration stage.

	Variable	Initial Value	Upper Bound	Lower Bound	Update Value
$f_{t,j}$ (MPa)	Masonry tensile strength	0.16	0.20	0.05	0.13
E_i (GPa)	Infill Young Modulus	0.80	1.00	0.05	0.50
E_m (GPa)	Masonry Young Modulus	1.22	0.89	1.33	0.90
β (-)	Shear retention factor	0.20	0.01	0.20	0.15

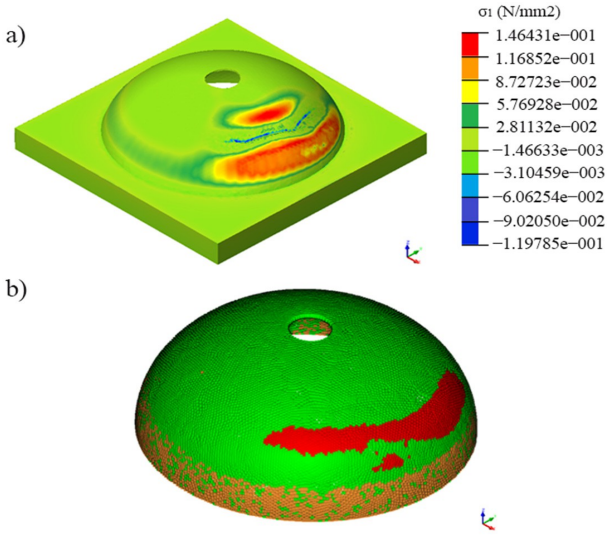

Figure 10. (**a**) First principal stress distribution, expressed in N/mm2 of the updated model; (**b**) Geometrical accuracy, in terms of Local Hausdorff metric (LHm_s) of the updated model; in green, values where the geometrical model improves the results, in orange values where no improvements are carried out and in red, areas where the updated numerical model displays worse behavior.

Noteworthy is the presence of a red area (Figure 10). The said phenomenon is associated with the presence of an offset in the spatial distribution of the plastic hinge in comparison to the photogrammetric one. Considering the results provided by the GHm_s and LHm_s indices (Figure 10b) (Table 7), a mild improvement in the geometrical similarity between the photogrammetric and numerical model (Figure 9b) is observable compared with the initial conditions (Figure 10a) and previous studies carried out on the dome [16] (presence of an infill, independent oculus, and manual calibration of the mechanical properties).

On one hand, the obtained numerical results, with a value of GHm_s of 7.40%, are insufficient to study the current stability of the dome based on an initial state model. The discrepancies, derived from the large number of currently unknown variables, call for the use of additional sensors as well as additional experimental campaigns (in laboratory and in field tests).

On the other hand, the causes of the current damage and deformation correspond to the initial one: a local failure of the timber structure (south wing) could be the cause of pathological agents acting on the wood (moisture and biological agents).

In order to understand the current stability of the construction it is required to evaluate it with the actual deformation and damage (cracks). Motivated by this, and given the geometrical and radiometric properties provided by the SfM systems, a geometric strategy is defined below.

Table 7. Comparison between expected and predicted displacement of the considered control nodes.

Control Node	Displacement Obtained (mm)	Displacement Expected (mm)
54	16.56	148.00
20256	22.80	46.00
56	26.10	198.00
21125	31.52	52.00
443	46.19	196.00
64123	38.92	25.00

4.2. Analysis of the Current Stability of the Construction Based on a SfM and NURBs Approach

It should be stressed that the structural evaluation of historical constructions not only implies the assessment of the damage's causes, but also requires a thorough understanding of the current stability (considering the actual deformation and damage), in order to take efficient restoration actions on the construction and to predict its integrity in case of different events (e.g., earthquakes). With the aim of improving the knowledge of the current stability, with respect to previous studies (Section 3.3 and [16]), a new approach is needed.

Although the point clouds obtained by the previously defined SfM approach, rich in geometric (density and accuracy) and radiometric (photorealistic texture) features, accurately represent the actual state of the construction, it is required to have additional strategies capable of exporting these properties into a numerical environment. The resulting mesh (triangulation of the SfM point cloud) has significant shortcomings to be considered as a suitable CAD/CAM model. Among its deficiencies, the following stand out [37]: (i) High density/resolution, which implies a large number of triangles and (ii) inadequate shapes.

Under the said framework, a methodology able to exploit these features based on the Non-Uniform Rational B-Splines (NURBs) and enhanced by the integration of structural pathologies (such as cracks and lack of material) is proposed. It follows the workflow shown below (Figure 11).

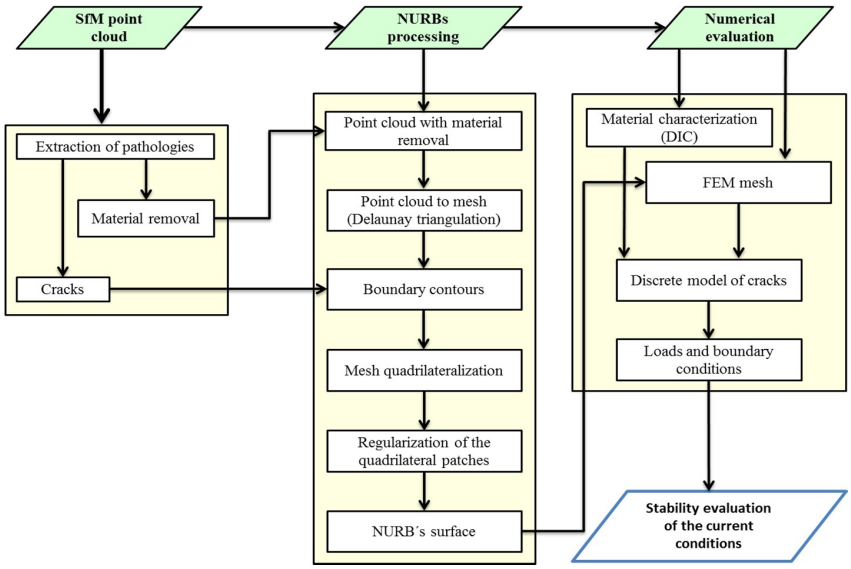

Figure 11. Proposed workflow for the study of the current stability of the construction.

Remote Sens. **2016**, *8*, 60

Considering the point cloud as the starting point, this product is firstly meshed by a standard Delaunay triangulation. Usually, these meshes present a non-manifold structure, which implies a low quality product with non-natural triangles which hinder the NURBs' generation. In order to minimize this drawback we use a topological reconstruction, which generates a maniflod mesh, based on the approach defined by [38].

Once the mesh has been correctly defined, a region clustering (boundary contours) was carried out, comprising two critical stages. In a first stage the boundary vertex (limits of the construction, lack of material and the absence of an oculus piece) of the mesh are extracted. Later, in a second stage, the cracks are integrated into these boundary contours, through a projection of the observed crack path on the SfM point cloud, as established [9].

After that, a correct representation of these regions by means of NURBS patches is required. For this purpose and in order to build a regular base on which to correctly estimate the parameters of the different regions, a quadrilaterization of the mesh is carried out. This procedure is based on the combination of Morse theory and Spectral mesh analysis according to [37]. This methodology guarantees a complete quadrilateral description of the mesh, with a C^1 (tangential continuity) between neighboring patches, ensuring a continuity along the edges.

Since the construction's surface needs to be fitted using different NURBs regions (quadrilaterial patches), a regularization process of these regions is necessary. This procedure comprises several steps [37]: (i) selection of one random border in the considered path and its opposite; (ii) border's regularization using B-Splines with a lambda density; and (iii) matching between points by means of the Fast Marching Method.

Finally, the points obtained by the regularization procedure are used as control points to fit each quadrilateral path to a NURBs' surface. It is worth mentioning, that, in construction elements such as arches, vaults or domes, the acquisition of its extrados (as a point cloud) is not possible in most of the cases, due to the presence of several setbacks (e.g., presence of infill, poor lighting conditions or lack of accessibility). Therefore, this previously shown strategy restricted the analysis of such constructions with the membrane theory (Mindlin-Reissner or Kirchhoff-Love theories). These theories limit the geometry of the numerical model's different elements to a minimum recommended size of ten times the construction's thickness. It implies as well the waste of the geometrical potentialities offered by the previously shown methodology.

Based on what is remarked above, a complementary strategy is proposed; able to estimate the construction's extrados based on its intrados geometry. This methodology is made up of the following stages: (i) decorative elements removal; (ii) normal estimation of the points by means of eigenvalue analysis of the covariance matrix [39]; (iii) translation of each point along the normal direction (with a value equivalent to the construction's thickness); (iv) point cloud meshing based on the Poisson approach and (v) projection of the cracks along its orthogonal direction. As a result, an accurate geometrical model of the construction is obtained with which to evaluate its actual stability (Figure 12).

Regarding the numerical aspect, and for the present case study, an incremental static non-linear FEM was carried out [40]. The material properties and the modelling strategy remain the same as those estimated for the initial model (considering the most appropriate ones) in Section 3.3, including a discrete model of the cracks.

For the present case study, this cracking is modelled considering the residual transversal stiffness (shear strength) through Equation (8). Concerning the normal stiffness, only a contribution in compression was considered, dismissing any contribution to the tensile regime according to Equation (9) (Table 8).

$$K_{t,c} = \frac{G_b G_m}{h_m(G_b - G_m)} \beta_{crack} \tag{8}$$

$$K_{n,c} = \frac{E_b E_m}{h_m(E_b - E_m)} \tag{9}$$

where $K_{t,c}$ and $K_{n,c}$ represent the tangential and normal stiffness respectively; G_b and G_m the shear modulus of brick and mortar, respectively; E_b and E_m the Young modulus of brick and mortar, respectively; h_m the mortar thickness; and β_{crack} the shear retention factor.

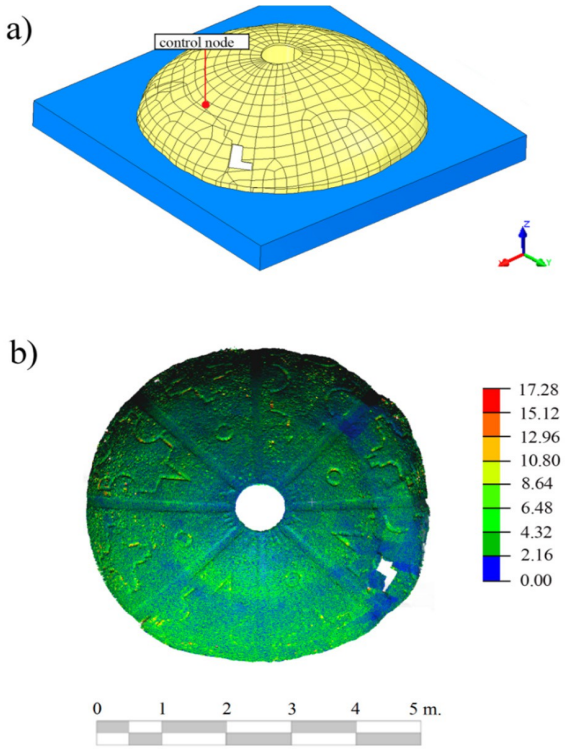

Figure 12. (**a**) Isometric view of the considered mesh model; (**b**) Discrepancies, expressed in mm, between the Non-Uniform Rational B-Splines (NURBs) and the photogrammetric models.

Table 8. Mechanical properties considered for the interaction between macroblocks (cracks).

Mechanical Properties of the Cracks		
h_m (mm)	Mortar thickness	15.00
G_b (N/mm^2)	Brick's shear modulus	1.27
G_m (N/mm^2)	Mortar's shear modulus	0.47
β_{crack}	Shear retention factor	$\beta_{c,m}$
$K_{t,c}$ (N/mm^3)	Tangential stiffness	121.88
$K_{n,c}$ (N/mm^3)	Normal stiffness (compression)	49.74

Finally a mesh for the numerical simulation is provided, with a total of 45,350 elements, clustered in: 45,196 high order solid elements and 154 high order interface elements.

For the stability analysis, all the loads acting on the dome (self-weight, infill pressure and asymmetric load) were considered. Afterwards, the estimated safety factor was established as the ratio between the current load and the collapse load obtained in the numerical simulation (Figure 13).

According to the study carried out in the Section 4.1 and the inspection of the SfM point cloud, the collapse mechanisms are mainly due to the formation of plastic hinges in the tensile regime.

The complexity of the model and the uncertainties associated with the variables (e.g., soil properties) require the study of the influence of different mechanical variables in the global stability of the construction, through parametrics analysis.

For these analyses, only the most important mechanical properties (to the tensile regime) were considered, namely: (i) Young modulus; (ii) tensile strength; and (iii) shear retention factor.

It can be observed, that the stability of the dome is mainly conditioned by the mechanical properties of the masonry, rather than the mechanical properties of the infill. Therefore, a safety factor (considering the initial mechanical properties) of 1.23 was established (Figure 13c).

However, it is worth mentioning that only the most important cracks were taken into account. By following a discrete strategy, minor and diffuse cracks were not considered. For this reason further investigation, integrating complementary approaches is necessary in order to obtain a better estimation of the actual stability.

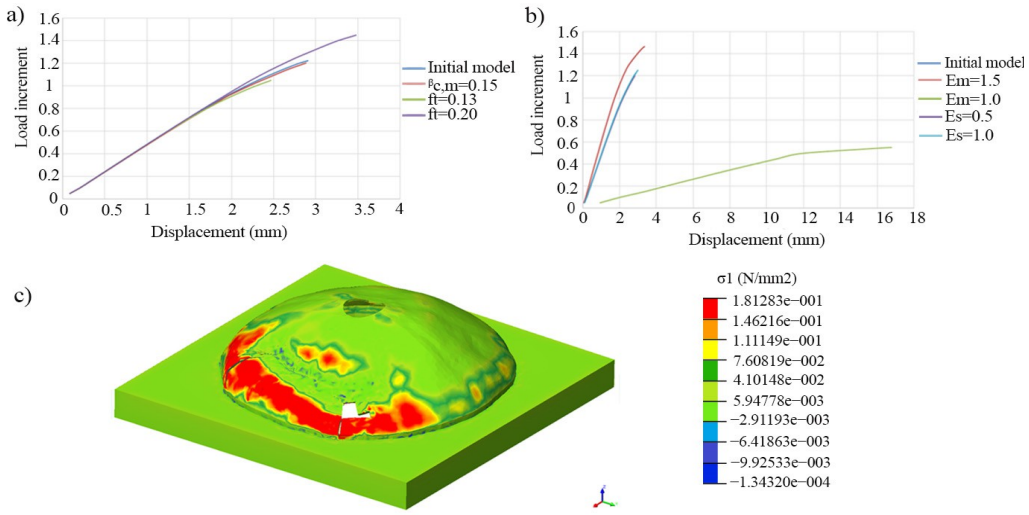

Figure 13. (**a**) Parametric analysis of different tensile strengths and shear retention factors; (**b**) Parametric analysis of different masonry and infill's Young modulus; (**c**) Maximum principal stress (σ_1), expressed in N/mm^2, at collapse of the initial considered model.

5. Conclusions

Based in the already established photogrammetric techniques of Digital Image Correlation (DIC) and image-based modelling (SfM), and complemented with geometrical (NURBs modelling and Hausdorff distance) and numerical methodologies (FEM), the strategies defined and used in the article allow the needs of structural evaluation of historical constructions to be met.

On one hand, two novel geometric quality indices are introduced and defined, called Global Hausdorff metric or GHm_s and Local Hausdorff metric or LHm_s. They allow to assess globally (GHm_s) and locally (LHm_s) the robustness, in geometric terms, of the obtained numerical model in comparison to the point cloud (deformed shape) of the construction. These indices can calibrate the different variables, based on the geometrical similarity between models acting on the numerical simulation.

On the other hand, with the aim of evaluating the actual stability of the construction and exploiting the geometrical and radiometric components of the obtained products (SfM point clouds), a modelling strategy based on NURBs is proposed. This strategy is able to profit from these properties to obtain an accurate geometrical model (with the actual deformation and damage), that serves as a basis for subsequent numerical analysis.

In order to validate these parameters and modelling methodology, it was applied to a real case study: the dome of the church of San Lorenzo in Sejas de Aliste (Zamora, Spain). Several simulations were carried out to understand the degradation process between the initial and the current state, and to corroborate the viability of the defined robustness parameters with a value of 7.40%, for the GHm_s.

When studying the current construction's stability, through the modelling strategy defined in the article, the results reveal a damaged construction with an estimate safety factor of 1.23.

However, the complexity of the model, the initial state, the absence of comprehensive knowledge of the different construction stages and the need of more experimental campaigns hinder the numerical results and the correct estimation of the safety factor. Taking this into account, further research will focus on the following aspects: (i) dynamical tests; and (ii) a robust calibration procedure (e.g., Non-Linear Square Minimization) based on the geometrical indices defined to enhance the numerical simulation of the dome.

Complementary to this, concerning the used image-based procedures, their potential includes: (i) flexibility (these may be used in the evaluation of mechanical properties of materials as well as geometrical models); (ii) wide range of applications, its use may be extended to other types of constructions such as tunnels or bridges; (iii) non-contact and non-destructive techniques; (iv) low associated cost; and (v) abundance of geometric and radiometric data. However, the methodology has some limitations: (i) the lack of geometrical information in non-visible areas, requiring complementary sensors such as electric tomography or ground penetration radar; and (ii) the model's accuracy, with several millimeters of error, restricting this strategy to constructions with large deformations.

Acknowledgments: Authors would like to thank Remote Sensing and the anonymous reviewers. Also the assistance provided by the University of Vigo and Minho. Authors would also like to thank architect Jose Luis Bordell for his valuable comments.

Author Contributions: All of the authors conceived and designed the study. Luis Javier Sánchez-Aparicio implemented the geometrical methodologies defined in the article. He also evaluated the structural behavior of the construction and carried out the experimental campaigns with the support of Alberto Villarino. Jesús García-Gago investigated the construction, its materials and constructive solutions, and also contributed to the experimental campaign. Luis Javier Sánchez-Aparicio, Alberto Villarino, Jesús García-Gago and Diego González-Aguilera wrote the manuscript.

Conflicts of Interest: The authors declare no conflict of interest.

References

1. Saloustros, S.; Pelà, L.; Roca, P.; Portal, J. Numerical analysis of structural damage in the church of the poblet monastery. *Eng. Fail. Anal.* **2015**, *48*, 41–61. [CrossRef]
2. Huerta, S. The analysis of masonry architecture: A historical approach: To the memory of professor Henry J. Cowan. *Arch. Sci. Rev.* **2008**, *51*, 297–328. [CrossRef]
3. Riveiro, B.; Solla, M.; de Arteaga, I.; Arias, P.; Morer, P. A novel approach to evaluate masonry arch stability on the basis of limit analysis theory and non-destructive geometric characterization. *Autom. Constr.* **2013**, *31*, 140–148. [CrossRef]
4. Heyman, J. *The Stone Skeleton: Structural Engineering of Masonry Architecture*; Cambridge University Press: Cambridge, UK, 1997.
5. Ramos, L.F.; Aguilar, R.; Lourenço, P.B.; Moreira, S. Dynamic structural health monitoring of Saint Torcato Church. *Mech. Syst. Signal Process.* **2013**, *35*, 1–15. [CrossRef]
6. Lourenço, P.B. Recent advances in masonry modelling: Micromodelling and homogenisation. *Multiscale Model. Solid Mech. Comput. Approaches* **2009**, *3*, 251–294.
7. Milani, G.; Simoni, M.; Tralli, A. Advanced numerical models for the analysis of masonry cross vaults: A case-study in italy. *Eng. Struct.* **2014**, *76*, 339–358. [CrossRef]
8. Del Pozo, S.; Herrero-Pascual, J.; Felipe-García, B.; Hernández-López, D.; Rodríguez-Gonzálvez, P.; González-Aguilera, D. Multi-sensor radiometric study to detect pathologies in historical buildings. *Int. Arch. Photogramm. Remote Sens. Spat. Inf. Sci.* **2015**. [CrossRef]
9. Sánchez-Aparicio, L.J.; Riveiro, B.; González-Aguilera, D.; Ramos, L.F. The combination of geomatic approaches and operational modal analysis to improve calibration of finite element models: A case of study in Saint Torcato Church (Guimarães, Portugal). *Constr. Build. Mater.* **2014**, *70*, 118–129. [CrossRef]
10. Villarino, A.; Riveiro, B.; Gonzalez-Aguilera, D.; Sánchez-Aparicio, L. The integration of geotechnologies in the evaluation of a wine cellar structure through the finite element method. *Remote Sens.* **2014**, *6*, 11107–11126. [CrossRef]

11. Hausdorff, F. *Felix Hausdorff-gesammelte Werke Band III: Mengenlehre (1927, 1935) Deskripte Mengenlehre und Topologie*; Springer-Verlag: Berlin, Germany, 2008; Volume 3.
12. García-Gago, J.; González-Aguilera, D.; Gómez-Lahoz, J.; san José-Alonso, J.I. A photogrammetric and computer vision-based approach for automated 3D architectural modeling and its typological analysis. *Remote Sens.* **2014**, *6*, 5671–5691. [CrossRef]
13. Rodríguez-Martín, M.; Lagüela, S.; González-Aguilera, D.; Rodríguez-Gonzálvez, P. Procedure for quality inspection of welds based on macro-photogrammetric three-dimensional reconstruction. *Opt. Laser Technol.* **2015**, *73*, 54–62. [CrossRef]
14. Ghorbani, R.; Matta, F.; Sutton, M. Full-field displacement measurement and crack mapping on masonry walls using digital image correlation. In *Advancement of Optical Methods in Experimental Mechanics*; Jin, H., Sciammarella, C., Yoshida, S., Lamberti, L., Eds.; Springer International Publishing: New York, NY, USA, 2014; Volume 3, pp. 187–196.
15. Salmanpour, A.; Mojsilovic, N. Application of digital image correlation for strain measurements of large masonry walls. In Proceedings of the 5th Asia Pacific Congress on Computational Mechanics, Queens Town, Singapore, 11–14 December 2013; pp. 11–14.
16. Sánchez-Aparicio, L.; Villarino, A.; García-Gago, J.; González-Aguilera, D. Non-contact photogrammetric methodology to evaluate the structural health of historical constructions. *Int. Arch. Photogramm. Remote Sens. Spat. Inf. Sci.* **2015**. [CrossRef]
17. Pan, B.; Lu, Z.; Xie, H. Mean intensity gradient: An effective global parameter for quality assessment of the speckle patterns used in digital image correlation. *Opt. Lasers Eng.* **2010**, *48*, 469–477. [CrossRef]
18. Schweighofer, G.; Pinz, A. Robust pose estimation from a planar target. *IEEE Trans. Pattern Anal. Mach. Intell.* **2006**, *28*, 2024–2030. [CrossRef] [PubMed]
19. Bouguet, J.-Y. Camera Calibration Toolbox for Matlab. 2004. Available online: http://www.vision.caltech.edu/bouguetj/calib_doc/ (accessed on 7 August 2015).
20. Pan, B.; Quian, K.; Xie, H.; Asundi, A. Two-dimensional digital image correlation for in-plane displacement and strain measurement: A review. *Meas. Sci. Technol.* **2009**, *20*, 062001. [CrossRef]
21. Xavier, J.; Fernandes, J.R.A.; Frazão, O.; Morais, J.J.L. Measuring mode I cohesive law of wood bonded joints based on digital image correlation and fibre Bragg grating sensors. *Compos. Struct.* **2015**, *121*, 83–89. [CrossRef]
22. Pan, B. Bias error reduction of digital image correlation using gaussian pre-filtering. *Opt. Lasers Eng.* **2013**, *51*, 1161–1167. [CrossRef]
23. Barazzetti, L.; Binda, L.; Scaioni, M.; Taranto, P. Photogrammetric survey of complex geometries with low-cost software: Application to the "G1" temple in Myson, Vietnam. *J. C Herit.* **2011**, *12*, 253–262. [CrossRef]
24. Pierrot-Deseilligny, M.; de Luca, L.; Remondino, F. Automated image-based procedures for accurate artifacts 3D modeling and orthoimage generation. *Geoinform. FCE CTU* **2011**, *6*, 291–299. [CrossRef]
25. Rodríguez-Gonzálvez, P.; Garcia-Gago, J.; Gomez-Lahoz, J.; González-Aguilera, D. Confronting passive and active sensors with non-gaussian statistics. *Sensors* **2014**, *14*, 13759–13777. [CrossRef] [PubMed]
26. Morel, J.-M.; Yu, G. Asift: A new framework for fully affine invariant image comparison. *SIAM J. Imaging Sci.* **2009**, *2*, 438–469. [CrossRef]
27. Selby, R.G.; Vecchio, F. *Three-dimensional Constitutive Relations for Reinforced Concrete*; Department of Civil Engineering, University of Toronto: Toronto, ON, Canada, 1993.
28. Freeda Christy, C.; Tensing, D.; Mercy Shanthi, R. Experimental study on axial compressive strength and elastic modulus of the clay and fly ash brick masonry. *J. Civil Eng.* **2013**, *4*, 134–141.
29. Atamturktur, S.; Li, T.; Ramage, M.H.; Farajpour, I. Load carrying capacity assessment of a scaled masonry dome: Simulations validated with non-destructive and destructive measurements. *Constr. Build. Mater.* **2012**, *34*, 418–429. [CrossRef]
30. Recommendations, Maritime Works. *Geotechnical Recommendations for the Design of Maritime and Harbour Works (ROM 0.5-94)*; Puertos del Estado: Madrid, Spain, 1995.
31. Manie, J.; Kikstra, W.P. *Finite Element Analysis User's Manual-Release 9.4.4*; TNO DIANA BV: Delft, The Netherlands, 2011.
32. Girardeau-Montaut, D.; Roux, M.; Marc, R.; Thibault, G. Change detection on points cloud data acquired with a ground laser scanner. *Int. Arch. Photogramm. Remote Sens. Spat. Inf. Sci.* **2005**, *36*, W19.

33. Aspert, N.; Santa Cruz, D.; Ebrahimi, T. MESH: Measuring errors between surfaces using the Hausdorff distance. In Proceedings of the IEEE International Conference in Multimedia and Expo (ICME), Lausanne, Switzerland, 26–29 August 2002; Volume 1, pp. 705–708.
34. Alexandre, L.A. Set distance functions for 3D object recognition. In *Progress in Pattern Recognition, Image Analysis, Computer Vision, and Applications*; Ruiz-Shulcloper, J., di Baja, G.S., Eds.; Springer: Berlin, Germany, 2013; pp. 57–64.
35. Wu, J.-M.; Jing, Z.; Wu, Z.; Feng, Y.; Xiao, G. Study on an improved Hausdorff distance for multi-sensor image matching. *Commun. Nonlinear Sci. Numer. Simul.* **2012**, *17*, 513–520. [CrossRef]
36. Ministerio delle Infrastructure. *Ntc (Nuove Norme Tecniche per le Construzioni)*; Ministerio delle Infrastructure: Rome, Italy, 2008.
37. Branch, J.W.; Prieto, F.; Boulanger, P. Automatic extraction of quadrilateral patches from triangulated surfaces using morse theory. In Proceedings of the 16th International Meshing Roundtable; Brewer, M.L., Marcum, D., Eds.; Springer: Berlin, Germany, 2008; pp. 199–212.
38. Attene, M. A lightweight approach to repairing digitized polygon meshes. *Vis. Comput.* **2010**, *26*, 1393–1406. [CrossRef]
39. Schaer, P.; Skaloud, J.; Landtwing, S.; Legat, K. Accuracy estimation for laser point cloud including scanning geometry. In Proceedings of the 5th International Symposium on Mobile Mapping Technology, Padova, Italy, 29–31 May 2007.
40. Milani, G.; Valente, M. Comparative pushover and limit analyses on seven masonry churches damaged by the 2012 Emilia-Romagna (Italy) seismic events: Possibilities of non-linear finite elements compared with pre-assigned failure mechanisms. *Eng. Fail. Anal.* **2015**, *47*, 129–161. [CrossRef]

Chapter IV

Practical use of multispectral techniques for the detection of pathologies in constructions.

Chapter 13

Practical Use of Multispectral Techniques for the Detection of Pathologies in Constructions

L.J. Sánchez-Aparicio, S. Del Pozo, P. Rodríguez-Gonzálvez, J. Herrero-Pascual, A. Muñoz-Nieto and D. González-Aguilera
Department of Cartographic and Land Engineering, High School of Ávila, University of Salamanca, Ávila, Spain

D. Hernández-López
Regional Development Institute-IDR, University of Castilla-La Mancha, Albacete, Spain

Abstract

Our approach to multispectral remote sensing assessment of constructive pathologies has been organized in two different parts. The first one (Chapter 7) dealt with equipment and methods. The second one, developed in this chapter, will be related to the application to real cases, encompassing relevant aspects such as: data acquisition (sensor type choice and field works planning), processing (filtering and segmentation), sensor registration, true orthophoto generation, orthophoto classifications (through supervised and unsupervised techniques) and the qualitative and quantitative analysis of results (by means of confusion matrix, spectral separability, overall accuracy, reliability and agreement of informational classes). Based on these premises three case studies have been addressed. On the one hand, two historical stone masonry constructions and on the other hand one modern reinforced concrete construction. These three case studies will be used as examples of best practices in multispectral dataset management and processing, and will serve to evaluate the flexibility of the methodology proposed for detecting and classifying accurately a wide range of constructive pathologies.

13.1 Introduction

Chapter 7 addressed, from a theoretical point of view, a study of instrumentation and methods to process multispectral datasets of different building elements. This chapter will describe and analyze a selected group of experiences resulting from the application of such methodologies in two of the most significant civil engineering fields such as cultural heritage constructions and buildings and civil infrastructures.

Safeguarding and enhancement of the built heritage can be considered a fundamental feature for modern developed societies. Sometimes by its own intrinsic value, and also for its artistic or cultural value, preservation of these types of constructions becomes extremely important. Due to their unique nature or their fragility it is necessary to know thoroughly their geometric and structural characteristics and, where appropriate,

provide information to establish intervention plans based on a comprehensive diagnosis and assessment of their pathologies. Experience in conservation and restoration projects highlights the need to use non-destructive techniques to acquire required datasets. This fact restricts the use of some techniques and sensors.

The exposure to chemically aggressive environments, moisture or biological organisms produces deteriorations that usually worsen over time. This situation is especially pronounced in constructions and old buildings. However, modern buildings and civil infrastructures that use different materials and construction techniques also suffer different types of deterioration.

The case studies submitted below have been selected within a broader set of experiences developed by the research group TIDOP (Armesto-González et al. 2010, Crespo et al. 2010, Del Pozo et al. 2015, González-Jorge et al. 2012, Rodríguez-Gonzálvez et al. 2013), which belongs to the University of Salamanca (http://tidop.usal.es), in order to offer a wide casuistry applying multispectral data in diagnosis and assessment of pathologies in constructions.

Following a common structure, the next items will be addressed in each case study:

- Description and building materials: after a brief introduction of the case study, a broad description of materials and construction technics will be done.
- Pathological assessment: as a result of the constructive elements analyzed, a brief description of the expected pathologies will be assessed.
- Sensors and methods: under these paragraphs the characteristics of the used sensors and the methodology applied in the data process will be explained.
- Experimental results: these paragraphs will show, by means of graphics and statistical analysis, an objective assessment of the followed methodology. The main issues to be considered in the analysis of multispectral images are: (i) Separability; (ii) Cohen's Kappa coefficient; (iii) Overall accuracy; and (iv) Comparative study between supervised and non-supervised classifications.

The following table (Table 13.1) synthesizes the technical specifications of the sensors that have been used. The next figure (Fig. 13.1) shows, schematically, the workflow applied to data processing, which is common for most cases.

To complete this chapter, a best practices guide, derived from case studies, will be presented in the conclusion section.

13.2 First Case Study: Ribeiriño Bridge (Ourense, Spain)

13.2.1 *Description and Building Materials of the Ribeiriño Bridge*

Located in Ourense county (northern Spain), Ribeiriño bridge (Fig. 13.2) is a key to the communication network between the cities of Santiago of Compostela and Madrid (capital and largest city of Spain). Predominantly built in reinforced and pre-stressed concrete (arc, abutments, bearings and piers) following the Spanish standard EH-68 (Ministerio de Fomento 1968). The construction entered in service in 1971.

Set in an environment with high level of humidity and under an average rainfall of 880 mm/yr, the bridge is 147 m long and it is supported by several piers along its structure. In the central span, these constructive elements are supported by a parabolic

Table 13.1 Technical specifications of the sensors used in the case studies.

		Trimble GX200	FARO Photon 80	Riegl LMS z390i
Active sensors	Measuring principle	Time of flight	Phase shift	Time of flight
	Wavelength	534 nm (green)	785 nm (VNIR)	1,550 nm (SWIR)
	Radiometric resolution	8 bits	11 bits	8 bits
	Deflection system	Oscillating flat mirror	Rotating mirror	Rotating mirror
	Field of view	360° H 60° V	360° H 320° V	360° H 80° V
	Standard deviation	1.4 mm for D $\leq$ 50 m	2 mm for D = 25 m	6 mm for D $\leq$ 50 m
	Range of measurement	2–350 m	0.60–76 m	1.50–400 m
	Angular resolution	Azimuth: 12″ Zenith: 14″	Azimuth and Zenith: 33″	Azimuth and Zenith: 3.6″
	Beam divergence	3 mm to 5 m	0.16 mrad	0.3 mrad
	Scan speed (p/s)	5,000	120,000	11,000
		Nikon D200	Nikon Coolpix L11	
Passive sensors	Camera type	Single-lens reflex camera	Compact digital camera	
	Sensor type	CCD	CCD	
	Sensor size	23.60 × 15.80 mm	5.76 × 4.29 mm	
	Pixels	2872 × 2592	2816 × 2112	
	Radiometric resolution	12 bits	8 bits	
	Focal length	18 mm	6.2 mm	
	Max aperture	3.5	2.8	

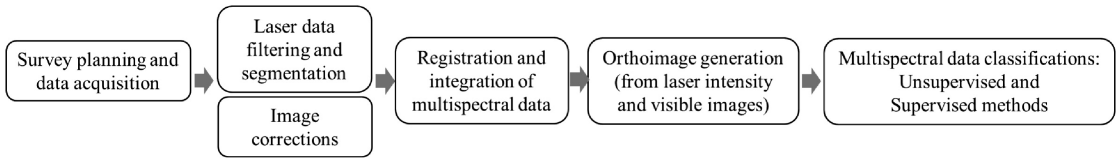

Figure 13.1 Workflow of the methodology proposed.

concrete arch. While the lateral spans (with a rectangular shape) are supported on several piers.

13.2.2 *Pathologies of the Structure*

Considering the environmental conditions previously defined: (i) High humidity on a cyclic basis; (ii) Concrete exposed to water contact; (iii) Presence of carbon dioxide; (iv) Possible attack of melting salts, the main pathological agent to be expected was the carbonatation corrosion. It can be also considered, to a lesser extent, to be chloride corrosion given the presence of a marine environment.

Although they have different origins, both corrosive processes, cause similar degrading result in concrete. For a better understanding, the concept of the steel passivation process should be reviewed.

Figure 13.2 Pier of the Ribeiriño bridge.

Passivation involves the formation of an inert film with a high pH (12.6–14) as a result of the hydration of Portland cement, in particular the calcium hydroxide component, forming the passive layer (physical protection against chemical aggressions).

Although this layer masks the steel against the action of external agents, the corrosion (presence of carbon dioxide and chloride) can promote the removal of this protective layer. As a consequence of its removal, a low pH environment is created and the steel is exposed to oxidation, causing a volume increase. This increase leads to the detachment of concrete areas and loss of mechanical adherence between steel and concrete. Complementarily, the presence of high levels of moisture, oxygen and a suitable temperature facilitates the growth of biological organisms on the bridge.

As a result of the different chemical attacks (mainly corrosion), the concrete durability is conditioned by the penetration of the several agents and the speed at which is attacked. Causing a decomposition of the elements and a loss of mechanical adherence between the steel and concrete.

To sum up two different pathologies will be expected:

- Biological colonization
- Moistures that can lead to corrosion by carbonation and chloride.

13.2.3 *Materials and Methods*

Considering the two pathologies mentioned above, it was decided to make a comparative multispectral study. To do this, we worked both with the radiometric results provided by the terrestrial laser scanner Riegl LMS z390i, in the SWIR range of the electromagnetic spectrum, and the photographs taken with a Nikon D200 camera built into the scanner (see Table 13.1).

The joint use of the laser scanner and the built in camera not only gives us an ideal 3D scene reconstruction. After a proper parallax-baseline correction, we can get a

true orthoimage with four multispectral channels (R, G, B and SWIR) increasing the spectral resolution of the study with the consequent enrichment in the pathological surveying of the bridge's pier.

The proposed methodology, which consists of several stages as shown in Figure 13.1, focuses on automation as a basic guideline to detect pathologies. Next, the procedures followed and its main characteristics are explained:

Planning and data acquisition. To carry out a proper data acquisition and to facilitate subsequent data process and orthoimage creation, the laser scanner was placed and leveled just once, 9 to 17 m far from the bridge. The spatial resolution achieved at this distance was 10 mm. Data acquisition was managed by Riscan Pro software, taking first data from laser intensity and then photographs in the selected area.

Filtering and segmentation. The first step of data processing consisted of point cloud filtering and segmentation of a selected area in which a great number of pathologies are presented, excluding all other irrelevant areas in the case study.

Data corrections. The separation of each RGB image in three different images (coming from red, green and blue channels), was performed through the free software DCRaw (Coffin 2011) by means of the Bayer demosaicing filter. As a result three images (1436 × 1296 pixels) were obtained.

Orthoimages generation. Once we have three separated images as mentioned above, and the SWIR one, coming from laser scanner, we obtained four orthoimages with Riscan Pro. Firstly, the orthoimage from the point cloud data, which incorporates intensity values in the SWIR range, was generated by the orthogonal projection of points in a plane parallel to the bridge structure. Then, to generate orthoimages in R, G and B channels the external camera orientation parameters with respect to the coordinate system of the laser model were obtained (registration). This step involves identifying and pointing out singular points in the images and the laser model. For this purpose we used external targets previously attached to the bridge. Finally, the projection of the points was performed using the collinearity condition (see Chapter 7). The final resolution of the orthoimages was 30 mm.

Multispectral data classification. The classification of these two groups (SWIR and SWIR+RGB) of orthoimages encloses a first *fuzzy k-means* unsupervised classification and a second *maximum likelihood* supervised classification:

- Unsupervised classification: the unsupervised classification algorithms based on the k-means approach is the most commonly used. It classifies a given data set in a certain number of clusters that are previously fixed. Within k-means algorithms, *fuzzy k-means* is one of the most frequently used. *Fuzzy k-means* give a specific weighting to each data associated with the inverse distance to the cluster's center.
- Supervised classification: the *maximum likelihood* classifier is the most complex, robust and reliable supervised algorithm, as it is closely based on the original data distribution. It considers that the radiometry (digital levels) of each category follows a normal distribution. It allows describing each category by a probability function from the mean vector and variance-covariance matrix. In this way, it is possible to calculate the probability that a given pixel belongs to a category.

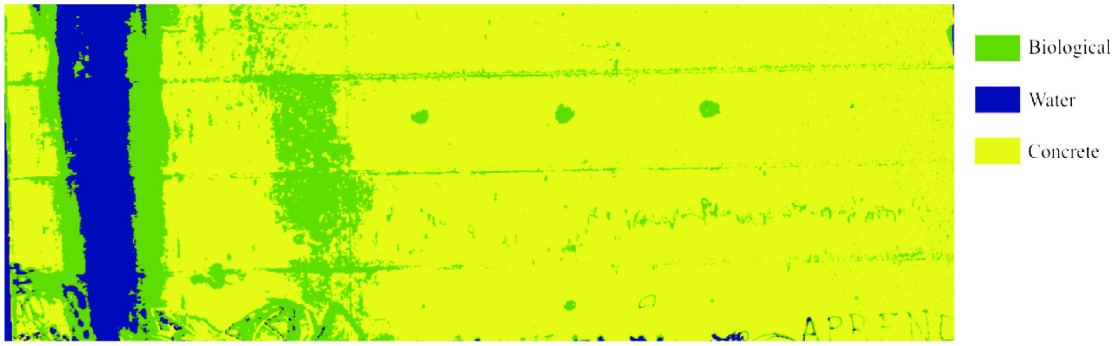

Figure 13.3 Supervised classification based on *fuzzy k-means* algorithm: SWIR (Laser) + RGB (Camera).

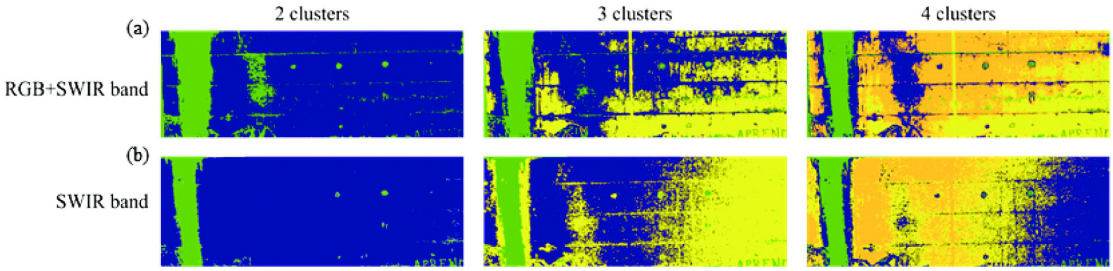

Figure 13.4 Unsupervised classification: (a) RGB + SWIR channels. (b) SWIR channel.

13.2.4 *Experimental Results*

At this point we must remember that the aim is to achieve an automatic process. This aim implies that the classification methodology should be a non-supervised classification one, which should be as close as possible to the ideal of a supervised process (which will act as a reference).

The supervised classification process, where user intervention to define training areas is required, was performed using the *maximum likelihood* algorithm (Fig. 13.3). For this purpose three informational classes were used, generating a Cohen's Kappa coefficient (Cohen 1968) of 0.97787.

The high value of Cohen's Kappa coefficient suggests good results in the classification process, but as seen in Figure 13.3, there are informational errors arising from classes not taken into account such as graffiti or drain pipes, where the presence of shadows generates several confusions. This fact reveals the limitations of the workflow based on the use of four channels, workflow applied in the discretization of informational classes that were not considered in the initial study.

Looking for the maximum possible automation, application of an unsupervised mono-channel classification (*fuzzy k-means*) (Fig. 13.4b) gives a biased result where clusters have no direct equivalence to informational classes (Fig. 13.3).

A four channels unsupervised *fuzzy k-means* classification (SWIR + RGB) gives better results (Fig. 13.4a). Using four clusters and applying an aggregation process to

guarantee the equivalence between clusters and informational classes, results are closer to the reality.

The quality assessment of the latest automated (non-supervised classification) results, contrasted with supervised process, shows an overall accuracy of 90.89%. The major errors come from the wrong assignment of concrete to biological class, and biological to water class. This second error has less effect because both classes represent aggressive pathologies for concrete, revealing the presence of moisture on it.

We can conclude that in a practical approach, when a general detection of pathologies is required, and the speed of data acquisition becomes important, a strategy based on the use of two sensors (active and passive) provides valid results in a completely automatic process. Moreover, from data acquired we can manage a metric 3D model of the construction.

13.3 Second Case Study: Santo Domingo Ruins (Pontevedra, Spain)

13.3.1 *Description and Building Materials of the Santo Domingo Ruins*

Popularly known as the "Ruins of Santo Domingo", which was once a Dominican monastery, is one of the most interesting historical-artistic properties of the Spanish north. The presence of tombs, heraldic shields and altarpieces rich in detail, unique and fragile, increases the value of the construction (Porto 1993). Built in granite, the beginning of its works dates from the first third of the XIV century. During its construction period, the monastery suffered different reforms, with the expansion of monastic stays. Nevertheless, the current building retains the main characteristics of the local Dominicans monasteries (Fig. 13.5).

Nowadays, the poor state of conservation of the different construction elements, together with the existence of biological colonization, loss of material, cracking and continuous leaks on the apses, expose this construction to a continued degradation process.

Figure 13.5 Santo Domingo ruins: (a) Front view of the façade. (b) Lateral view of the ruins.

The main construction material is the two-mica granite (at least in the area of the monastery ruins) (Montojo Santos et al. 2014). Such material was used to form the different masonry elements along the monastery. The different blocks were joined by lime mortar and complemented by underpinning rubbles.

For the artistic elements, the high level of biological colonization hinders the identification of the granite. It should be noted that the presence of accumulations of dark minerals (biotite and turmalita), with oxidation strips (iron oxide-hydroxides) gives a characteristic brown-rusty tone (Fig. 13.5).

13.3.2 *Pathologies of the Structure*

Subject to a wide variety of biological, atmospheric and structural degradation agents, the Santo Domingo ruins are an artistic-cultural property in an advanced state of degradation. Within the wide range of pathologies present in the building, the following degradation processes are expected to be detected:

- Efflorescence (white layer): given the presence of soluble salts, due to environmental conditions, mortars used in the restoration process, decorative materials employed in the different constructive elements or by capillary rise from the ground. This pathological effect starts with the crystallization of the salts, outside or into the material, causing a wedge effect (expansion) which degraded the material properties.
- Biological activity: materialized with the presence of moss, lichens, algae, plants with stem and remains of metabolic activity on the construction. This pathology causes a degradation of the mortar and rocks present on the different constructive elements (chemical erosion and fracture).
- Damp spots: on the pavement and walls, caused mostly by capillary rise. They are also visible on the ledges of the construction as a result of different runoffs.
- Crusts (black color): they appear throughout the building, their origin can be attributed to: (i) Biological colonization; and (ii) Contamination from urban activity. Both causes create dark color crusts with different grip levels on the affected area.

13.3.3 *Materials and Methods*

Although there are several tests capable of detecting damage, caused by different pathological agents, in the construction (e.g. X-ray diffraction, microscopes or chemical assays) (Montojo Santos et al. 2014), it is required to provide a quantification procedure, as was explained in the previous case study. Due to the characteristic of the construction, and the needed of a geometrical monitoring, the terrestrial laser scanner was the a priori best solution. Complementary to the geometrical data captured by this sensor, the radiometric information was employed, in order to carry out a multispectral image classification procedure.

Since the main goal of the present chapter is focused on the pathological detection by the radiometry captured by the different sensors used, the geometrical processing was omitted. For the present case study, and given the variety of pathologies presented, four sensors (three terrestrial laser scanners and a visible camera) were used. On the one hand, and in order to capture the visible spectrum, a time of flight

Trimble GX200 laser scanner (Green-534 nm) and a Nikon D200 digital camera were utilized. On the other hand and with the purpose of acquiring the near (NIR) and medium (SWIR) infrared spectrum, a FARO Photon (785 nm) and Riegl LMS z390i (1,550 nm) laser scanners were used (to see more about its technical specifications see Table 13.1).

As shown Figure 13.1, the methodology followed for the acquisition and evaluation of the results comprise a total of five stages, as explained below:

Planning and data acquisition. Prior to data collection, a visual inspection was performed to evaluate the different pathologies presented in the construction. Also it was to assess the accessibility and restrictions in the area. Additionally to the localization and the value of the construction, the environmental conditions were considered (e.g. high probability of rain and high humidity).

During the data acquisition process, the different laser scanners used were placed according to a plan previously prepared and at a distance from the façade between 5–10 m getting thirty one point clouds with a 10 mm of spatial resolution. This process was assisted by different software: Realworks Survey for Trimble, Scene 3D for Faro Photon 80 and Riscan Pro for Riegl LMS z390i. The number of scan stations was selected according to the different technical specifications provided by the manufacturer (Table 13.1).

Filtering and segmentation. Applied after data gathering, this stage comprises the filtering (denoising) and registration of the different point clouds. For the point clouds the alignment was considered the ICP (Iterative Closest Point) strategy.

Data corrections. Encloses the images demosaicking, since the camera used in this work utilizes a Bayer filter. For more details about this process consult the previous case study.

Orthoimages generation. For each point cloud registered, an orthoimage was generated providing a total of six channels: Four orthoimages in the visible range (R, G1, $G2_{Trimble}$ and B) and two in the infrared (NIR and SWIR) one. Taking the advantage of the registration performed in the previous step (with the different point clouds captured) the ortoimages were generated (see previous case study). As result 10 mm resolution images were obtained.

Multispectral data classification. The multispectral dataset, evaluated in the present case study, enclose a total of six orthoimages. A *fuzzy k-means* algorithm was used in the unsupervised classification (for more details see the previous case of study). Also a supervised classification was required with the aim of improving the results, by the addition of informational classes introduced by an expert.

13.3.4 *Experimental Results*

Starting from the geometrical base, provided by the orthoimage previously defined (with 10 mm of spatial resolution), the main goal now is the pathological clustering identification (in contrast to the material classification which is not considered). For this purpose an initial analysis (non-supervised) classification was carried out. Six informational classes were considered and a *fuzzy k-means* algorithm was used. The results of this process are shown in Figure 13.6, considering the following classes: (i) Granite without pathological affections; (ii) Pathologies arising from water (dampness) and

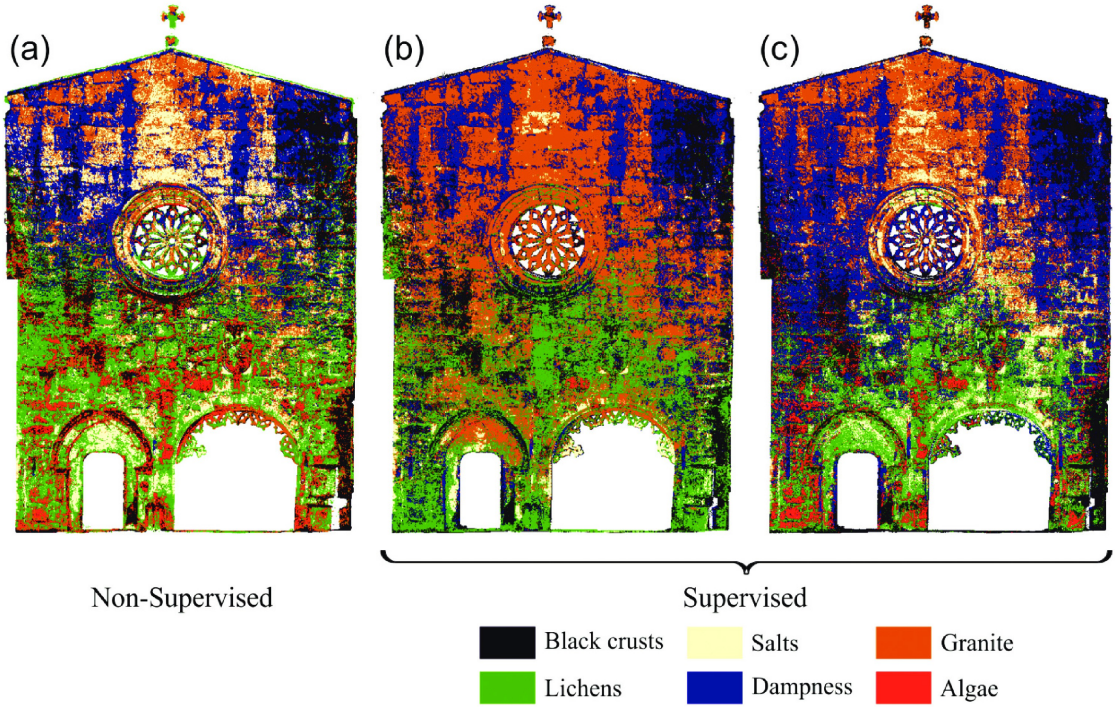

Figure 13.6 (a) Non supervised classification with merged classes. (b) Supervised classification with six channels. (c) Supervised classification with three channels (only active sensors).

salts; (iii) Two types of biological elements (lichens and algae); and (iv) Pathologies of decay (black crusts). Despite this initial study, the unsupervised classification, with six clusters and the employment of *fuzzy k-means* algorithm, fails to yield results close to real ones, even using all available channels.

Given the large variety of pathological processes presented in this construction, and some of them with similar origin (algae-lichen), the resulting analysis shows a radiometric overlap. Therefore it was required to increase the number of clusters to improve the separability between classes.

In order to enhance the unsupervised classification performance, it was necessary to establish an aggregation process (merge phase) attended by the user. The main goal of this process is to approximate the new clusters to the informational class showed in Figure 13.6a. This process is applied to the Biological colonization, moss and lichen classes, shown in Section 13.3.2.

Despite the aggregation process, classification results are far from optimal, with an overestimation of the affected areas by the pathological processes. The greatest variations were shown between biological agents. In view of the obvious errors occurring in the non-supervised process, it was necessary to use a supervised approach based on a *maximum likelihood* algorithm. Six classes, from the initial hypothesis and the six channels available, were considered in this classification process (Fig. 13.6b). Results (Table 13.2) show an overall accuracy of 0.8844 and a Cohen's Kappa coefficient of 0.8157 (excluding the null class).

Table 13.2 Supervised classification: confusion matrix with six channels.

	Black crusts	Lichens	Salts	Dampness	Granite	Algae
Black crusts	15.16%	0.18%	0.00%	1.73%	0.02%	0.02%
Lichens	0.02%	4.03%	0.02%	0.00%	0.02%	0.02%
Salts	0.00%	0.00%	1.44%	0.00%	0.02%	0.00%
Dampness	1.17%	0.25%	0.00%	17.29%	1.97%	0.04%
Granite	0.08%	1.52%	0.25%	4.17%	50.17%	0.06%
Algae	0.00%	0.00%	0.00%	0.00%	0.00%	0.35%

Table 13.3 Supervised classification: confusion matrix with five channels.

	Black crusts	Lichens	Salts	Dampness	Granite	Algae
Black crusts	15.01%	0.37%	0.00%	1.70%	0.00%	0.02%
Lichens	0.10%	3.98%	0.00%	0.02%	0.02%	0.02%
Salts	0.00%	0.02%	1.44%	0.00%	0.00%	0.00%
Dampness	1.13%	0.74%	0.00%	16.65%	2.18%	0.04%
Granite	0.14%	1.95%	0.31%	4.33%	49.41%	0.06%
Algae	0.00%	0.00%	0.00%	0.00%	0.00%	0.35%

Since the black crusts were associated to the granite decay caused by a granular disintegration due to the presence of dampness and/or soiling, there was a class overlap as shown in Table 13.3. In a similar way, the high level of deterioration of the façade (approx. half of it is affected by some kind of pathology) hindered the granite discretization for the different wavelengths.

Regarding the wavelengths and the overlap between green channels (Trimble GX200 and visible camera), the results provided by classifications carried out with five (excluding passive green channel) and six channels had a similar efficiency (Table 13.2 and Table 13.3).

Evaluating the statistical results, it is possible to observe a slight decline. The overall accuracy and Kappa coefficient go down to 0.8684 and 0.7916 respectively. This decline hardly has a negative effect on the final result, from a qualitative point of view. This change has its origin in the slight variations (during the classification) between lichens-dampness and lichens-granite classes. For the algae class any variation was observed given its spectral signature, with high variations in the visible zone (manifested through red/orange tonalities).

Classification results derived from the independent use of the active channels, three in total (Fig. 13.6c) corresponding with the different laser scanner used, seem to be insufficient. With an overall accuracy of 0.7526 and a Cohen's Kappa coefficient of 0.6367 (Table 13.4) this classification cannot be considered as the best one. It may lead to the wrong considerations for later restoration actions.

For these purposes, sensor hybridization was applied considering two classifications: (i) Five channels classification (three from the active sensors and two from the red and blue channel of the camera) and (ii) Six channels classification (adding to the previous channels clustering the green channel of the camera). As a result of this hybridization the classification improved (Table 13.2 and Table 13.3).

Table 13.4 Supervised classification: confusion matrix with three channels.

	Black crusts	Lichens	Salts	Dampness	Granite	Algae
Black crusts	14.92%	0.31%	0.00%	1.71%	0.00%	0.16%
Lichens	0.14%	2.84%	0.10%	0.02%	0.02%	0.97%
Salts	0.00%	0.27%	1.01%	0.00%	0.18%	0.00%
Dampness	0.95%	0.88%	0.08%	16.15%	2.32%	0.39%
Granite	0.08%	3.74%	6.55%	5.10%	40.02%	0.76%
Algae	0.00%	0.00%	0.00%	0.00%	0.00%	0.33%

Also there is a remarkable worsening in the unaffected material classification, since the granite used in this construction presents a heterogeneous texture, with large variations in the grain size and mineral distribution, requiring for instance an expansion in the number of channels used or the use of an additional algorithm based on spatio-contextual classification techniques (Li et al. 2014), in order to have an optimal result.

As shown in the results (Table 13.2 and Table 13.3), the addition of redundant channels, with overlapping (in terms of spectral signatures) areas, did not generate significant improvements. Regarding the use of channels from the cameras, despite having a bad radiometric resolution, they achieve better classification results in areas with several classes (that need to be classified), even without the presence of large pathologies on it.

13.4 Church of San Pedro Case Study (Avila, Spain)

13.4.1 *Description and Building Materials of the San Pedro Church*

The historical and cultural heritage of the city of Ávila is famous mainly due to its variety of medieval constructions both religious and civil in origin. Within this wide range of buildings the predominant use of granite masonry is certainly highlighted.

It is worth to noting that the construction material depended on its availability close to the working area. The presence of a granite deposit in the village of "La Colilla", just a few kilometers from the city, served as a quarry for the extraction of this construction material for buildings.

Much of the appeal of this heritage architecture lies in the wide variety of types of granites present in this quarry. A total of 5 granite varieties can be recognized and all of them have been used as building material in historical constructions in Ávila (Molina Ballesteros 1993): (i) Unaltered grey coarse-grained granite; (ii) Unaltered grey fine-grained granite; (iii) Ochre granite; (iv) Red granite and (v) White granite. Each of the three latter granite types is the result of several alterations produced during the Iberian Hercynian Base and presents its own physical and mechanical properties that were considered in the multispectral analysis.

The church of San Pedro is located in the old big market square devoted to Santa Teresa, facing the medieval door of the Alcazar, and is one of the most characteristic monuments of Romanesque architecture in the city. With a cross-shaped layout, it consists of three naves with five sections topped by three apses. It has a recognized dome base and a tower in the northern arm of the transept.

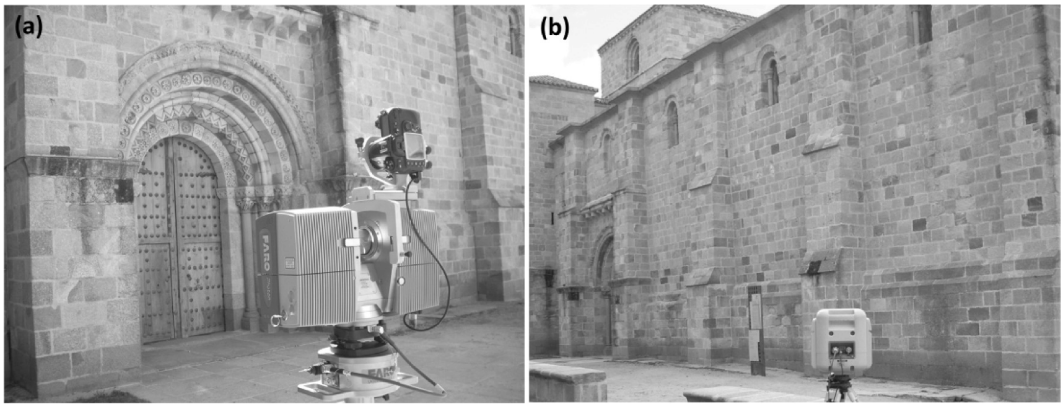

Figure 13.7 Church of San Pedro: (a) Detail view of the north entrance. (b) General view of the north façade (Flórez García, 2009).

Here, the different granite types of masonry combined on the façade are generally assessed (Fig. 13.7):

- The main façade (westward orientation): consists of a plinth and buttress of grey granite blocks. The use of this constructive solution in the upper archivolts and the pinnacles should be highlighted. The rest of the façade is built with ochre and red granite blocks.
- The eastern façade: consisting, similarly to the main façade, of a grey granite plinth (variable in height) and walls with ochre and red granite blocks.
- The north façade: slightly different from the rest, presents a red granite plinth and the rest of the elements are erected with ochre granite as predominant construction material.
- The southern façade: similarly to the western façade has a buttress fully erected in grey granite.
- The inside of the church: consists of a combination of ochre and grey granite. The grey granite was used for the pillars, since ochre granite was used for the rest of the structural elements (walls, arches, vaults, etc.).

13.4.2 *Pathologies of the Structure*

While white, ochre and red granites present better properties to be hewed and become part of the façade ornamentation: their physical-mechanical properties, such as water absorption, frost resistance, bending strength, shock and compression resistance, are worse than those of the grey granite from bedrock (García-Talegón et al. 1993). That is why a complete pathological evaluation with a comprehensive knowledge of the structure (finite element analysis, limit analysis, etc.) may yield not only a correct identification of the different construction materials but also detect possible pathologies of such materials as listed below:

- Grey granite: mainly composed of quartz, feldspar, mica and chlorite.
- Ochre granite: altered granite without chlorites, biotites and plagioclases. Its mineralogical composition consists of iron oxyhydroxides and phyllosilicates.

- Granite of reddish color: weathered granite that has undergone a kaolinization process with long periods of water saturation. It has a greater content of iron oxides.
- Degree of moisture: as a result of filtration and capillarity processes.
- Biological colonization: the effects of specific atmospheric conditions such as high humidity and temperature and the presence of oxygen lead to the proliferation and persistence of certain organisms on the rock.
- Color changes: as patinas of dirt, a damage due to environmental pollution.

13.4.3 *Materials and Methods*

In this case study, technologies such as terrestrial laser scanning and close range photogrammetry were again applied to analyze and diagnose the diseases presented in the different construction materials of the north façade of the church, because this façade is the most affected of the church.

A pathological assessment of the constructions was undertaken in response to the damage caused by external factors in the previous case studies. However, in this case the variability of different types of granites was examined as an intrinsic factor of the origin of pathologies. Thus it was decided to work in the visible and near infrared range to analyze the potential of these two spectral ranges in order to distinguish building materials. For the visible range and as an active sensor the laser scanner Trimble GX200 was used, whereas the compact camera Nikon Coolpix L11 was applied as passive sensor. For the near infrared range, the laser scanner FARO Photon 80 was selected (the technical characteristics of each sensor are listed in Table 13.1).

The methodology for the data analysis and the workflow followed are proposed in Figure 13.1: planning and data acquisition, filtering and segmentation, some data corrections, orthoimages generation and multispectral data classification.

Planning and data acquisition. An initial assessment and inspection of the area under study were essential to plan the multisensory data acquisition. Some possible limitations during data capture and the accessibility to the area depend on the time of day, number of stations and the distance established to the structure, among other factors. Therefore, the success in the fieldwork depends largely on the previous inspection. In this particular study various problems were observed: hidden areas caused by the projected shadows by two nearby buildings, inability to station the sensors in the desired position and frequent pedestrian traffic. Finally, the ideal moment was selected to achieve a homogeneous lighting to ensure uniformity in the radiometric values of the field campaign.

With laser scanners leveled properly, a total of 2 stations at a distance to the façade that varied between 6 and 3 m were performed. The final spatial resolution of the point cloud was 8 mm. As in previous cases, Trimble Realworks Survey and Scene 3D software were used for the data acquisition. Meanwhile, the Nikon Coolpix L11 was integrated into the FARO Photon 80 to take pictures simultaneously from the same point of view.

Filtering and segmentation. As has been mentioned, since the church was located in a city center and surrounded by some buildings, the multispectral study was very interrupted by pedestrian traffic and affected by the shadows projected by neighboring

buildings. Therefore, the first step of data processing was the segmentation of the point clouds leaving only data belonging to the façade of interest.

Data corrections. Some data required corrections such as carry out a proper registration and alignment of all stations belonging to each sensor. The targets disposed on the walls were used to perform the alignments, and therefore these targets should appear in each laser scan.

Orthoimages generation. After getting all the scans aligned and registered in the same coordinate system, the three orthoimages (from: RGB, $G_{Trimble}$, and NIR) were created. The orthoimage generation was carried out with the Trimble Realworks Survey software. Firstly, orthoimages from both laser scanners point clouds in the green and NIR ranges respectively were created and orthoimages from the RGB afterwards (similarly as in the previous case). The spatial resolution reached for the orthoimages was 20 mm.

Multispectral data classification. Finally, the set of three orthoimages arranged in a three-channels multispectral image was initially classified in an unsupervised way and subsequently in a supervised way. For the unsupervised classification the *fuzzy k-means* algorithm was used.

13.4.4 *Experimental Results*

The methodology required to ensure a right pathological classification of the structural materials involved performing a supervised classification. To this end, it was necessary to establish the suitable number of a priori informational classes and their connection with the data collected by all the sensors.

The initial hypothesis was set based on: (i) Three classes for construction materials (granites); (ii) Three classes for pathologies (two classes for moisture and one for biological factors); (iii) wood structures; and (iv) null class.

The study of mortar between blocks was not possible since its thickness was less than the GSD achieved with all sensors. This building material was perceptible only in the joints with a widest thickness of 3 cm while the spatial resolution of the orthoimages was 2 cm. Therefore, it was decided to dismiss it from the classification process.

Regarding the *fuzzy k-means* unsupervised classification, where the aforementioned hypothesis of clusters was established, provided results were not comparable even with the visual inspection. Therefore, it was necessary to fix other informational classes (a total of seven) including artificial elements of the guttering system, excluding wooden class present in the door and the union of the two types of unaltered granites in one class. This was necessary since the spectral resolution of the five-channels images generated was not enough.

The overall accuracy achieved in the classification shown in Figure 13.8 was 0.8835 with a Cohen's Kappa coefficient of 0.8328 for six informational classes (Table 13.5).

After the unsupervised classification by setting seven clusters, the roof gutters and metal rivets of the door were classified within the same class. Regarding the detection of pathologies on the façade, the confusion between moisture and biological factors should be noted (Table 13.6). This fact occurs because both pathologies are usually interrelated.

Moreover, the classes for which the worst value of separability (1.735/2.000) was obtained were "unaltered granite" and "penetrating damp", as shown in Table 13.6.

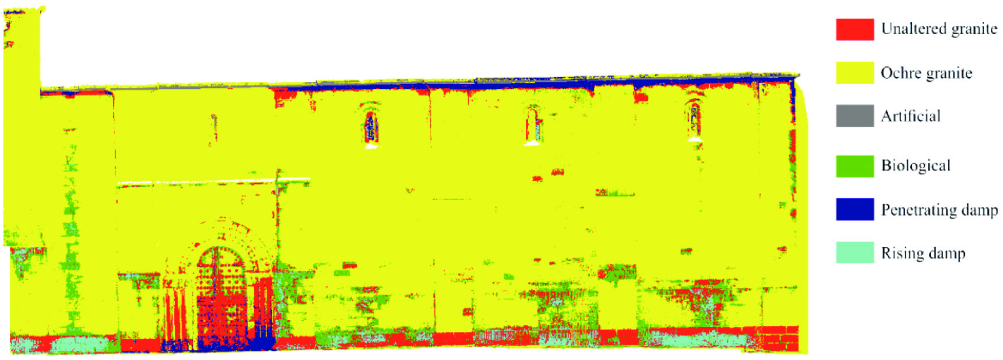

Figure 13.8 Orthoimage classification result after the supervised classification.

Table 13.5 Supervised classification: confusion matrix with six channels.

	Unaltered granite	Ochre granite	Artificial elements (e.g. gutter)	Biological colonization	Penetrating damp	Rising damp
Unaltered granite	82.28%	0.96%	0.00%	1.26%	15.48%	0.02%
Ochre granite	0.73%	98.70%	0.00%	0.57%	0.00%	0.00%
Artificial elements	0.00%	0.00%	100.00%	0.00%	0.00%	0.00%
Biological colonization	1.90%	1.33%	0.00%	84.30%	12.46%	0.00%
Penetrating damp	2.53%	0.00%	0.00%	6.41%	91.05%	0.00%
Rising damp	3.36%	0.00%	0.00%	0.00%	0.00%	96.64%

Table 13.6 Separability between classes.

	Unaltered granite	Ochre granite	Artificial elements	Biological colonization	Penetrating damp	Rising damp
Unaltered granite	–					
Ochre granite	1.99642	–				
Artificial elements	2.00000	2.00000	–			
Biological colonization	1.83363	1.98558	2.00000	–		
Penetrating damp	1.73514	2.00000	2.00000	1.87890	–	
Rising damp	1.98978	2.00000	2.00000	2.00000	1.99994	–

The main reason is the similar radiometric response of the unaltered granite and slightly damp unaltered granite and due to unaltered granite is only part of the façade plinth and this part of the structure is likely to be affected by rising damp.

As a general conclusion, it is important to highlight that limitations in robust discrimination potential of pathologies after the classification process is not only due to the radiometric resolution, which depends on the available sensors for each case study, but also depends on the smallest element that it is possible to discriminate, i.e. the spatial resolution of the orthoimages.

An approximate knowledge of the spectral signatures of the materials studied, although they come from laboratory tests, would help in the selection of the optimal wavelengths for the definition of effective informational classes.

13.5 Conclusions

Although the described methodology based on multispectral dataset management allows detecting and classifying accurately a variety of constructive pathologies, certain aspects such as peelings, cracks or disaggregation processes (abundant in masonry elements) are not completely explained. Given the flexibility of this methodology, which allows the analysis of data obtained by laser scanning and photogrammetry techniques, such degradation processes can be completely characterized through a geometric analysis of the construction. Also, the possibility of a large scale evaluation (large evaluated areas) and pathologies quantification are the strong points of photogrammetry and laser systems, making them valuable resources within the buildings' pathological assessment. However, as noted above, certain geometric aspects are not fully defined, as well as qualitative data on the material affected by pathological processes (which can be obtained by in-situ or laboratory test).

In order to make a full pathological assessment it is recommended to perform the following stages: (i) Geometric analysis (measuring deformations, settlements, kaolinization, etc.); (ii) Multispectral classification (using the described methodology); and (iii) Complementary qualitative in-situ and laboratory tests (use of reagents to assess biological colonization, mineralogical analysis, mechanical analysis, etc.).

Also essential is planning periodic field campaigns which will allow monitoring and assessing the pathological condition and the effectiveness of the applied restoration techniques.

Regarding the field campaigns, a series of particular best practices have been covered in the previous subsections. However, the optimal data acquisition protocol changes for the different spectral regions. When the discretization of the textural differences is required, the visible region is advisable, so the acquisition should be done with uniform light conditions. However, for a more detailed analysis of moisture (different degree of moisture) it is recommended to add a thermal infrared channel, which requires a light absence (mainly the solar effects) for an optimal data gathering. Although it is possible a priori knowledge of the material spectral signature, this information comes from laboratory test where not only the light conditions are controlled, but also specimens are optimal. In the field campaign, the constructive materials may have a heterogeneous appearance due to the textural differences which hinder their correct classification. In this regard, the use of additional SWIR channels, despite its worst geometric resolution, will improve their classification. Finally, the 3D spatial characterization of the study object is a strong point when the quantitative metric analysis associated to the areas affected is required. As additional advantage, the quantification of the prevention measures and their associated cost is directly drawn. When only a qualitative analysis is required, a pure 2D approach could be applied, supported by a projective transformation. However, the results and the resultant conclusions will be valid, only if the error budget is admissible and has been taken into account.

The current emergence of BIM (Building Information Modeling) and HBIM (Historical Building Information Modeling) multilayer models can be the perfect complement

to the methodology presented. As a result, it would be possible to create a complete information model including in it an exhaustive material characterization and pathological evaluation through time. As a result, analyses based on predictive models allow us to anticipate possible events, allowing to safeguard the integrity of the construction. It is in this field where the methodology presented could play a crucial role and provide added value.

References

Armesto-González, J., Riveiro-Rodríguez, B., González-Aguilera, D., & Rivas-Brea, M. T. (2010). Terrestrial laser scanning intensity data applied to damage detection for historical buildings. *Journal of Archaeological Science,* 37(12): 3037–3047. doi: http://dx.doi.org/10.1016/j.jas.2010.06.031.

Coffin, D. (2011). Raw digital photo decoding. Retrieved January 24, 2015.

Cohen, J. (1968). Weighted kappa: Nominal scale agreement provision for scaled disagreement or partial credit. *Psychological bulletin,* 70(4): 213.

Crespo, C., Armesto, J., González-Aguilera, D., & Arias, P. (2010). Damage Detection on Historical Buildings Using Unsupervised Classification Techniques. *ISPRS-International Archives of the Photogrammetry, Remote Sensing and Spatial Information Sciences, XXXVIII*, 184–188.

Del Pozo, S., Herrero-Pascual, J., Felipe-García, B., Hernández-López, D., Rodríguez-Gonzálvez, P., & González-Aguilera, D. (2015). Multi-Sensor Radiometric Study to Detect Pathologies in Historical Buildings. *ISPRS-International Archives of the Photogrammetry, Remote Sensing and Spatial Information Sciences, XL-5/W4*, 193–200.

Flórez García, E. (2009). *Aplicación de técnicas geomáticas al análisis y diagnóstico de patologías en edificios del patrimonio histórico*. Departamento de Ingeniería Cartográfica y del Terreno. Politécnica Superior de Ávila. Ávila.

García-Talegón, J., García del Amo, D., Iñigo, A., Menduiña, J., Molina Ballesteros, E., & Hernández, V. (1993). Propiedades físico mecánicas de los granitos empleados en la catedral de Avila procedentes del yacimiento de "La Colilla" (Avila).

González-Jorge, H., Gonzalez-Aguilera, D., Rodriguez-Gonzalvez, P., & Arias, P. (2012). Monitoring biological crusts in civil engineering structures using intensity data from terrestrial laser scanners. *Construction and Building Materials*, 31(0): 119–128. doi: http://dx.doi.org/10.1016/j.conbuildmat.2011.12.053.

Instrucción del Hormigón Estructural, E. (2008). EHE-08. *Madrid, Ministerio de Fomento, Secretaría General Técnica.*

Li, M., Zang, S., Zhang, B., Li, S., & Wu, C. (2014). A Review of Remote Sensing Image Classification Techniques: the Role of Spatio-contextual Information. *European Journal of Remote Sensing*, 47, 389–411.

Lu, W., & Tan, Y.-P. (2003). Color filter array demosaicking: new method and performance measures. *IEEE Transactions on Image Processing, 12*(10), 1194–1210.

Ministerio de Fomento (1968). Instrucción para el proyecto y ejecución del obras de hormigón en masa o armado. Madrid.

Molina Ballesteros, E. (1993). *Incidencia de las alteraciones del zocalo hercinico iberico en las caracteristicas de las rocas afectadas, empleadas como materiales de construccion. Los granitos de "La Colilla" (Ávila).* Paper presented at the Alteracion de granitos y rocas afines, empleados como materiales de construccion: deterioro de monumentos historicos. Actas del workshop, Consejo Superior de Investigaciones Cientificas, Avila, Spain, 1993.

Montojo Santos, C., López de Silanes Vázquez, M., Álvarez Andrés, J., Sánchez-Biezma Serrano, M. J., Prieto Lamas, B., Silva Hermo, B. M., & López Díaz, A. J. (2014). Las ruinas de Santo Domingo de Pontevedra.

Porto, C. M. (1993). Arte gótico en Galicia: los dominicos I.

Rodríguez-González, P., Pascual, J. H., Aguilera, D. G., Nieto, Á. L. M., Mancera-Taboada, J., Martín, N. S., & Hidalgo, M. Á. M. (2013). Aplicación de técnicas geomáticas al análisis y diagnóstico de patologías en el Patrimonio Arquitectónico. *Mapping* (161), 4–19.

Sánchez-Aparicio, L. J., Riveiro, B., González-Aguilera, D., & Ramos, L. F. (2014). The combination of geomatic approaches and operational modal analysis to improve calibration of finite element models: A case of study in Saint Torcato Church (Guimarães, Portugal). *Construction and Building Materials*, 70(0): 118–129. doi: http://dx.doi.org/10.1016/j.conbuildmat.2014.07.106.

Chapter V

Conclusions and Future Research Topics

This Doctoral Thesis aims at making a contribution to one of the most challenging fields in civil engineering, the detection and quantification of damages in infrastructures and its contribution into the structural response of them. The major conclusions and contributions of the Thesis are expressed in more detail below, in accordance with the objectives defined previously:

I. **Evaluation of the applicability of geomatic sensors (Terrestrial Laser Scanner and digital cameras) in buildings with structural damages.**

   a) The geometrical and radiometrical component of the points clouds derived from Terrestrial Laser Scanner and digital cameras have shown strong potentialities as sensors for *SHM.*

   b) The Digital Image Correlation approach has proven to be a powerful technique for the mechanical evaluation of materials. Throwing a non-contact, low-cost methodology able to compete with the traditional sensors such as the Linear Variable Differential Transformers (*LVDTs*) or strain gauges.

   c) The use of Unmanned Aerial Vehicles equipped with digital cameras offers a powerful photogrammetric tool for reconstructing inaccesible areas or buildings.

   d) The combination of photogrammetry (Structure from Motion) and the Terrestrial Laser Scanner allows a complete reconstruction and *CAD* creation of complex buildings.

   e) Although cracks are geometrical phenomena, they can be evaluated through radiometric approaches (such as edge detectors).

II. **Development of modeling strategies and construction of *CAD* models on structures with pathological processes with a clear geometric component (deformations and cracks), suitable for its subsequent numerical analysis.**

   a) The curvature segmentation technique holds a special position among the different segmentation strategies, maintaining details and decimating flat areas.

b) For a correct point cloud to *CAD* conversion a manifold mesh is needed. In a maniflod mesh each edge is incident to only one or two faces and the faces incient to a vertex form a closed or an open fan.

c) The Functional Decomposition approach (based on the Morse theory) has proven to be a powerful methodology for the segmentation of meshes into smooth regions.

d) Parametric (planes, cylinders, etc.) and non-parametric (*NURBs*) surfaces can be used in the geometrical models for numerical simulations.

e) The NURBS approach based on the mesh quadrilaterization (Morse theory and Spectral anlaysis) and regularization shows good results for *CAD* modeling.

f) The consideration of structural pathologies (such as cracks or lack of material) can be integrated into NURBS environment through boundary conditions.

III. The use of structures' dynamic evaluation strategies based on Operational Modal Analysis (OMA) in the evaluation of damage.

a) Operational Modal Analysis (output-only modal analysis) has proven to be a powerful approach for different types of constructions.

b) The Stochastic Subspace Identification (*SSI*) and Enhanced Frequency Domain Decomposition (*EFDD*) require random excitations with ambient noise, which makes the estimation of the modal parameters simple and cost-effective.

c) The detection of the damage (with influence in the global behavior of the structure) can be carried out by frequency changes.

d) Local damage presents an important relation with the mode shapes. Therefore not only a sufficient number of measuring points is needed to capture them, but also indicators such as the *MAC* or *COMAC* .

IV. Application and development of methodologies of robust calibration of numeric models, able

to locate and interpret the core damage present in buildings, using the above-mentioned techniques.

a) The static and dymanic variables of the structure (deflections, frequencies, modal shapes, etc.) can be used to calibrate the structural response of the numerical simulation.

b) The point cloud features (geometrical ones) can be used as indicator of robustness of the numerical model.

c) Global Hausdorff metric (GHm_s) and Local Hausdorff metric (GHm_s) seem to have strong potentialities in the evaluation of the similarities between the simulated deformation and the current one.

d) The Finite Element Method shows strong capabilities. However the diversity of variables acting on it need to be calibrated in order to improve the results.

e) The Douglas-Reid and the Deterministic calibration methods can be used for the calibration of complex finite element models.

f) Damage functions (discrete and substructures) can be used to detect and quantifying cracks in damage constructions.

g) Damage functions can be used in conjunction with robust calibration strategies to enhance the response of numerical simulations.

V. Application of techniques for the analysis of multispectral images in the extraction and quantification of pathologies with an eminently radiometric component (e.g. characterization of materials, humidity in concrete, biological attacks, etc.) that show a close connection with the stability and the useful life of constructions.

a) Laser Scanning and Photogrammetry provide useful information (radiometric component) about the pathological state of the construction.

b) Unsupervised and Supervised classification algorithms (such as Fuzzy k-means or Maximum Likelihood) have proven to be potential tools in the detection of a wide variety of pathologies (e.g. algae, lichens or humidity in concretes).

c) The spectral response of the structure´s materials and pathologies is needed for their correct evaluation.

d) Sensor hybridization (laser scanner and digital cameras) was successfully achieved, improving the results of the multispectral classification.

e) The laser scanner or photogrammetric point cloud can be used as a metric support on which the damages presented in the building can be quantified.

In more practical terms and concerning their reach, the sensors used as well as the methodologies developed have been tested in different types of damaged buildings: from historical and vernacular architecture, to reinforced concrete constructions and constructive solutions in an experimental phase.

The work carried out in this Doctoral Thesis provides means to respond to common pathological processes presented in constructions, allowing the evaluation of their stability and life cycle. Nevertheless, part of these procedures require future works to boost their applicability, including:

I. Sensor hybridization.

a) Using thermograpic cameras with dynamic analysis to evaluate the influence of temperature in the structure´s dynamic behaviour.

II. *CAD* modeling strategies for numerical simulations.

a) Developing the connection with more sophisticated numeric computational strategies, such as isogeometric analysis or Nurbs-Enhanced Finite Element Method (NEFEM method) able to exploit with the geometry provided by the laser scanning and the photogrammetry through a *NURBs* modeling.

b) Improving the segmentation process with curvature mean-shifting strategies.

c) Advancing in the automatic classification of segmented zones and connections by means of parametric or non-parametric surfaces.

d) Labeling the mesh segmentation by means of learning and expert classifiers, allowing the classification of different structural components and their posible pathologies.

III. Model/non-model based damage-detection.

a) Developing model-based damage-detection methods using improved damage functions (e.g. considering crack depth and path).

b) Using non-model based methods as space delimiting agents, with the purpose of implementing damage functions on these areas.

c) Progressing on the validation of geometric-quality indexes, GHm_s and LHm_s, for the calibration of numerical models.

IV. Multispectral classification.

a) Enhancing the sensor fusion by means of an automatic registration (multimodal matching).

b) Employing multispectral/ hyperspectral cameras to evaluate different spectrum ranges in the detection of pathologies.

c) Extending the multispectral classification to a 3D environment with the aim of integrating the materials and pathologies in models fit for numerical analysis or advanced construction information systems (Building Information Models-*BIM*).

d) Complementing the multispectral classification with the Neural Network approach in order to enhance the recognition and classification of materials and pathologies.

REFERENCES

A

Adewole, K. K., & Bull, S. J. (2013). Prediction of the fracture performance of defect-free steel bars for civil engineering applications using finite element simulation. *Construction and Building Materials, 41*, 9-14. doi: http://dx.doi.org/10.1016/j.conbuildmat.2012.11.089

Akca, D., & Grün, A. (2007). *Least Squares 3D surface matching*: Inst. für Geodäsie und Photogrammetrie.

Armesto-González, J., Riveiro-Rodríguez, B., González-Aguilera, D., & Rivas-Brea, M. T. (2010). Terrestrial laser scanning intensity data applied to damage detection for historical buildings. *Journal of Archaeological Science, 37*(12), 3037-3047. doi: http://dx.doi.org/10.1016/j.jas.2010.06.031

Armesto, J., Roca-Pardiñas, J., Lorenzo, H., & Arias, P. (2010). Modelling masonry arches shape using terrestrial laser scanning data and nonparametric methods. *Engineering Structures, 32*(2), 607-615. doi: http://dx.doi.org/10.1016/j.engstruct.2009.11.007

Attene, M. (2010). A lightweight approach to repairing digitized polygon meshes. *The Visual Computer, 26*(11), 1393-1406.

B

Barazzetti, L., Binda, L., Scaioni, M., & Taranto, P. (2011). Photogrammetric survey of complex geometries with low-cost software: Application to the 'G1' temple in Myson, Vietnam. *Journal of cultural heritage, 12*(3), 253-262.

Besl, P. J., & McKay, N. D. (1992). *Method for registration of 3-D shapes.* Paper presented at the Robotics-DL tentative.

Branch, J. W., Prieto, F., & Boulanger, P. (2008). *Automatic Extraction of Quadrilateral Patches from Triangulated Surfaces Using Morse Theory.* Paper presented at the Proceedings of the 16th International Meshing Roundtable.

C

Cabaleiro, M., Riveiro, B., Arias, P., Caamaño, J., & Vilán, J. (2014). Automatic 3D modelling o f metal frame connections from LiDAR data for structural engineering purposes. *ISPRS Journal of Photogrammetry and Remote Sensing, 96*, 47-56.

Campbell, J. B. (2002). *Introduction to remote sensing*: CRC Press.

Castellazzi, G., D'Altri, A. M., Bitelli, G., Selvaggi, I., & Lambertini, A. (2015). From laser scanning to finite element analysis of complex buildings by using a semi-automatic procedure. *Sensors, 15*(8), 18360-18380.

Conde, B., Villarino, A., Cabaleiro, M., & Gonzalez-Aguilera, D. (2015). Geometrical Issues on the Structural Analysis of Transmission Electricity Towers Thanks to Laser Scanning Technology and Finite Element Method. *Remote Sensing, 7*(9), 11551-11569.

D

De Borst, R., Remmers, J. J., Needleman, A., & Abellan, M.-A. (2004). Discrete vs smeared crack models for concrete fracture: bridging the gap. *International Journal for Numerical and Analytical Methods in Geomechanics*(28), 583-607.

Del Pozo, S., Lindenbergh, R., Rodríguez-Gonzálvez, P., Blom, J. K., & González-Aguilera, D. (2015). Discrimination between Sedimentary Rocks from Close-Range Visible and Very-Near-Infrared Images. *PloS one, 10*(7), e0132471.

Del Pozo, S., Rodríguez-Gonzálvez, P., Hernández-López, D., & Felipe-García, B. (2014). Vicarious radiometric calibration of a multispectral camera on board an unmanned aerial system. *Remote Sensing, 6*(3), 1918-1937.

Dong, C., Zhang, P., Feng, W., & Huang, T. (1994). *The sensitivity study of the modal parameters of a cracked beam.* Paper presented at the Proceedings of the 12th International Modal Analysis.

Douglas, B. M., & Reid, W. H. (1982). Dynamic tests and system identification of bridges. *Journal of the Structural Division, 108*(ST10).

F

Farrar, C. R. (2003). *Damage prognosis: current status and future needs*: Los Alamos National Laboratory.

Farrar, C. R., & Worden, K. (2007). An introduction to structural health monitoring. *Philosophical Transactions of the Royal Society of London A: Mathematical, Physical and Engineering Sciences, 365*(1851), 303-315.

G

García-Talegón, J., García del Amo, D., Iñigo, A., Menduiña, J., Molina Ballesteros, E., & Hernández, V. (1993). Propiedades físico mecánicas de los granitos empleados en la catedral de Avila procedentes del yacimiento de" La Colilla"(Avila).

Gentile, C., & Saisi, A. (2007). Ambient vibration testing of historic masonry towers for structural identification and damage assessment. *Construction and Building Materials, 21*(6), 1311-1321.

Gonilha, J. A., Barros, J., Correia, J. R., Sena-Cruz, J., Branco, F. A., Ramos, L. F., . . . Santos, T. (2014). Static, dynamic and creep behaviour of a full-scale GFRP-SFRSCC hybrid footbridge. *Composite Structures, 118*, 496-509. doi: http://dx.doi.org/10.1016/j.compstruct.2014.08.009

H

Haque, M., Zain, M., Hannan, M., Jamil, M., & Johari, H. (2012). Recent application of structural civil health monitoring using WSN and FBG. *World Applied Sciences Journal, 20*(4), 585-590.

Hausdorff, F. (2008). *Felix Hausdorff-Gesammelte Werke Band III: Mengenlehre (1927, 1935) Deskripte Mengenlehre und Topologie* (Vol. 3): Springer-Verlag.

Heyman, J. (1997). *The stone skeleton: structural engineering of masonry architecture*: Cambridge University Press.

Housner, G. W., Bergman, L. A., Caughey, T., Chassiakos, A., Claus, R., Masri, S., . . . Yao, J. T. (1997). Structural control: past, present, and future. *Journal of Engineering Mechanics, 123*(9), 897-971.

Huerta, S. (2008). The Analysis of Masonry Architecture: A Historical Approach: To the memory of Professor Henry J. Cowan. *Architectural Science Review, 51*(4), 297-328.

L

Li, M., Zang, S., Zhang, B., Li, S., & Wu, C. (2014). A Review of Remote Sensing Image Classification Techniques: the Role of Spatio-contextual Information. *European Journal of Remote Sensing, 47*, 389-411.

Liang, D., & Yuan, S. (2015). Structural health monitoring system based on multi-agent coordination and fusion for large structure. *Advances in Engineering Software, 86*, 1-12.

Lorenzoni, F., Casarin, F., Modena, C., Caldon, M., Islami, K., & da Porto, F. (2013). Structural health monitoring of the Roman Arena of Verona, Italy. *Journal of Civil Structural Health Monitoring, 3*(4), 227-246.

M

Milani, G., & Valente, M. (2015). Comparative pushover and limit analyses on seven masonry churches damaged by the 2012 Emilia-Romagna (Italy) seismic events: Possibilities of non-linear finite elements compared with pre-assigned failure mechanisms. *Engineering Failure Analysis, 47, Part A*(0), 129-161. doi: http://dx.doi.org/10.1016/j.engfailanal.2014.09.016

Moody, D. I., Brumby, S. P., Rowland, J. C., & Altmann, G. L. (2014). Land cover classification in multispectral imagery using clustering of sparse approximations over learned feature dictionaries. *Journal of Applied Remote Sensing, 8*(1), 084793-

084793.

Mottershead, J., & Friswell, M. (1993). Model updating in structural dynamics: a survey. *Journal of sound and vibration, 167*(2), 347-375.

O

Osmancikli, G., Bayraktar, A., Türker, T., Uçak, Ş., & Mosallam, A. (2015). Finite element model calibration of precast structures using ambient vibrations. *Construction and Building Materials, 93*, 10-21. doi: http://dx.doi.org/10.1016/j.conbuildmat.2015.05.096

P

Pandey, A., Biswas, M., & Samman, M. (1991). Damage detection from changes in curvature mode shapes. *Journal of sound and vibration, 145*(2), 321-332.

Peeters, B., & De Roeck, G. (2001). One-year monitoring of the Z 24-Bridge: environmental effects versus damage events. *Earthquake engineering & structural dynamics, 30*(2), 149-171.

Piegl, L., & Tiller, W. (2012). *The NURBS book*: Springer Science & Business Media.

Pope, A., & Rees, W. G. (2014). Impact of spatial, spectral, and radiometric properties of multispectral imagers on glacier surface classification. *Remote sensing of environment, 141*, 1-13.

R

Rainieri, C., & Fabbrocino, G. (2014). *Operational modal analysis of civil engineering structures*: Springer.

Ramos, L. F. (2007). Damage identification on masonry structures based on vibration signatures.

Ramos, L. F., Aguilar, R., Lourenço, P. B., & Moreira, S. (2013). Dynamic structural health monitoring of Saint Torcato church. *Mechanical Systems and Signal Processing, 35*(1–2), 1-15. doi: http://dx.doi.org/10.1016/j.ymssp.2012.09.007

Ramos, L. F., Marques, L., Lourenço, P. B., De Roeck, G., Campos-Costa, A., & Roque, J. (2010). Monitoring historical masonry structures with operational modal analysis: Two case studies. *Mechanical Systems and Signal Processing, 24*(5), 1291-1305
.

Riveiro, B., Morer, P., Arias, P., & de Arteaga, I. (2011). Terrestrial laser scanning and limit analysis of masonry arch bridges. *Construction and Building Materials, 25*(4), 1726-1735. doi: http://dx.doi.org/10.1016/j.conbuildmat.2010.11.094

Rytter, A. (1993). *Vibrational based inspection of civil engineering structures.* Unknown.

S

Saloustros, S., Pelà, L., Roca, P., & Portal, J. (2015). Numerical analysis of structural damage in the church of the Poblet Monastery. *Engineering Failure Analysis, 48*(0), 41-61. doi: http://dx.doi.org/10.1016/j.engfailanal.2014.10.015

Scaioni, M., Barazzetti, L., Brumana, R., Cuca, B., Fassi, F., & Prandi, F. (2009). *RC-Heli and Structure & Motion techniques for the 3-D reconstruction of a Milan Dome spire.* Paper presented at the Proceedings of the 3rd ISPRS International Workshop 3D-ARCH.

Simoen, E., De Roeck, G., & Lombaert, G. (2015). Dealing with uncertainty in model updating for damage assessment: A review. *Mechanical Systems and Signal Processing, 56–57*(0), 123-149. doi: http://dx.doi.org/10.1016/j.ymssp.2014.11.001

Solıs, M., He, L., Lombaert, G., & De Roeck, G. (2013). FINITE ELEMENT MODEL UPDATING OF A FOOTBRIDGE BASED ON STATIC AND DYNAMIC MEASUREMENTS. *ECCOMAS*.

Stubbs, N. (1987). A general theory of non-destructive damage detection in structures *Structural Control* (pp. 694-713): Springer.

Stubbs, N., Kim, J., & Topole, K. (1992). *An efficient and robust algorithm for damage localization in offshore platforms.* Paper presented at the Proceedings of the ASCE Tenth Structures Congress.

T

Teughels, A., & De Roeck, G. (2003). *Damage assessment of the Z24 bridge by FE model updating.* Paper presented at the Key engineering materials.

Titurus, B., & Friswell, M. (2008). Regularization in model updating. *International Journal for numerical methods in engineering, 75*(4), 440-478.

Tognaccini, R. (2009). La chiesa di Santa Maria del Mar a Barcellona: dal rilievo tridimensionale all'analisi strutturale.

Toldo, R., Beinat, A., & Crosilla, F. (2010). *Global registration of multiple point clouds embedding the Generalized Procrustes Analysis into an ICP framework.* Paper presented at the 3DPVT 2010 Conference.

Türker, T., & Bayraktar, A. (2014). Structural safety assessment of bowstring type RC arch bridges using ambient vibration testing and finite element model calibration. *Measurement, 58*, 33-45. doi: http://dx.doi.org/10.1016/j.measurement.2014.08.002

V

Várady, T., Facello, M. A., & Terék, Z. (2007). Automatic extraction of surface structures in digital shape reconstruction. *Computer-Aided Design, 39*(5), 379-388. doi: http://dx.doi.org/10.1016/j.cad.2007.02.011

Villarino, A., Riveiro, B., Gonzalez-Aguilera, D., & Sánchez-Aparicio, L. (2014). The Integration of Geotechnologies in the Evaluation of a Wine Cellar Structure through the Finite Element Method. *Remote Sensing, 6*(11), 11107-11126.

W

Watt, D. S. (1999). *Building pathology: Principles and practice*: Blackwell Science.

Worden, K., & Dulieu-Barton, J. (2004). An overview of intelligent fault detection in systems and structures. *Structural Health Monitoring, 3*(1), 85-98.

Y

Yan, Y., Cheng, L., Wu, Z., & Yam, L. (2007). Development in vibration-based structural damage detection technique. *Mechanical Systems and Signal Processing, 21*(5), 2198-2211.

Z

Zienkiewicz, O., & Taylor, R. (1994). El método de los elementos finitos. Volumen 1: Formulación básica y problemas lineales: CIMNE, Barcelona.

Zordan, T., Briseghella, B., & Liu, T. (2014). Finite element model updating of a tied-arch bridge using Douglas-Reid method and Rosenbrock optimization algorithm. *Journal of Traffic and Transportation Engineering (English Edition), 1*(4), 280-292.

Annex I

Enchance your Finite Element Models software

Developed in Matlab®, Enhance your Finite Element Models (*EyFEM*) is a non-official add-on for the TNO-DIANA® software developed during this Doctoral Thesis. *EyFEM* includes all the procedures built in the Chapter II and Chapter III:

- Discrete damage functions.
- Substructure damage functions.
- Hybrid damage funtions (discrete functions and substructures).
- Robust calibration procedures (dynamic, static and a combination of them) based on Deterministic approaches.
- Geometric quality indixes (GHm_s and LHm_s) based on the similarity between the numerical simulation and the real state captured by a geomatic sensor.

EyFEM was conceived with the aim to calibrate complex numerical simulations (static, dynamic or combination of both) based on the Finite Element Method (Fig. 1).

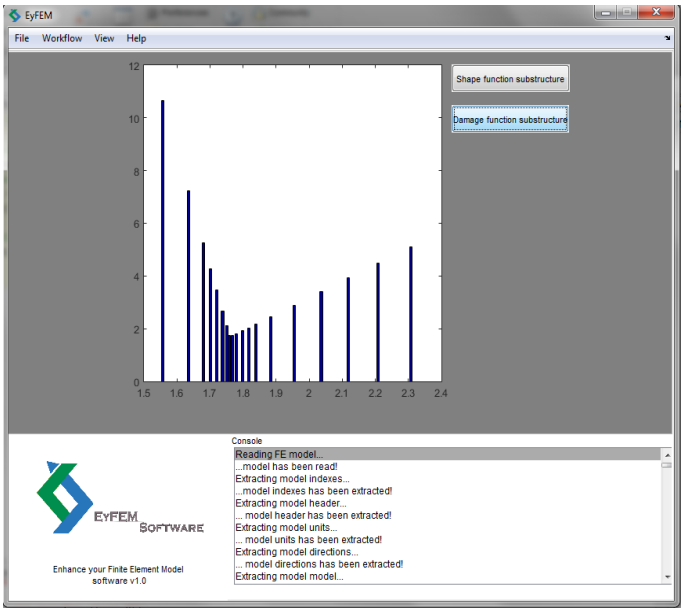

Figure 1. EyFEM interface

Its operational framework includes procedures for damage identification and quantification based on the damage function concept (1) (2).

$$X^e = X_o^e(1 - a^e) \tag{1}$$

$$a^e = \sum_{i=1}^{n} p_i N_i(X^e) \tag{2}$$

Where X^e_o is the physical property related with the damage (e.g. Young Modulus) in its initial value, X^e is the updated value, p_i is the multiplication factor and N_i is the damage function (discrete or substructure damage function).

This is all supported by a constrained Deterministic approach (assuming a relation between the experimental and the numerical variables) which tries to find the minimum value of the objective function (3) (4).

$$J^{sta} = 1/2 \mathrm{W}_\delta \sum_{j=1}^{m} (\delta_j^{num} - \delta_j^{\exp})/(\delta_j^{\exp})^2 \tag{3}$$

$$J^{din} = 1/2[W_f \sum_{i=1}^{m} ((f_i^{num} - f_i^{\exp})/(f_i^{\exp}))^2 + W_\varphi \sum_{i=1}^{m} (\phi_i^{num}(\phi_i^{\exp})/\phi_{ref}^{\exp})^2] \tag{4}$$

Where W_f, W_Φ, and W_δ are the weights considered for the frequency, vibration modes and static displacements, respectively, f is the frecuency, ϕ the modal displacements, δ the static displacements, and ϕ_{ref} is a scaling factor (normalization) that enable a comparison between the experimental and numerical modes displacements. For the dynamic functions (J^{din}) the *i* index indicates the mode shape and for the static one (J^{sta}) the *j* index indicates the load case.

This objective function is stated as a non-linear least square problem by (5) and follows a gradient-based optimization method (Gauss-Newton approach).

$$r = 1/2 \left\| \begin{matrix} J^{sta} \\ J^{din} \end{matrix} \right\|^2 \tag{5}$$

Where ||*|| denotes the Euclidean norm, *r* is the residual vector of and J^{sta}, J^{din} (static and dynamic objective functions, respectively).

It is noted that the gradient and the Hessian play an important role in this optimization method. For this reason firstly, the gradient is constructed from the sensitivity matrix (based on the concept of finite differences)(6). Later, the Hessian of the objective function is built following the next equation (7).

$$\nabla J(\Theta)=\sum_{i=1}^{m} r_i(\Theta)\nabla r_i(\Theta)=Jacob(\Theta)^T r(\Theta) \quad (6)$$

$$\nabla^2 J(\Theta)=Jacob(\Theta)^T Jacob(\Theta)+\sum_{(i=1)}^{n} r_i(\Theta)\nabla^2 r_i(\Theta)\cong Jacob(\Theta)^T Jacob(\Theta) \quad (7)$$

Where *Jacob* is the Jacobian matrix, *r* the vector which contains the residuals, Θ the different variables that will be optimized,∇ $r_i(\Theta)$ the residual´s gradient,∇ $J(\Theta)$ is the first derivate of the objective function and ∇^2 $J(\Theta)$ the second one. The index *n* indicates the number of variables consider during the optimization.

Additionally, *EyFEM* includes the geometrical indexes defined in Chapter IIIfor the evaluation of the robustness of Finite Element Models based on the geometrical similarity between the numerical and the real shape (point cloud captured by laser scanner or photogrammetry) (8) (9).

$$GHm_s=\left(\sum_{(a=1)}^{n} d_{SH}(a)-\sum_{(a=1)}^{n} d_{SHb}(a)\right)/\left(\sum_{(a=1)}^{n} d_{SHb}(a)\right) x100 \quad (8)$$

$$LHm_s=d_{SH}(a)/d_{SHref}(a) \quad (9)$$

Where GHm_s represent the Global Hausdorff metric index and LHm_s the Local Hausdorff metric index, $d_{SH}(a)$the symmetrical Hausdorff distance to cluster *a* considered for the model, $d_{SHb}(a)$ the symmetrical Hausdorff distance for the cluster *a* of the base model and $d_{SHref}(a)$ the symmetrical Hausdorff distance from cluster *a* to the reference one.

Annex II

Quality Description of the articles published

QUALITY INDEXES FOR PUBLICATIONS:

- **SJR INDICATOR:** Expresses the average number of weighted citations received in the selectec year by the documents published in the selected journal in the three previous years.

- **H INDEX:** H index expresses the journal´s number of articles *(h)* that have received at least h citations. It quantifies both journal scientific productivity and scientific impact and it is also applicable to scientist, countries, etc.

- **TOTAL DOCS.:** Output of the selected period. All types of documents are considered, including citable and non citable documents.

- **TOTAL DOCS.(3 YEARS):** Published documents in the three previous years (selected year documents are excluded). All types of documents are considered, including citable and non citable documents.

- **TOTAL REFERENCES:** Includes all the blibiographical references in a jorunal in the selected period.

- **TOTAL CITES (3 ºYEARS):** Number of citations received in the selected year by a journal to the document published in the three previous years. All types of documents are considered.

- **CITABLE DOCUMENTS:** Number of citable documents published by a journal in the three previous years (selected year documents are excluded). Exclusively artibles, reviews and conference papers are consideres.

- **CITES PER DOCUMENTS (2 YEARS):** Average citations per document in a 2 years period. It is computed considering the number of citations received by a journal in the current year to the documents published in the two previous years.

- **CITES PER DOCUMENTS (3 YEARS):** Average citations per document in a 3 years period. It is computed considering the number of citations received by a journal in the current year to the documents published in the three previous years.

- **CITES PER DOCUMENTS (4 YEARS):** Average citations per document in a 4 years period. It is computed considering the number of citations received by a journal in the current year to the documents published in the four previous years.

- **REF./DOC.:** Average number of references per document in the selected year.

- **SELFT CITES:** Number of journal´s self-citations in the selected year to its own documents published in the three previous years. All types of documents are considered.

- **NON-CITABLE DOCUMENTS (AVALIABLE IN THE GRAPHICS):** Non-ciable documents ratio in the period being considered.

- **UNCITED DOCUMENTS (UNCITED DOCS.):** number of uncited documents in the three prevous years.

- **% INTERNATIONAL COLLABORATION:** Document ratio whose affiliation includes more than one country address.

QUALITY INDEXES FOR BOOK CHAPTERS:

- **PBK:** Total number of books publised by a given publisher in a certain filed or disciline in the last five years.

- **PCH:** Total number of book chapters published by a given publisher in a certain field or discipline in the last five years.

- **CIT:** Total number of citations received by a given publisher in a certain field or discipline at the time of the data retreival process.

- **FNCS:** Normalized citations received according to the *"crown"* indicator.

JOURNAL:	Construction & Building Materials Journal
URL:	http://www.journals.elsevier.com/construction-and-building-materials/
EDITORAL:	Elsevier
IMPACT FACTOR:	2,29
H INDEX:	70
QUARTILE:	Q1 **(FIRST DECILE)**
RANK:	12(124)

SJR indicator vs. Cites per Doc (2y)

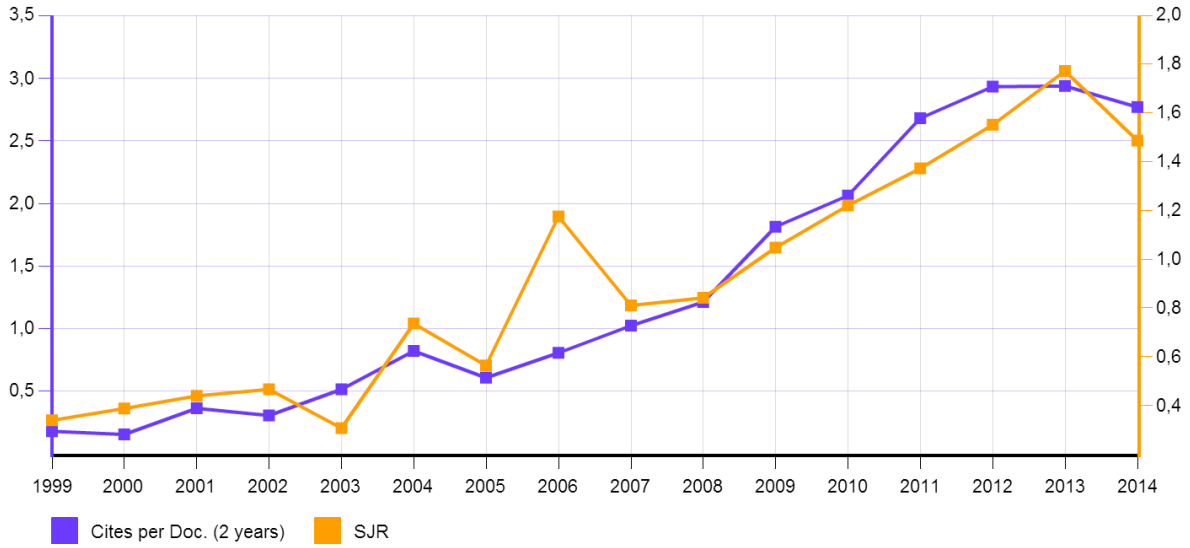

Citation vs. Self-Citation

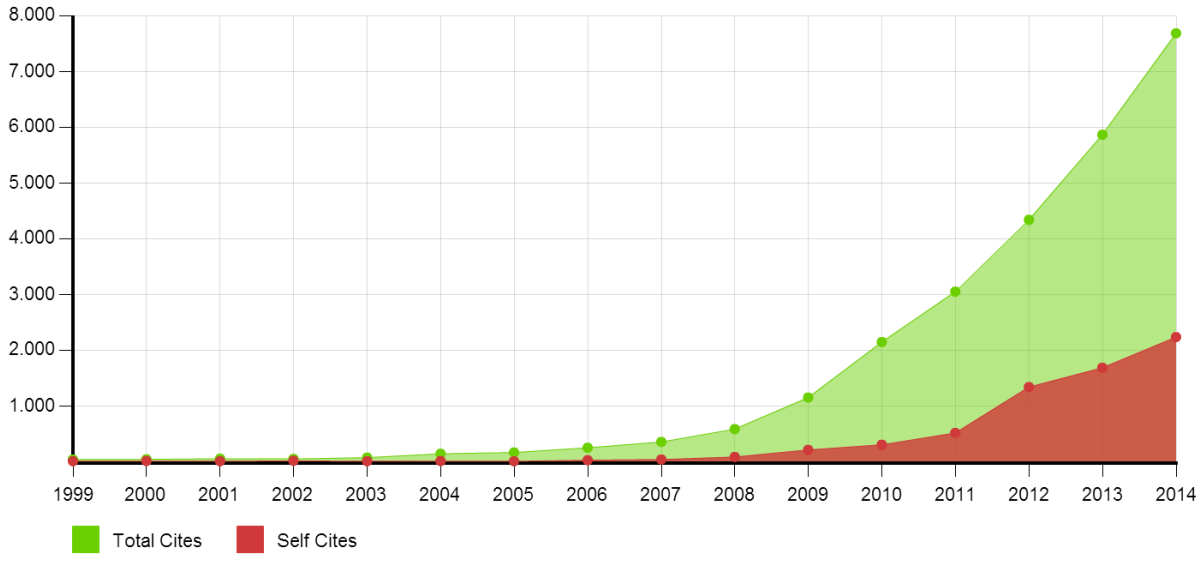

Cites per Document vs. External Cites per Document

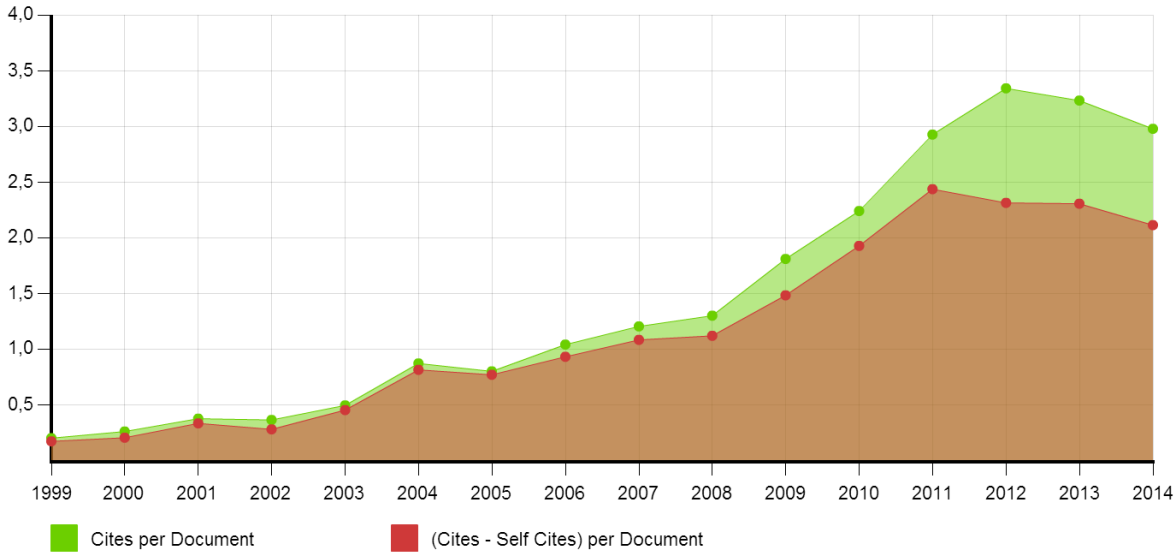

Cites per Document in 2, 3 and 4 years windows

International Collaboration

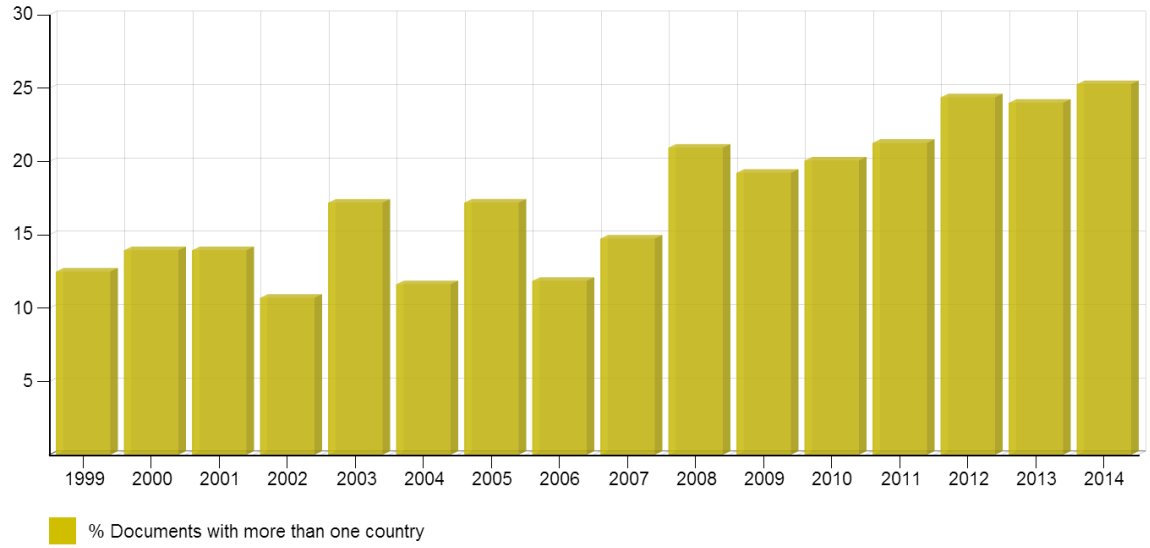

Journal's Citable vs. Non Citable Documents

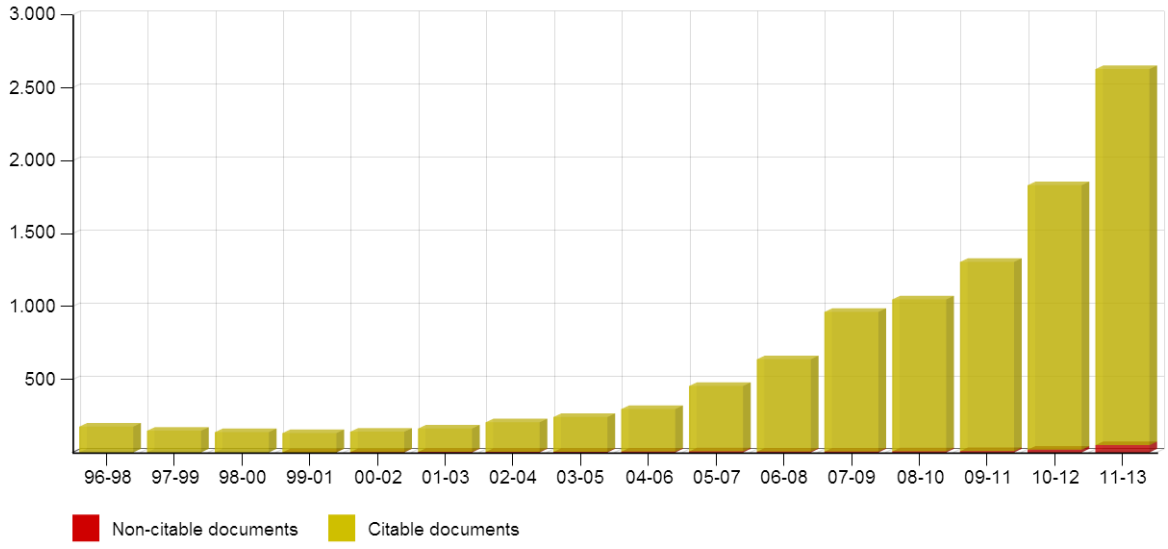

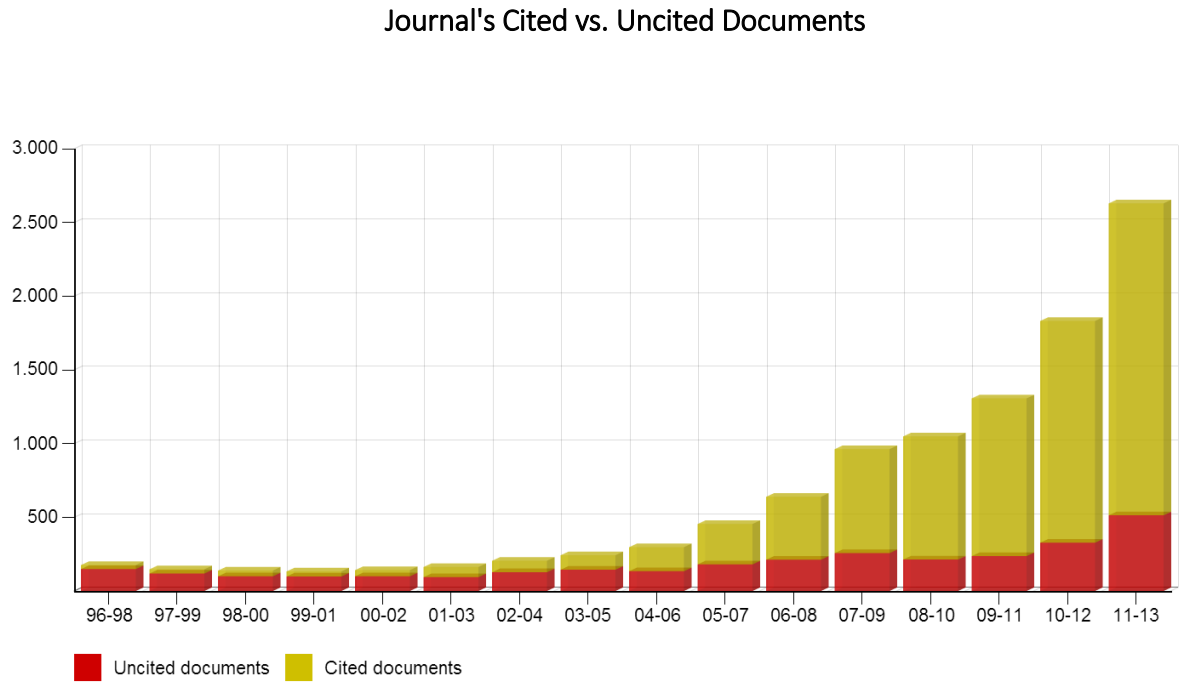
Journal's Cited vs. Uncited Documents
3.000
2.500
2.000
1.500
1.000
500
96-98
97-99
98-00
99-01
00-02
01-03
02-04
03-05
04-06
05-07
06-08
07-09
08-10
09-11
10-12
11-13
Uncited documents
Cited documents

JOURNAL:	Composite Structures Journal
URL:	http://www.journals.elsevier.com/composite-structures/
EDITORAL:	Elsevier
IMPACT FACTOR:	3,32
H INDEX:	82
QUARTILE:	Q1
RANK:	3(24)

SJR indicator vs. Cites per Doc (2y)

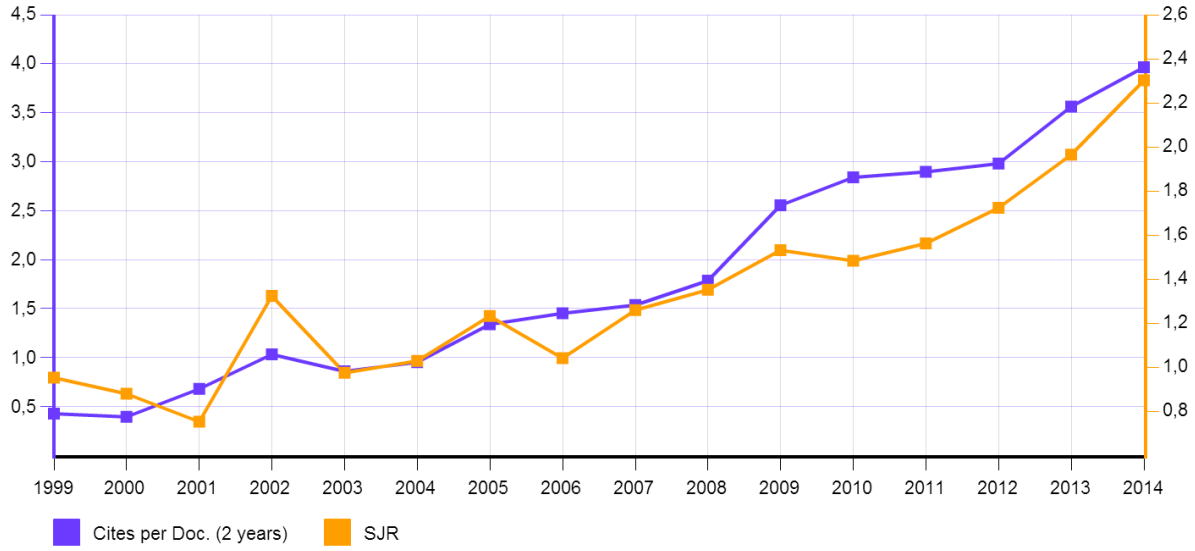

Citation vs. Self-Citation

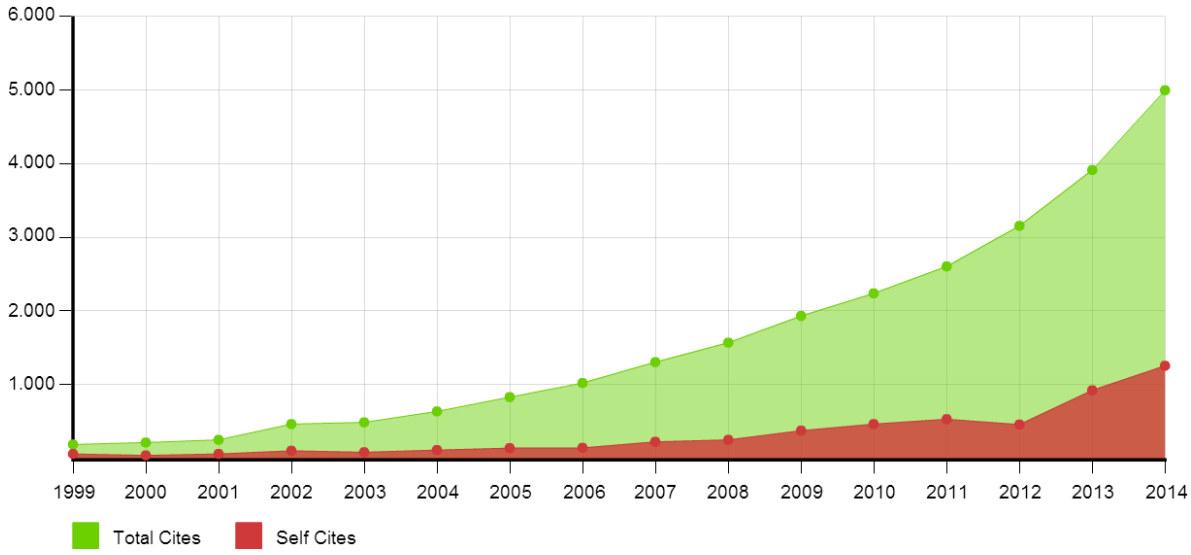

Cites per Document vs. External Cites per Document

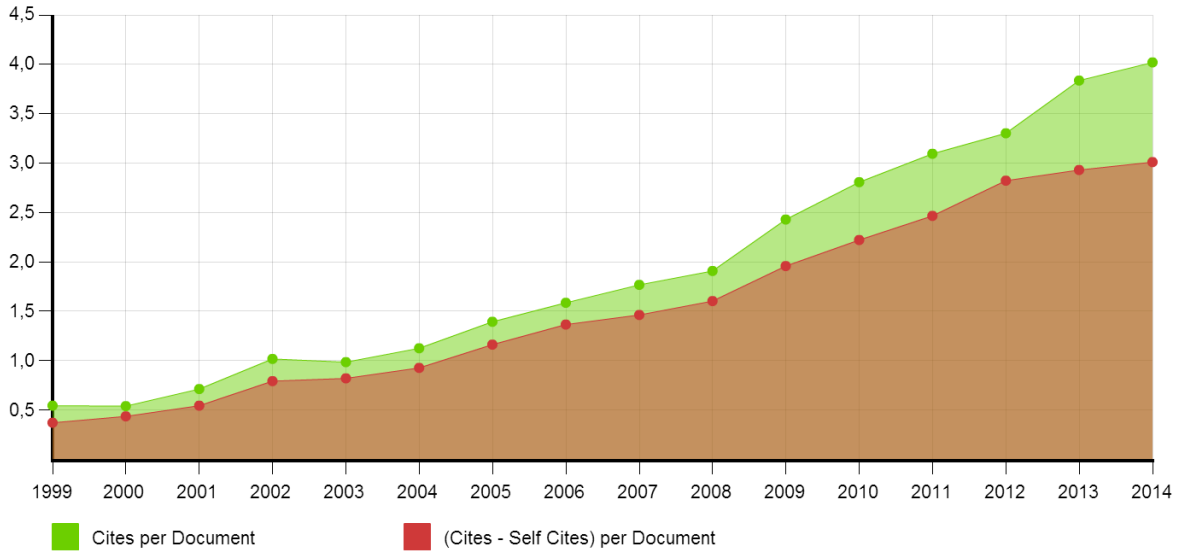

Cites per Document in 2, 3 and 4 years windows

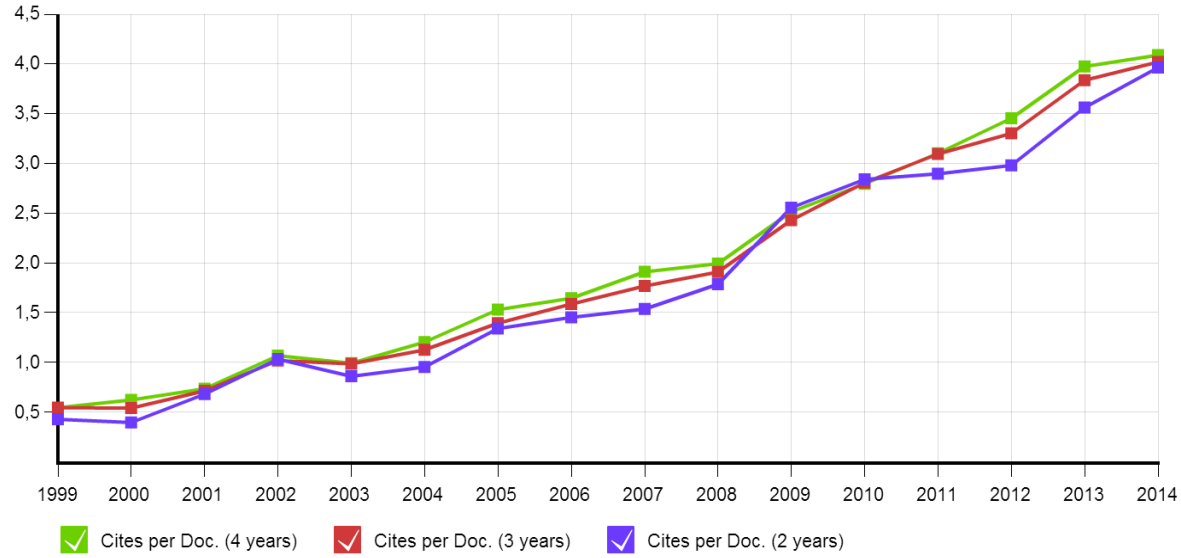

International Collaboration

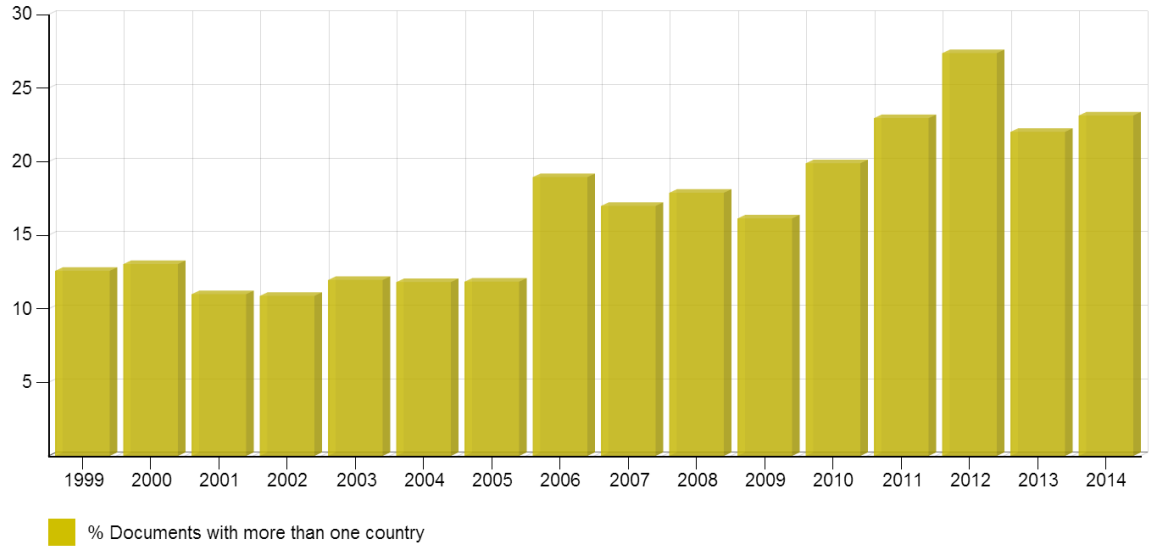

Journal's Citable vs. Non Citable Documents

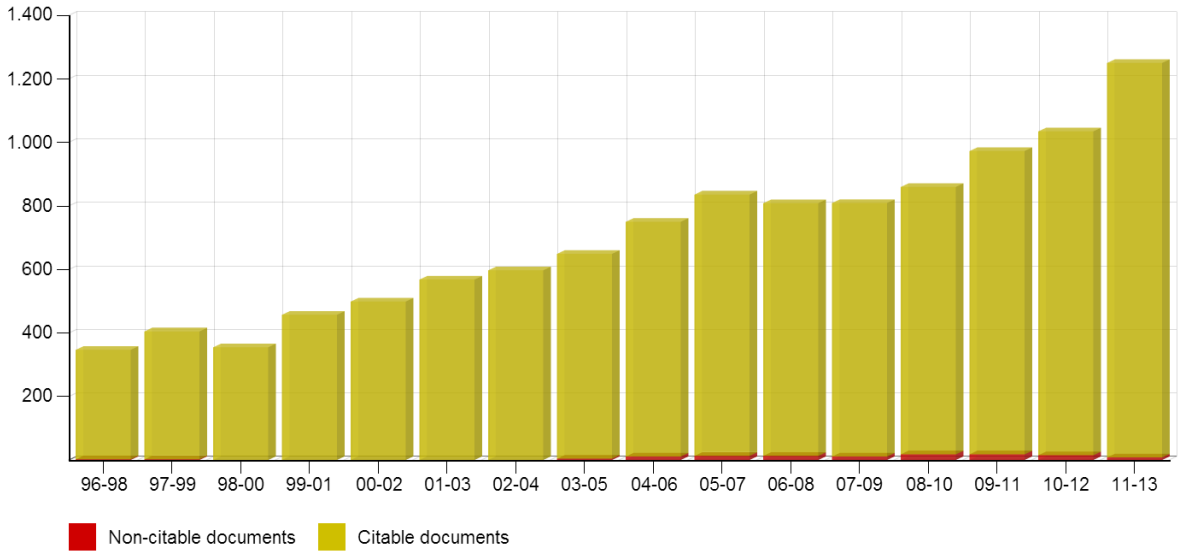

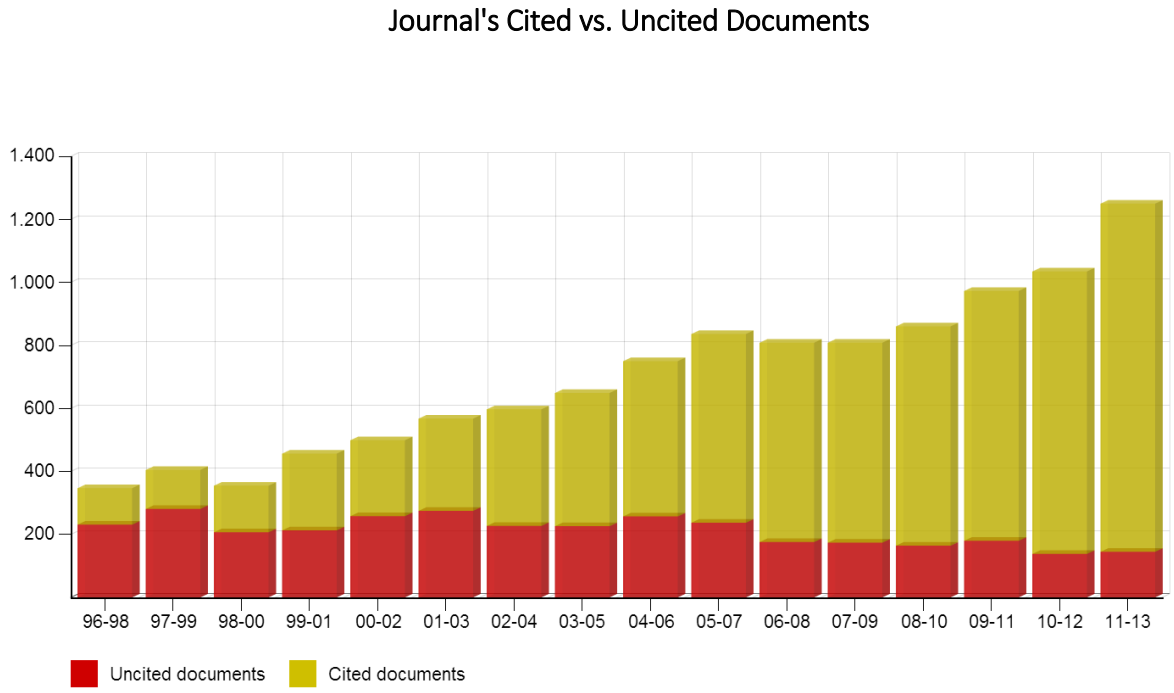
Journal's Cited vs. Uncited Documents
1.400
1.200
1.000
800
600
400
200
96-98
97-99
98-00
99-01
00-02
01-03
02-04
03-05
04-06
05-07
06-08
07-09
08-10
09-11
10-12
11-13
Uncited documents
Cited documents

JOURNAL:	Remote Sensing
URL:	http://www.mdpi.com/journal/remotesensing
EDITORAL:	MDPI
IMPACT FACTOR:	3,18
H INDEX:	70
QUARTILE:	Q1
RANK:	5(28)

SJR indicator vs. Cites per Doc (2y)

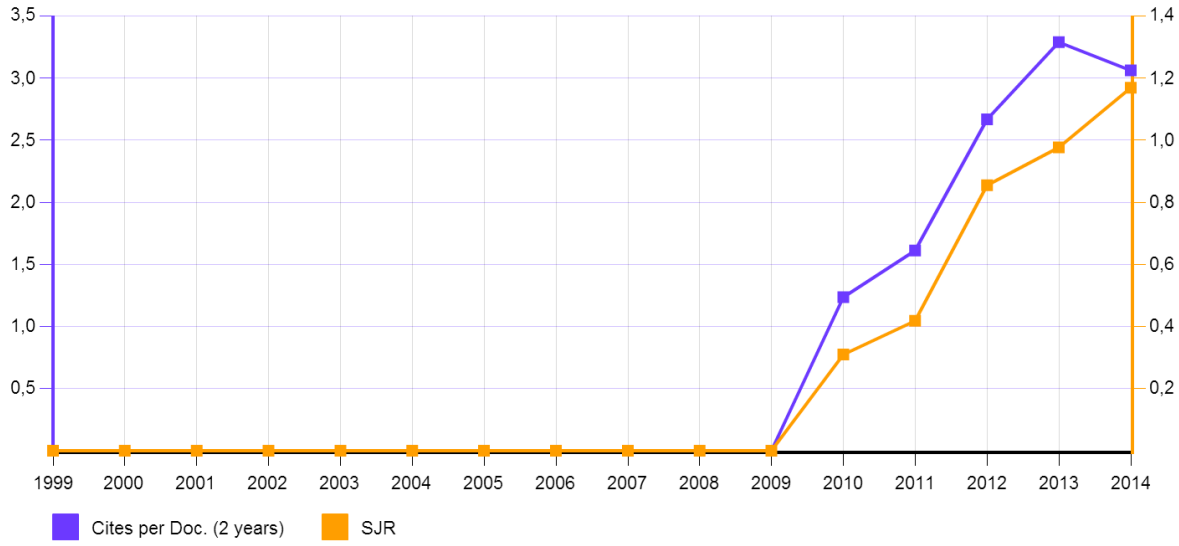

Citation vs. Self-Citation

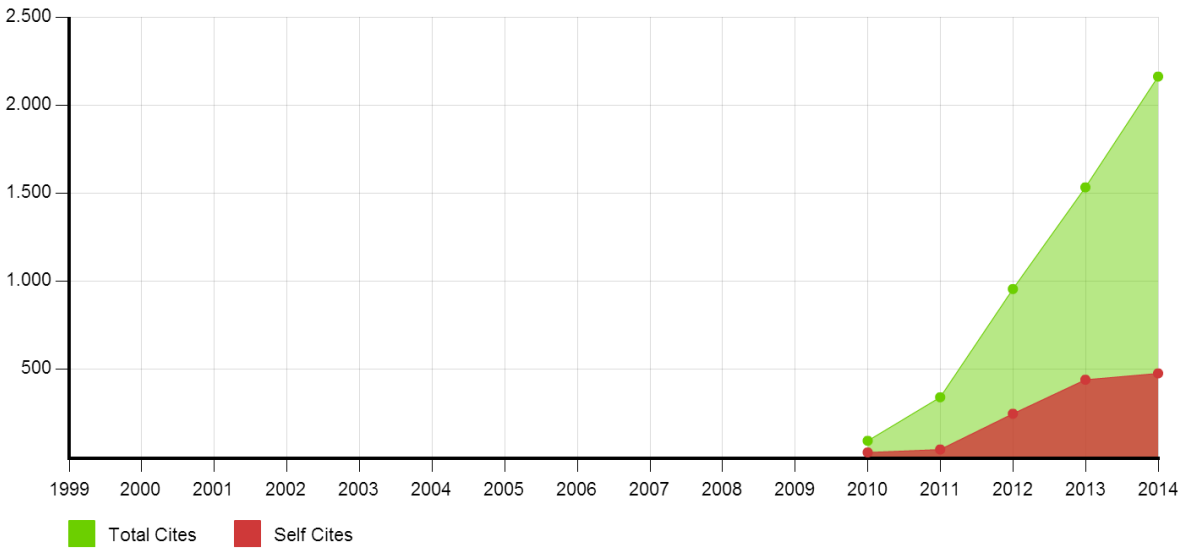

Cites per Document vs. External Cites per Document

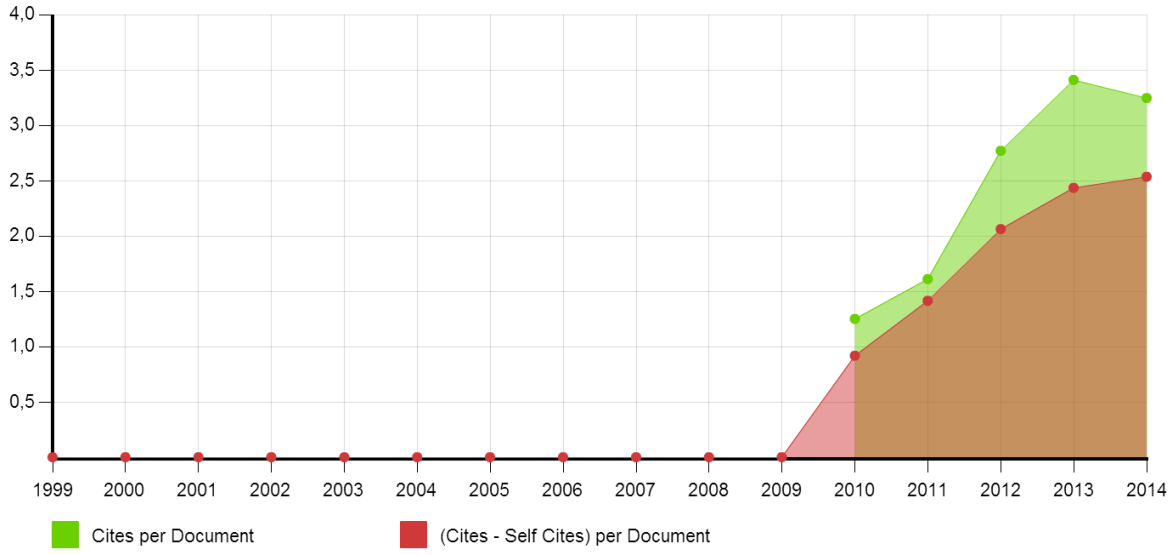

Cites per Document in 2, 3 and 4 years windows

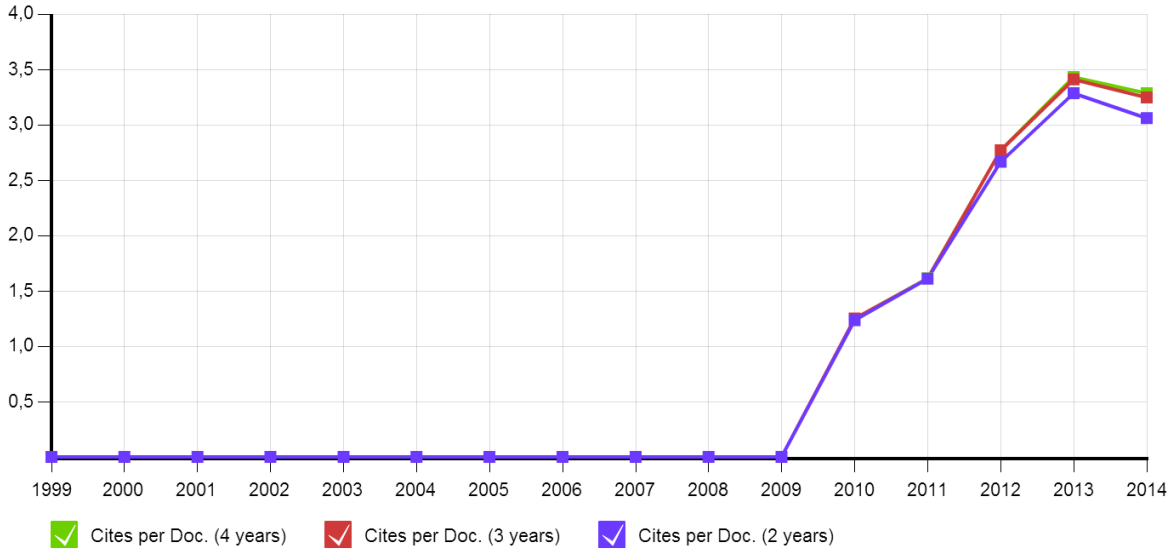

International Collaboration

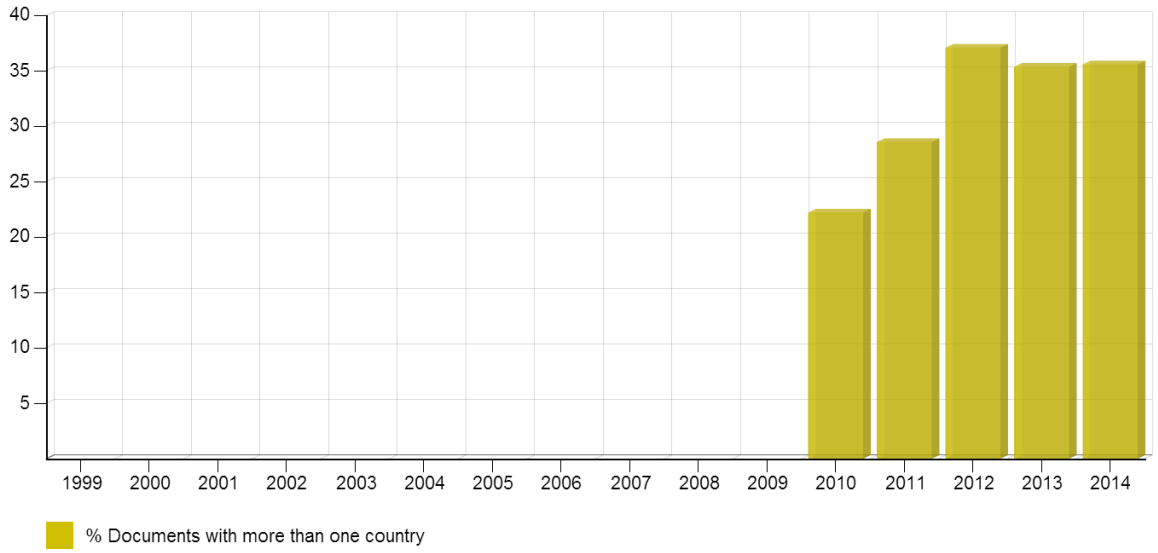

Journal's Citable vs. Non Citable Documents

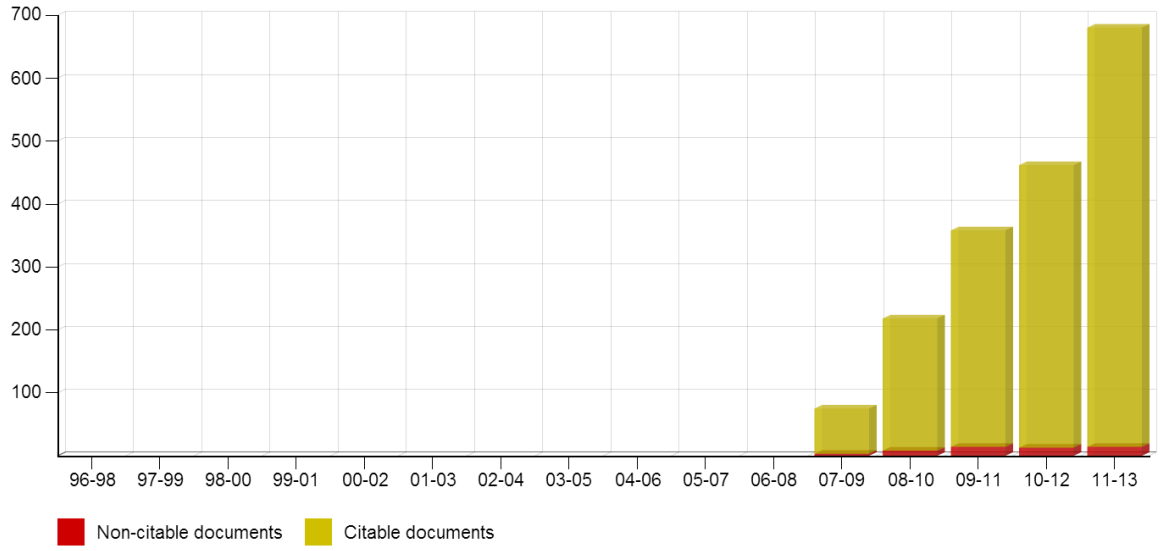

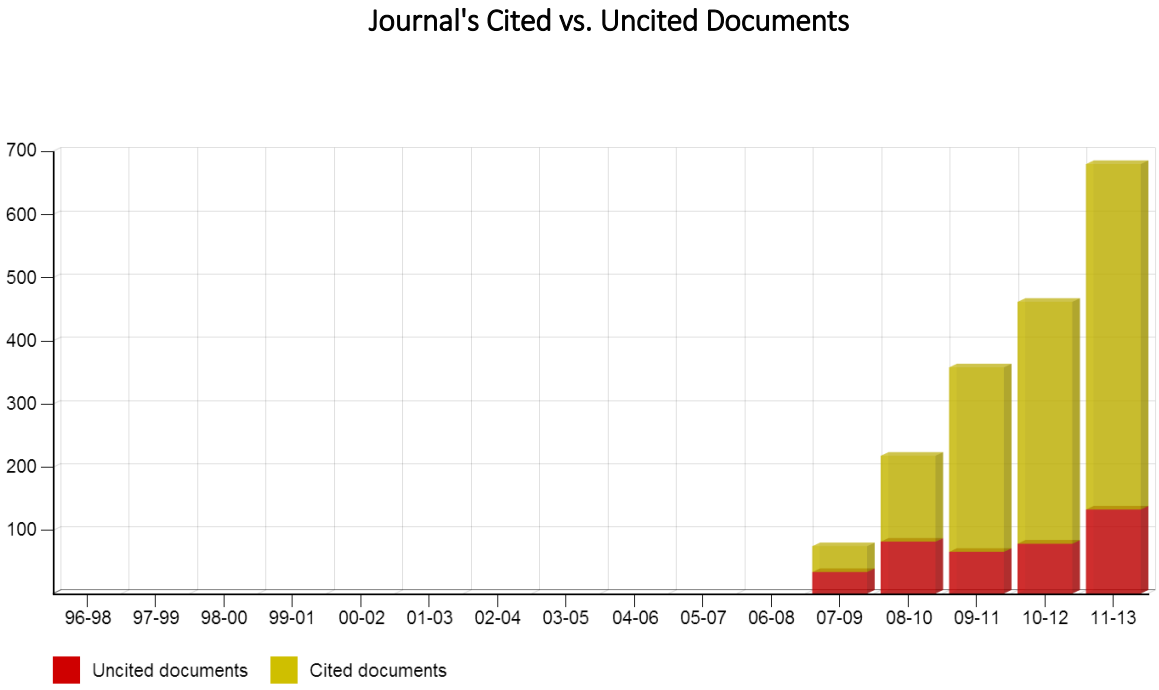
Journal's Cited vs. Uncited Documents
700
600
500
400
300
200
100
96-98
97-99
98-00
99-01
00-02
01-03
02-04
03-05
04-06
05-07
06-08
07-09
08-10
09-11
10-12
11-13
Uncited documents
Cited documents

JOURNAL:	CRC Press Balkema
URL:	http://www.balkema.nl/
EDITORAL:	Taylor & Francis
PBK:	126
PCH:	1832
CIT:	2400
FNCS:	1,22
RANK:	6(75) **(FIRST DECILE)**

	PBK	PCH	CIT	FNCS
Springer	1054	12139	14831	1,29
Elservier	387	5238	3943	1,19
Nova Science Publishers	267	2665	954	0,28
Woodhead Publishing	192	2482	878	0,43
Artech House	142	1759	676	0,55
CRC Press	126	1832	2400	1,22
Cambridge University Press	99	966	1543	2,08
Pan-Stanford	79	845	405	1,12
Wiley-Blackwell	49	542	194	1,21
MIT Press	47	580	437	1,36
IGI Global	48	593	92	0,38
William Andrew	35	481	169	0,62
De Gruyter	25	296	368	1,08
IWA Publishing	22	249	78	0,89
SAE International	16	200	16	0,17
SIAM	16	142	248	1,67
Scientific Publishing Co Pte Ltd	13	134	80	0,97
Edward Elgar	12	147	81	0,82
Taylor & Francis	11	172	73	0,46
ASTM International	10	206	9	0,06
Routledge	10	143	33	0,45

SPON PRESS	9	85	56	0,93
EDITIONS TECHNIP-TECHNICAL BOOKS	8	114	26	0,88
WIT PRESS	8	84	11	0,15
ISTE LTD	7	76	12	0,21
PALGRAVE MACMILLAN	7	60	35	0,74
AM. SOCIETY OF MECHANICAL ENGINEERS	6	72	20	0,33
IOS PRESS	6	122	35	0,31
WORLD BANK	6	52	22	0,51
AM. INST. AERONAUTICS ASTRONAUTICS	5	73	18	0,21